

Analysis of Electrogenenerated Chemiluminescence of PPV type Conducting Polymers

DISSERTATION

zur Erlangung des akademischen Grades

doctor rerum naturalium

(Dr. rer. nat.)

im Fach Chemie

eingereicht an der

Mathematisch-Naturwissenschaftlichen Fakultät I

der Humboldt-Universität zu Berlin

von

Umamaheswari Janakiraman

geb. am 18.11.1974 in Indien

Präsident der Humboldt-Universität zu Berlin

Prof. Dr. Jürgen Mlynek

Dekan der Mathematisch-Naturwissenschaftlichen Fakultät I

Prof. Dr. Michael Linscheid

Gutachter:

1. Prof. Dr. Erhard Kemnitz
2. Prof. Dr. Werner Abraham
3. Prof. Dr. Michael Linscheid

Tag der mündlichen Prüfung: 20.05.2003

Dedicated to my parents

TABLE OF CONTENTS

1: INTRODUCTION

1.1. Electrogenenerated Chemiluminescence (ECL)	5
1.2. Energetics of the ECL	7
1.3. Analysis of ECL reaction mechanism	
1.3.1. Distinguishing singlet route from triplet route	11
1.3.2. Identification of other possible mechanisms for the production of an excited state	14
1.4. Factors affecting the ECL and precautionary measures	14
1.5. Conducting polymers	16
1.6. Electroluminescence (EL)	21
1.7. Objectives of the present study	23

2. EXPERIMENTAL TECHNIQUES AND PROCEDURES

2.1. Electrochemical techniques	
2.1.1. Cyclic voltammetry	24
2.1.2. Potential Step Experiments	
2.1.2.i. Electrode reaction kinetics	27
2.1.2.ii. Measurement of double layer parameters	29
2.1.2.iii. Double layer charging and charge transfer	30
2.2. Experimental procedures	31
2.3. Optical methods	
2.3.1. Absorbance and fluorescence spectroscopy	32
2.3.2. Raman spectroscopy	34
2.3.3. Photomultiplier tubes	36
2.4. Polymer cross-linking by synchrotron radiation	37

3. THE ELECTROCHEMILUMINESCENCE EXPERIMENTS

3.1. Solution phase ECL: DPA	40
3.1.1 Experimental details	40

3.1.2 Cyclic voltammetry	41
3.1.3. Current transients	41
3.1.4. The ECL experiment	43
3.1.5. The ECL emission spectrum	51
3.2. Polymer phase ECL: MEH-PPV	52
3.2.1. Experimental details	52
3.2.2. Cyclic voltammogram	53
3.2.3. Current transients	55
3.2.4. The ECL experiment	56
3.3. Polymer phase ECL: DB-PPV	61
3.3.1. Experimental details	61
3.3.2. Cyclic voltammogram	62
3.3.3. Current transients	65
3.3.4. The ECL experiment	67
3.3.5. Studies concerning the stability of DB-PPV	70
3.3.6. Energetics of the ECL in DB-PPV	77

4. THEORETICAL ANALYSIS OF THE KINETICS OF ECL

4.1. Solution phase ECL - 9,10 diphenylanthracene (DPA)	81
4.1.1. Kinetics of the ECL process in solution phase	81
4.1.2. Double layer charging	83
4.1.3. Digital simulation technique	84
4.1.4. Conditions for simulation	86
4.1.5. Inclusion of the IR drop in the electrochemical solution and double layer charging at the electrode/solution interface	87
4.1.6. Simulation of the experimental ECL transient for DPA	88
4.2. Polymer phase ECL: MEH-PPV	91
4.2.1. Kinetics of the ECL process in the polymer phase	91
4.2.2. Double layer charging	98
4.2.3. Digital simulation technique	98
4.2.4. Conditions for simulation	99
4.2.5. Inclusion of the IR drop in the conducting polymer and double layer charging at the electrode/polymer interface	100
4.2.6. Simulation of the experimental transients of MEH-PPV	100
4.3. Simulation of the experimental transients of DB-PPV	104

5. SUMMARY, CONCLUSIONS AND OUTLOOK

5.1 Symmetrical ECL	106
5.2. Stability of the polymers	107
5.3. Influence of counterions	108
5.4. Kinetics of the ECL process	109
5.5. Mechanism of ECL in PPV type polymers	110
5.6. Outlook	111

6. LITERATURE

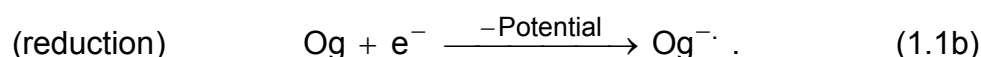
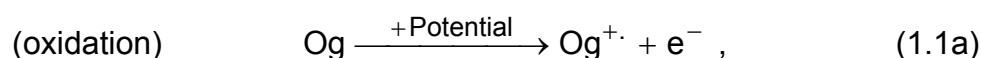
Table of Figures	117
List of Symbols	125
Abbreviations	136

1. Introduction

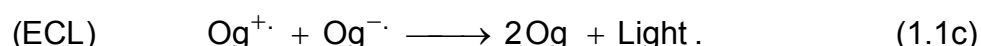
The first report about the generation of electrochemiluminescence (ECL) in conducting polymers (CP) came in the year 1994 [1] from the group of A.J. Bard. After that there have been only three publications about the electrogenerated chemiluminescence [2] in conducting polymers until to date [3-5]. But there have been several works done on the ECL in the solution phase containing organic molecules [6,7]. The generation of electroluminescence (EL) in conducting polymers is another field of research that is widely reported in the literature [8]. However ECL in conducting polymers is different from that in the solution phase and the EL process. In order to understand the significance of the ECL in conducting polymers, first the principles of the ECL process in the solution phase will be discussed, as it is relatively simple. Then the unique properties of conducting polymers such as the nature and transport of charges in them will be described. The characteristics of the electroluminescence (EL) process in CP will be described in brief to understand the uniqueness of the ECL process.

1.1. Electrogenenerated chemiluminescence

Electrogenenerated chemiluminescence is the production of light by the reaction between the charged species generated by electrochemical means. The first report of this kind appeared in 1964 [9]. The electrochemical generation of reactants may be formulated (for organic compound Og) as:



The redox process between the reactants produces neutral molecules in an excited electronic state that relaxes by emission of photons.

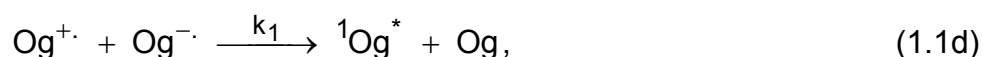


This chemiluminescence reaction is electron transfer luminescence since the sequence oxidation-reduction can be as effective as reduction-oxidation. The heterogeneous electron transfer reactions at the electrode/solution interface are fast. The luminescence observed is fluorescence. Therefore the schemes to be considered must be the ones, which provide sufficient energy to yield an

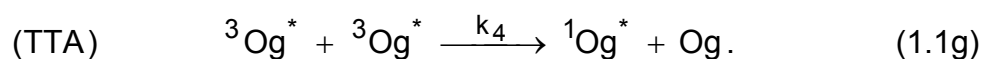
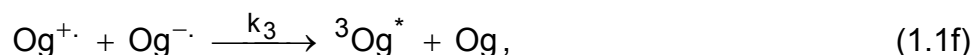
aromatic hydrocarbon in its first excited singlet state, $^1\text{Og}^*$.

The mechanisms considered to date for the formation of $^1\text{Og}^*$ in these systems can be classified into four types:

(1) The first mechanism postulates the direct formation of $^1\text{Og}^*$ via the annihilation of electrogenerated $\text{Og}^{\cdot+}$ by electrogenerated $\text{Og}^{\cdot-}$. The process may yield $^1\text{Og}^*$ or an excimer $^1\text{Og}_2^*$ [10].



(2) The second mechanism envisions the formation of $^3\text{Og}^*$ via the same annihilation reaction as above. This is then followed by the known process of triplet-triplet annihilation (TTA) to yield $^1\text{Og}^*$ provided that sufficient energy is available from two triplets. The presumably efficient quenching of $^3\text{Og}^*$ by $\text{Og}^{\cdot+}$ and/or $\text{Og}^{\cdot-}$ must be recognized in discussing mechanisms involving triplets.



(3) A third mechanism was postulated describing the direct generation of excited states, $^3\text{Og}^*$ or $^1\text{Og}^*$, by a heterogeneous electron transfer reaction at the electrode [11]. Oxidation of $\text{Og}^{\cdot-}$ or reduction of $\text{Og}^{\cdot+}$, under certain polarization conditions was said to generate $^3\text{Og}^*$.

(4) The fourth type is the chemiluminescence reaction of $\text{Og}^{\cdot-}$ with products resulting from the decomposition of $\text{Og}^{\cdot+}$ and/or the solvent. Chemiluminescence reaction of stable $\text{Og}^{\cdot+}$, with the decomposition products of $\text{Og}^{\cdot-}$ or with the solvent also belongs to this class. This mechanism was operative in a number of other cases, particularly those in which $\text{Og}^{\cdot+}$ is able of oxidizing or otherwise reacting with the solvent, e.g., 9,10-diphenylanthracene (DPA) or 9,10-dimethylantracene in dimethylformamide (DMF). In the rubrene system, as in the DPA in acetonitrile, luminescence was observed only when

both $\text{Og}^{\cdot+}$ and $\text{Og}^{\cdot-}$ are electrogenerated. The pre-annihilation ECL reported earlier in some cases [12] is absent when the solute-solvent electrode system yields stable $\text{Og}^{\cdot+}$ and $\text{Og}^{\cdot-}$.

1.2. Energetics of the ECL

In the usual thermal electron transfer reaction, the products are formed in their electronic ground states, for only these are usually conveniently accessible energetically. Nevertheless, the potential energy surface of the reactants can "cross" the surface of the products, in which one (or more) product(s) is (are) electronically excited in some other region of configuration space. If this latter intersection region is easily accessible (energetically and entropically, Marcus [13]), a reaction to form an excited product can occur. The excited product may either emit light or react. An example of such a reaction is a possible triplet-triplet annihilation to form an excited singlet, which later fluoresces. [14].

The electron transfer theory yields the rate constant to form a particular electronic state of the products as

$$k_{\text{ex}} = Z \kappa \rho \exp(-\Delta F^*/kT), \quad (1.2a)$$

where Z is about $10^{11} \text{ l mole}^{-1} \text{ s}^{-1}$, κ is a factor close to unity unless the splitting is extremely small, $\rho \approx 1$, and the ΔF^* reflects the accessibility of the intersection region.

$$\Delta F^* = w^r + (\lambda/4) \left\{ 1 + \left(\Delta F_{\text{R}^{\circ'}}/\lambda \right)^2 \right\}, \quad (1.2b)$$

$$\Delta F_{\text{R}^{\circ'}} = \Delta F^{\circ'} + w^p - w^r. \quad (1.2c)$$

In these equations w^r is the work required to bring the reactants together to the most probable separation distance R in the intersection region, i.e., in the "activated complex"; w^p is the corresponding work to bring the products together, each 'w' refers to the given state of excitation. $\Delta F^{\circ'}$ is the "standard" free energy of reaction in the prevailing medium, λ is a reorganization term. It is expressible in terms of differences in equilibrium bond lengths of each reacting

species in its initial and final electronic states in terms of dielectric properties (related to differences in equilibrium orientation polarization) in these electronic states; λ is typically on the order of 0.4-0.6 eV for solvents such as acetonitrile or dimethylformamide. The activation energy has a minimum value at $\Delta F^\circ = -\lambda$. If ΔF° is larger than $-\lambda$, we are dealing with a normal activation process. If, on the other hand, ΔF° is smaller than $-\lambda$, the intersection of the adiabatic potential curves occurs in the abnormal region.

In a sufficiently exothermic electron transfer reaction the region where the surface of ground-state products "intersects" that of ground-state reactants is not readily accessible and becomes less accessible with increasing exothermicity. Under such conditions the region where the potential energy surface involving an excited product intersects that for the unexcited reactants may be readily accessible. The formation of an excited product can then occur easily. This formation of an electronically excited Og is allowed because it represents a favourable way of accommodating the energy released by the electron transfer reaction. The actual transfer presumably does not involve any large changes in molecular geometry or co-ordination and could occur rapidly on the time scale of molecular vibrations. Such a time scale makes it difficult to convert this energy into thermal energy. Thus, the creation of an excited state and emission from it are possible in an electron transfer reaction under special conditions. This process is analogous to the combination of an electron with a hole in the solid state. An even closer analogy is the phenomenon of recombination luminescence of organic compounds held in rigid matrices at low temperatures [15].

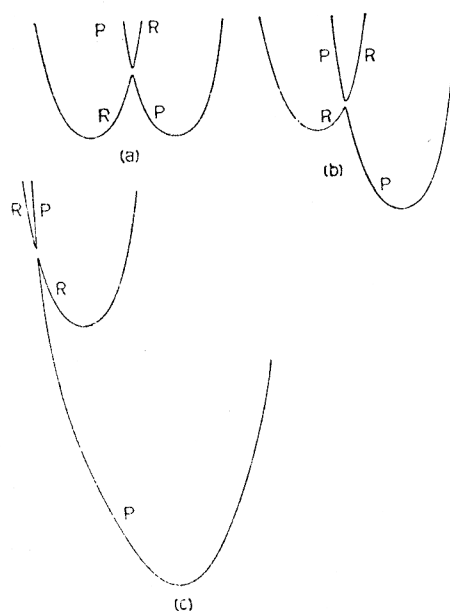


Fig 1.2a: Scheme of potential energy surfaces for an electron transfer reaction.

To understand the mechanism of electron transfer leading to the singlet or triplet excited state, we consider the simple molecular orbital picture representing the lowest unoccupied molecular orbital (LUMO) and highest occupied molecular orbital (HOMO).

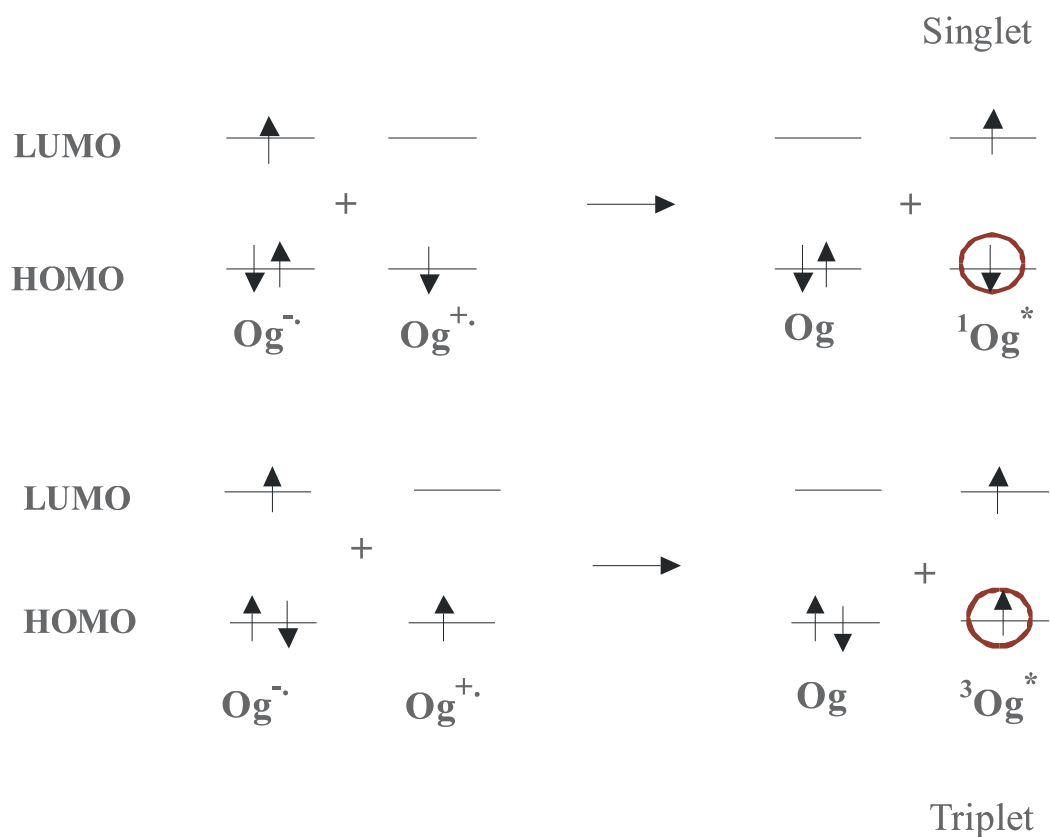


Fig. 1.2b: Molecular orbital representation of an electron transfer reaction.

An initial one-electron transfer with the formation of a radical ion generally characterizes the redox activity of an aromatic molecule in an aprotic solvent. Reductions are pictured as an addition of an electron to the lowest vacant molecular orbital (MO), and oxidations as a removal of an electron from the highest filled MO. Good correlations are found between electrochemical half-wave potentials and eigen values of these MO's which has been shown in the following table [reproduced from 16]:

Table 1.2a: Correlations between the electrochemical half-wave potentials and the energies of the excited singlet and triplet levels

Compound	$E^\circ(\text{Og}^{+\cdot}/\text{Og})$ V vs. SCE	$E^\circ(\text{Og}/\text{Og}^{-\cdot})$ V vs. SCE	$-\Delta G^\circ = n \Delta E^\circ$ (eV)	Energy Levels (eV)	
				First Excited Singlet	Lowest Triplet
Anthracene	1.36	-2.00	3.36	3.20	1.8
DPA	1.35	-1.89	3.24	3.00	1.8
TPP	1.25	-1.83	3.08	2.95	2.0
Rubrene	0.97	-1.48	2.45	2.30	1.1 - 1.2
p-Benzo quinone	not oxidized	-0.52	0.52	2.8	2.3
TMPD	0.24	not reduced	0.24	3.5	2.7

Process energetics has weighed heavily in mechanistic arguments, because it is easy to characterize the redox reactions thermodynamically via the standard potentials of the couples involved.

$$-\Delta H^\circ = E^\circ(\text{Og}^{+\cdot}/\text{Og}) - E^\circ(\text{Og}/\text{Og}^{-\cdot}) - T\Delta S. \quad (1.2d)$$

From the cyclic voltammogram of the organic compound, e.g., DPA (9,10-diphenylanthracene) the difference in the standard potentials for oxidation and reduction can be calculated using Eq. (1.2d). This corresponds to the free energy of the radical ion pair compared to the ground state DPA pair, which is ≈ 3.2 eV in acetonitrile. The free energy of $^1\text{Og}^* + \text{Og}$ was calculated from the 0-0

transition energy of the fluorescence spectrum to be 3.0 eV. Thus, the energy supplied in the electrochemical generation of the radical ions is sufficient for the production of DPA excited state. Such systems are called energy sufficient systems, and the corresponding electron transfer reaction can result in the ECL.

1.3. Analysis of the ECL reaction mechanism

1.3.1. Distinguishing singlet route from triplet route

In section 1.1 four possible ways of ECL generation were mentioned. The identification of the actual mechanism is indeed a difficult task, especially differentiating the mechanisms 1 from 2. The ECL emission spectrum yields the energy of the emitted light, which can be used as a tool to identify the nature of the excited state, whether it is a singlet or triplet excited state. But the problem is the identification of the triplet-triplet annihilation (TTA, Eq. (1.1g)) giving rise to the singlet-excited state. If the lowest triplet has less than half the energy of the first excited singlet, then TTA will not occur, as in the case of naphthalene [17]. However it cannot be generalised so easily. Especially in systems like DPA, where $^3\text{Og}^* + \text{Og}$ has larger energy, 1.8 eV than the half of the singlet energy.

Feldberg [18,19] did a kinetic analysis of the processes to identify the mechanism. The reactions (1.1a) and (1.1b) corresponding to the generation of radical cation and radical anion respectively can be achieved by the application of two successive potentiostatic steps of appropriate magnitudes. In which case reaction(s) (1.1d) (singlet) or (1.1f) and (1.1g) (triplet) take place in the second potential step. Let t_f and t_r be the duration of the first and second potential steps. Feldberg has calculated that when $k_1 t_f C$ is larger than 10^3 , the intensity of the fluorescence radiation will be given by:

$$\log_{10} \left(P t_f^{1/2} \right) = 1.45 \left[(t - t_f) / t_f \right]^{1/2} + \text{constant}, \quad (1.3.1a)$$

for times where $[(t - t_f) / t_f]^{1/2} > 0.4$ and where P is the photometer output and C is the bulk concentration. This equation is valid for direct formation of excited

singlets (reaction (1.1d)) or for triplet formation followed by TTA to give an excited singlet (reactions (1.1 f) and (1.1g)). For the latter case the constant is smaller by a factor of 2 than for the case of direct singlet formation. Thus, this method though helped to identify the production of the singlet state; a conclusion about whether it is a direct singlet formation or singlet formation through TTA is not possible. The details of the theoretical analysis will be discussed in detail in chapter 4.

Since the triplet-excited state has a paramagnetic spin, method of electron spin resonance (ESR) spectroscopy coupled with the ECL experiments was performed [20, 21]. TTA was tried to be identified by this technique. An initial report dealt with two energy-deficient systems, TMPD(+) / DPA(-) and TMPD(+)/anthracene(-), and one energy-sufficient systems, DPA(+) / DPA(-). Monotonically increasing intensities with field strength were observed for the former cases, but the latter did not show any effect. These results demonstrated the presence of a field influenced step in the emission scheme for the two TMPD(+) oxidations and the absence of such a process in the DPA(+) / DPA(-) case. The influenced reactions were presumed to involve paramagnetic species, and triplet-triplet annihilation was suggested as an appealing candidate. Thus, these findings were cited as possible evidence that the two energy-deficient systems proceed via the T-route, whereas the S-route yields the emission from DPA(+) / DPA(-) [22]. This method was not successful in all the cases. In DPA the ECL was ESR silent, but the ECL efficiency (ratio of the number of emitted photons in unit time to the faradaic current) was just about 1.5 % when it is expected to be 100% based on a pure singlet route [23]. Thus, the differentiation between direct singlet formation and that due to TTA is still uncertain. However the other possibilities can be identified. The complications due to excimer formation were often eliminated by phenyl substituents at reactive sites.

Also on the basis of the magnetic field effects it is not really possible to confirm or deny this mechanistic position, because one cannot predict the magnitude of an ECL field effect in any qualitative fashion. In principle, it could be calculated if a host of rate constants, the quencher concentrations, and molecular parameters in the spin Hamiltonians were all available [24]. In ECL the quencher concentrations within the reaction zone have unknown (and possibly

unknowable) magnitudes and time dependencies. Even though a quantitative description is not feasible, this technique is still a very powerful qualitative aid for distinguishing ECL processes involving triplets from those that do not.

A very sensitive means for probing T-route systems involved intercepting a triplet intermediate $^3D^*$ by triplet energy transfer to an acceptor species A [25,26]:



The acceptor triplet can itself undergo triplet annihilation; hence, the acceptor's addition may transform the ECL spectrum from donor emission to that of the acceptor. Alternatively, it might undergo rapid radiationless decay resulting in quenching of the ECL emission. Either effect provides support for the operation of the T-route in any case for which it is suspected. Moreover, the acceptor triplet can undergo a "photochemical annihilation" created by a known number of redox events and can give triplet yields in an attractively straightforward manner. Although it is a common tool in photochemistry, it is very difficult with ECL systems, because the conditions for unambiguous transfer are quite stringent. The basic problem is that the acceptor triplet will ordinarily get reduced or oxidized more easily than one of the ion precursors. It therefore interferes severely with ECL generation, and any modification in behaviour upon its addition is practically uninterpretable. A less severe, but important problem is the need for a chemical inertness of the acceptor toward the ion radicals. Very few systems have met these demands so far, and all of them have involved the fluorantharene triplet as a donor. Since this molecule has a small S^1-T^1 splitting, it exhibits high triplet energy (2.3 eV) for a species that reduces so easily (- 1.70 V vs. SCE). There are several suitable acceptors for its triplet, and interception studies of oxidations of its anion have proved quite fruitful. However, quantitative calculation of the triplet yield ϕ_t is difficult, even if the productions of the radical ions are controlled because of the interference by any quenchers present in the system [27].

1.3.2. Identification of other possible mechanisms for the production of an excited state

Regarding the formation of an excited state, by the reaction of the radical ions with the electrode, which is the possibility 3 mentioned in section 1.1: It depends on the free energy for the formation of the radical ion. If it is larger (≈ 3 eV), then there will be no chance to form an excited species in the solution. If the standard energy for the formation of the radical anion is higher, then when the potential of the electrode is switched to a positive value, the electron from the radical anion can go easily to one of the unoccupied orbitals of the metal. Thus, the radical anion becomes oxidized to the neutral species instead of becoming excited. Similar remarks apply to a very exothermic electron transfer from an electrode to a molecule or a radical cation in solution. In this case the electron can relieve the exothermicity by coming from one of the filled half of the conduction band of the metal. Thus the molecule or the radical cation becomes, reduced when the polarity of the electrode becomes more negative [13].

The possibility 4, i.e., the reaction between one of the radical ions with the decomposed products of the electrochemical system, depends on the stability of the system. In such cases ECL is observed before reaching the appropriate potentials for the electrogeneration of one of the radical ions. This phenomenon is termed as pre-annihilation ECL. For example, Rubrene in dimethylformamide (DMF) has the pre-annihilation ECL due to the reaction of the radical cation with the solvent. Whereas DPA or Rubrene in acetonitrile yields luminescence, only when both $\text{Og}^{\cdot+}$ and $\text{Og}^{\cdot-}$ are electrogenerated [28].

1.4. Factors affecting the ECL and the precautionary measures

The electrogenerated chemiluminescence is affected by the stability of the exciton as well as that of the precursor radical ions. The definition of quenching is a process, which reduces the lifetime of the excited state. A reduction in the lifetime usually implies a decrease in the quantum yield. Some of the processes that reduce the quantum yield are: collisional quenching, static quenching and energy transfer. Light scattering can appear as quenching (loss of fluorescence

signal). Both, collisional and static quenching require a contact between the fluorophore and the quenchers. Thus, these methods are useful to measure rates of diffusion and exposure of fluorescent species to the quencher. A large number of quenchers are known, and a partial list is: molecular oxygen, amides, BrO_4^- , xenon, peroxides, nitroxides and acrylamide.

The mechanism of quenching was difficult to determine. In some cases, such as acrylamide, the quenching mechanism seems to involve a transfer of charge from the excited fluorophore to the quenching agent.

In the case of the conducting polymers, the chemical nature of the polymer plays a crucial role in determining the stability of the exciton. The movement of the exciton along the polymer, which is enhanced by the presence of delocalized bonds in CP, as well as the dissociation of the exciton, which is caused by the lack of delocalization, lead to the loss of the excitons.

Considering the stability of the radical ions, again, oxygen is the foremost threat to it. It is invariably present in the chemicals and in the environment. This even in a minute amount is a threat to the excited state because of its paramagnetic nature [29]. And hence, traces of water in the solvent or the supporting electrolyte is also detrimental. It can produce the superoxide during the electrochemical potential sweep/step necessary for the production of ECL. Hence, the success of ECL experiments depends strongly on the removal of oxygen and water from the experimental system. The radical ions, especially those with extensive delocalization and blocked reactive sites, may be stable or they may undergo a number of different types of reaction [30]. Electrogeneration of dianions and dications at potentials beyond the initial reduction and oxidation waves is also possible. But these species are usually quite unstable in the solvents employed for ECL.

The solvent supporting electrolyte systems are chosen for their lack of reactivity with the electrogenerated species, their wide potential limits and their good conductivities. Purity of the medium is important in determining both, the quality of the electrolytic background and the stabilities of the ECL reactants, hence, special attention must be given to it. The common solvents used for the ECL experiments are acetonitrile (AN), benzonitrile (BN), N,N-dimethylformamide

(DMF), methylene chloride, propylene carbonate (PC) and tetrahydrofuran (THF). The supporting electrolytes are tetraalkylammonium salts with the anions as tetrafluoroborate (BF_4^-), hexafluorophosphate (PF_6^-) and perchlorate (ClO_4^-).

Excellent purification procedures are described in the literature for dimethylformamide (DMF) and acetonitrile [31]. Since these solvents are hygroscopic, they must be isolated from the atmosphere during storage. These solvents are kept under argon and when needed can be dispensed through the spigot by slightly pressurizing the flask with the inert gas on a vacuum line. Greaseless fittings are used when dealing with solvents. The supporting electrolytes can often be used as received. Recrystallisation may be required [32]. Hygroscopic electrolytes must be dried for 24-28 hours at 90-100 °C and should be kept in a desiccator. Drying them overnight prior to the experiment also helps to reduce the moisture content.

Vacuum systems are generally used which offer convenience in continuous removal of water from the system. The vacuum level is approximately 10^{-5} Torr. The system should be filled with argon during the experiment. Bubbling the electrolytic solution with argon also helps to remove the traces of oxygen along with the above said procedure.

Platinum is the most frequently used electrode material for ECL studies. Although the oxide films that occur in aqueous solutions do not affect it, some pre-treatment is generally done before use. Polishing the platinum to a high finish, with very fine emery paper or diamond paste, are some of the regular procedures.

1.5. Conducting polymers

Conducting polymers (CP) contain electronic states that can be reversibly occupied and emptied with electrochemical techniques. In fact, the electrochemistry of conducting polymers has enormous potential for wide ranging practical applications, e.g., in batteries, displays, etc. [33-35]. As polymers, these materials have a highly anisotropic quasi-one-dimensional electronic structure that is fundamentally different from the structures of

conventional inorganic semiconductors. This has two consequences: First, their chain like structure leads to strong coupling of the electronic states to conformational excitations peculiar to the one-dimensional (1D) system [36], and second, the relatively weak interchain binding allows diffusion of dopant molecules into the structure (between chains), whereas the strong intrachain carbon-carbon bond maintains the integrity of the polymer. In their neutral form, these polymers are semiconductors with an energy gap of ≈ 2 eV. However, when they are in the doped state (i.e., oxidized or reduced), their conductivity increases by many orders of magnitude; conductivities in the range of $\approx 10^3 - 10^4$ S/cm are not unusual [37].

The conductivity in doped polymers, optical and magnetic properties that are far from those of traditional metals provided the direct evidence that the description of electronic excitations in CPs is very different from that of three-dimensionally bonded materials. The anisotropic bonding in the polymers allows a local rearrangement of the chain geometry to better accommodate an electronic excitation, without requiring a large lattice strain in the directions perpendicular to the chain. And it allows, in general, formation of "polaronic" excited states, for both charged and neutral excitations (excitons).

The character of these polaronic states was first established for the case of polyacetylene, for which, in the trans isomer, the degeneracy with respect to the sense of bond alternation causes these states to take the form of topological, soliton-like chain excitations, which have associated with them a nonbonding π level that is situated at the middle of the π - π^* semiconductor gap [38]. In polymers with a nondegenerate ground state, such as PPV, the two alternative senses of bond alternation do not have equivalent energies; the charged excitations of a nondegenerate ground state polymer are termed polarons or bipolarons and represent localized charges on the polymer chain with an accompanying local rearrangement of bond alternation. The neutral excited state shows similar structural reorganization, as shown in the following Fig. 1.5a.

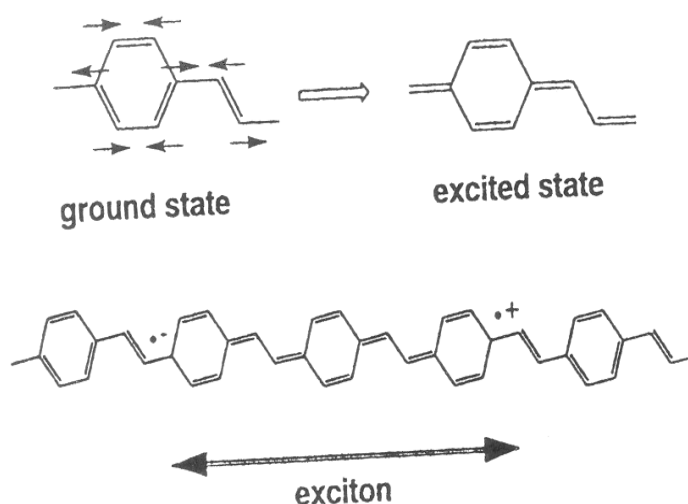


Fig. 1.5a: Configuration of the exciton in PPV.

These states may be considered equivalent to a confined soliton pair, and in this model the two nonbonding midgap "soliton" states form bonding and antibonding combinations, thus producing two gap states symmetrically displaced about the midgap as shown in Fig.1.5b. These levels can be occupied by 0, 1, 2, 3, or 4 electrons, giving a positive bipolaron (bp^{2+}), positive polaron (p^+), polaron exciton, negative polaron (p^-), or negative bipolaron (bp^{2-}), respectively.

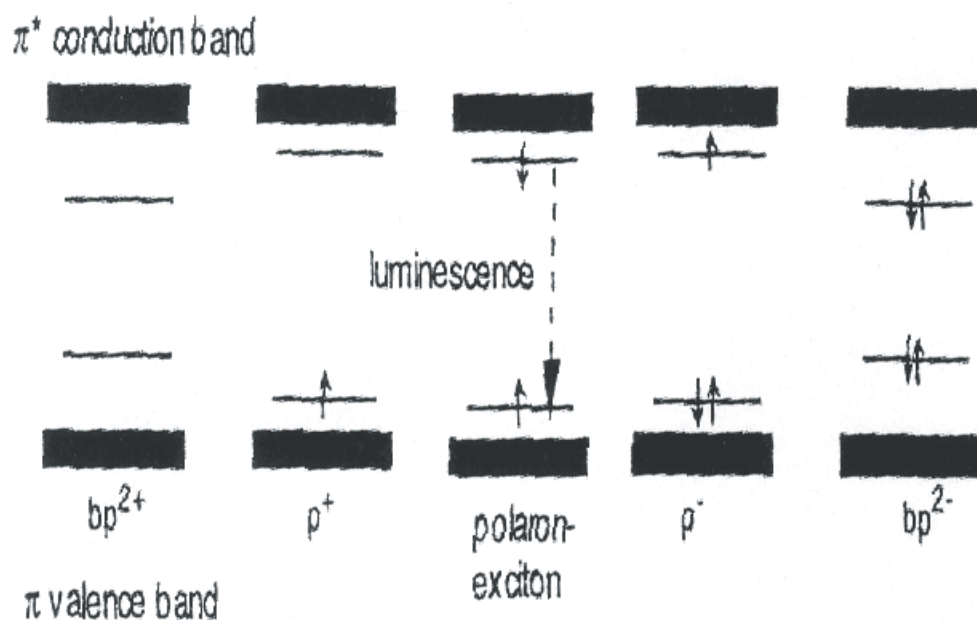


Fig. 1.5b: Scheme of the valence and conduction bands of polarons and bipolarons.

The case of near degeneracy allows the polarons to be relatively extended with

electronic levels near the center of the gap, while strong breaking of the degeneracy keeps them much more compact with levels near the band edges. The singly charged polaron is expected to have gap states that are more closely tied to the band edges than is the case for a bipolaron or exciton. The greater degree of relaxation of the bipolaron in comparison to the polaron stabilizes the coalescence of two like-charged polarons to form a bipolaron. There are many theoretical works concerned with the modelling of these polaronic levels [39, 40]. The success of these models lies in their ability to account for the appearance of new optical absorption bands within the semiconductor gap on chemical doping (e.g., at 0.6 eV and 1.6 eV for the case of PPV [41]) and at the same time to account for low paramagnetic response (bipolarons being low spin). The quantum chemical techniques that have been used to describe the ground state electronic structure have also been used with considerable success to model the electronic structure and chain geometry of charged excited states [42, 43]. But these predict that the energy of the photons emitted by luminescence should be equal to the spacing between the two-bipolaron levels. Whereas experimentally the luminescence is found to occur at significantly higher energy than the bipolaron spacing as determined from photo induced absorption. Such discrepancies are overcome by taking the electron-electron interactions into account in the model calculations [44]. Further improvements are made by considering interchain interactions [45]. Describing the excited states, especially the neutral excited states that are excitonic, is still complex. Excitons are electron hole pairs, which may either be localized on one molecular unit or spread over many molecular units. A complete description of the excitons was done by considering the electron-electron (Coulombic) and the electron-lattice interactions. One consequence of the electron-electron is that singlet and triplet excitons are no longer of the same energy or of the same size. The triplet exciton is considerably more localized than the singlet exciton, which is confirmed for PPV and its oligomers [46]. Based on these theoretical studies, the arrangement of ground and excited state energies for PPV is depicted as shown in Fig. 1.5c.

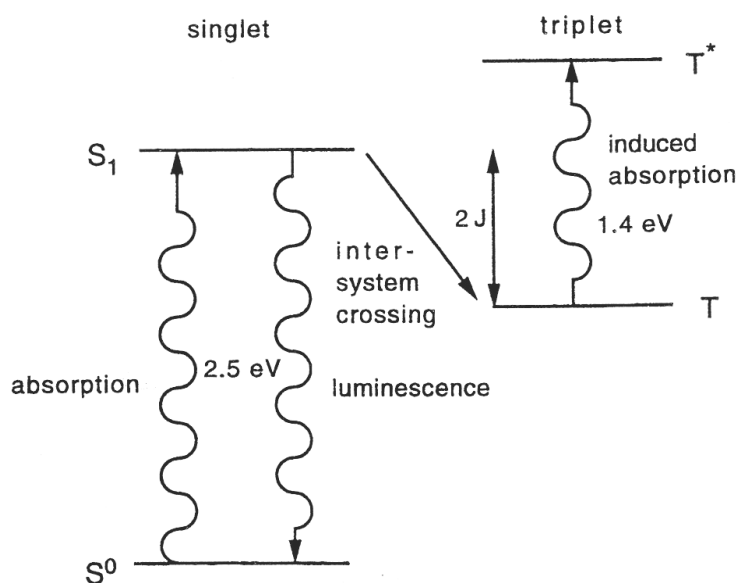


Fig. 1.5c: Ground and excited states of PPV polymer.

Thus, the energy levels in the case of CPs are different from the organic monomer molecules and are strongly influenced by the electronic and lattice interactions. The understanding of this is necessary to assign the spectroscopic features of these polymers. Polymers with larger π - π^* energy gaps have poor intrachain delocalization and can show changes in optical properties as they are brought together in the solid. Interchain interactions are therefore important for these materials and lead to the formation of more extended excited states, which would be described as charge transfer excitons within the framework of molecular semiconductors. If the intermolecular contacts are optimized via a geometrical change following excitation, such excitons are described as excimers (where the exciton extends over identical molecular units) or exciplexes (where the exciton extends over two or more different molecular units).

The other important factor need to be known is the movement of the charges and excitons in CP. Let us consider excitons alone at first. Excitons are mobile within the solid, and their motion, either coherent or diffusive, plays a very important part in the photophysics of conjugated polymers. When there are appreciable nearest-neighbor interactions between the molecular units of CP, the exciton becomes delocalized, the exciton then drifts along the delocalized band. When there is a significant electron-phonon interaction, the exciton loses

its coherence, and it becomes a localized state that moves by hopping between sites. In practice, disorder in site energies plays a very important part in causing this loss of coherence.

The transport of charges (positive polaron, negative polaron and the corresponding bipolarons) resembles that of the exciton. The presence of ions from the supporting electrolyte with CP in an electrochemical environment yields a characteristic charge transport mechanism in them. This is discussed in detail in chapter 4.

Since the electron-electron and interchain interactions determine the polaronic and excitonic energy levels in the CP, they can be tuned to achieve the desired emission. This is done by changing the substituents of the conducting polymer to achieve characteristics like the emission in the desired energy range and of desired solubility [47].

1.6. Electroluminescence

Due to the tunability of the energy of emission and the ease of handling them, conducting polymers are used in solid-state light emitting devices (LED), emission of which is called electroluminescence (EL). Electroluminescence (EL) from conjugated polymers was first reported in 1990 [48] using poly(*p*-phenylenevinylene) (PPV) as the single semiconductor layer between metallic electrodes, as illustrated in Fig. 1.6a.

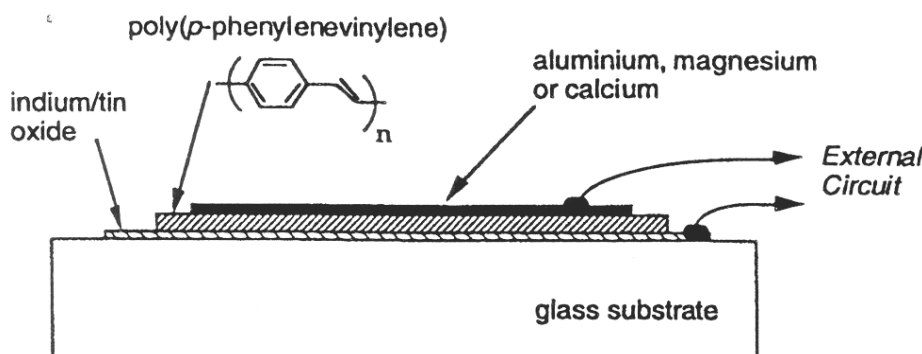


Fig. 1.6a: Construction of a light emitting diode (LED).

PPV has an energy gap between π and π^* states of about 2.5 eV and produces

luminescence in a band below this energy, as shown in Fig. 1.6b. Operation of LED is achieved when the diode is sufficiently biased to achieve injection of positive and negative charge carriers from opposite electrodes. Capture of oppositely charged carriers within the region of the polymer layer can then result in the formation of the singlet exciton, which is generated by photo excitation across the π - π^* gap, and this can then decay radiatively to produce the same emission spectrum as that produced by photo excitation. The absorption and emission spectra for PPV are shown in Fig 1.6b. Note that the absorption rises rapidly above the onset of the π - π^* threshold and that the emission spectrum appears on the low energy side of the absorption. Both, absorption and emission spectra show a broadening due to vibronic coupling, as is characteristic for optical transitions in molecular semiconductors where the excited state is a singlet exciton. The similarity of the emission spectra produced by photo excitation and by charge injection establishes that the excited state responsible for light generation in the LED is the same as that produced by photoexcitation.

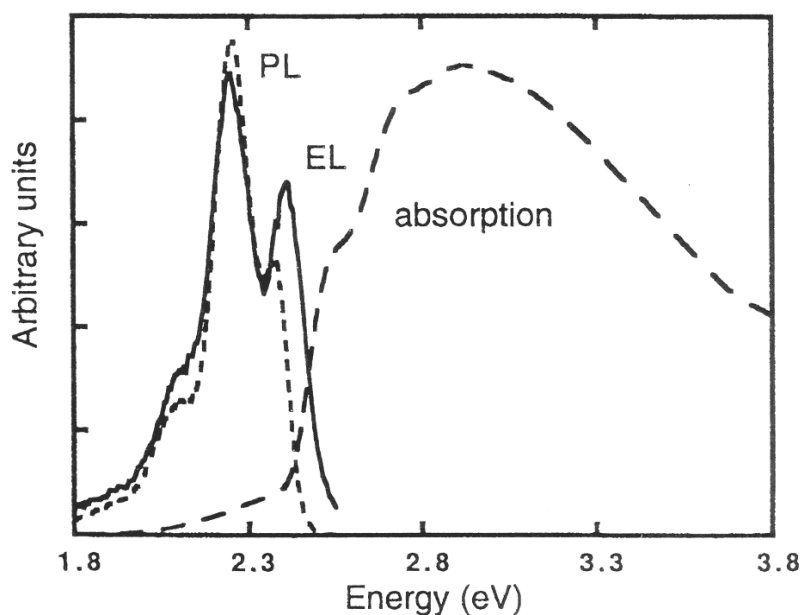


Fig. 1.6b: Absorption, photoluminescence (PL) and electroluminescence (EL) spectra of PPV.

The levels of efficiency of the first, simple LEDs based on PPV, which were fabricated with aluminium negative electrodes, were relatively low, on the order of 1 photon generated within the device per 10^4 charges injected (an internal quantum efficiency of 0.01 %) [48]. External quantum efficiencies are strongly

affected by the refractive index of the emissive layer, and the relationship between the two has been discussed by Greenham et al. [49]. These values have risen rapidly over the past few years as improved understanding of the operation of these devices, aided in considerable measure by parallel developments made with sublimed molecular film devices, has allowed considerable optimization of the devices characteristics. The use of negative electrodes with lower work functions was shown to improve efficiency to as high as 1 % in devices made with ITO/MEH-PPV/Ca [50].

1.7. Objectives of the Present Study

The conducting polymers behave electrically different in the solid state and in contact with the solution. Since CPs yield both, electroluminescence (EL) in the solid state and electrogenerated chemiluminescence (ECL) in contact with electrochemical solution. Therefore, it is of interest to analyze the mechanism of the ECL process in the conducting polymers, to find out whether is it similar to the EL process or to the ECL process in solution phase. If it is different, in what way does it differ from the other two processes? In order to achieve that, theoretical modeling of the ECL reaction and charge transport mechanism and comparison with the experimental findings are required. This study can also throw some light on the charge transport mechanism of CP in electrochemical conditions. These are the objectives of the present study.

2. Experimental Techniques and Procedures

2.1. Electrochemical techniques

Throughout the work, electrochemical methods were used in which the electrode potential was controlled via a potentiostat. Two electrochemical techniques involved in the analysis of electrochemiluminescence (ECL) are cyclic voltammetry (CV) and potential step experiments. In these experiments, the potential of the working electrode (Wk) is controlled by a potentiostat (Fig. 2.1a) either directly or following the program from a function generator, as in the case of potential step experiments. Reference and counter electrodes are represented as Ref and Ctr in the figure.

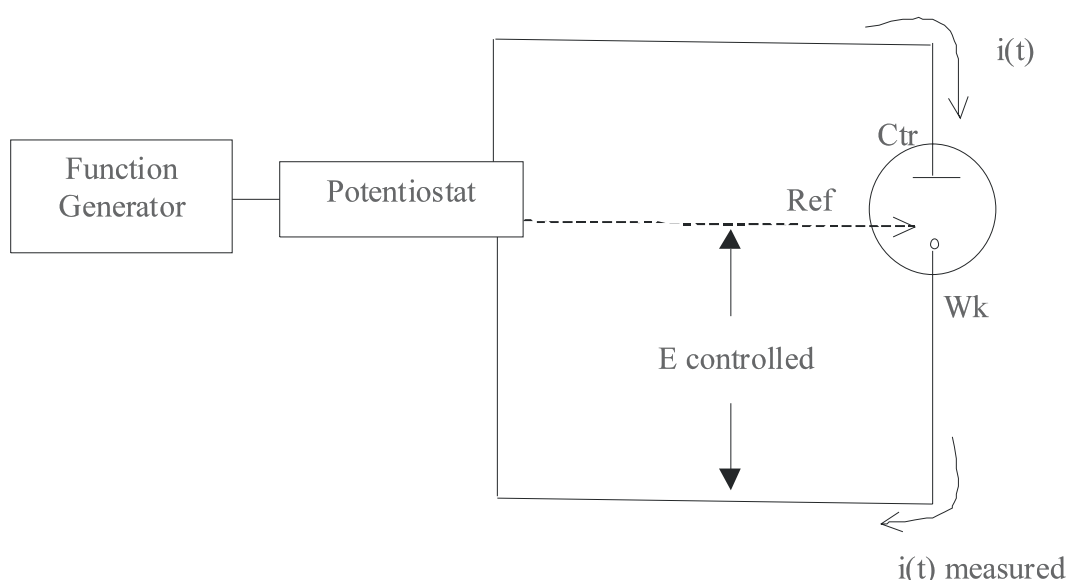


Fig. 2.1a: Scheme for controlled potential experiments.

2.1.1. Cyclic voltammetry

Cyclic voltammetry (CV) is a very popular technique for initial electrochemical studies of new systems and even to derive information about fairly complicated electrode reactions. The technique is based on applying a triangular potential sweep at a rate v ($=dE/dt$), in V/sec, to the electrochemical system.

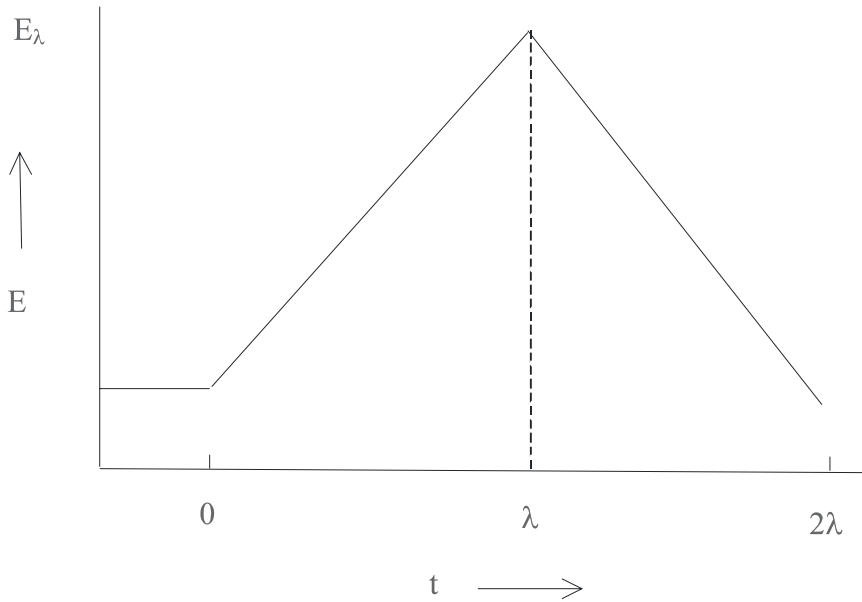


Fig. 2.1.1a. Triangular waveform of the potential in potential sweep techniques.

The potential (E) at any time is given by

$$(0 < t \leq \lambda) \quad E = E_i + v t, \quad (2.1.1a)$$

$$(\lambda < t \leq 2\lambda) \quad E = E_i + 2v\lambda - v t, \quad (2.1.1b)$$

where t is the time of the potential sweep, λ is the time corresponding to the switching potential, E_λ , E_i is the initial potential and v is the scan rate [51].

Let us consider the oxidation of DPA to its radical cation $\text{DPA}^{+\cdot}$ at a platinum (Pt) electrode in an electrolytic solution, with an initial concentration of DPA, C_{DPA} . When the potential is swept in the positive direction, initially there is charging of the double layer at the electrode/electrolytic solution interface giving rise to a current that is proportional to the double layer capacitance, C_{dl} ,

$$i_{\text{dl}} = \frac{dq_{\text{dl}}}{dt} = C_{\text{dl}} \frac{dE}{dt}. \quad (2.1.1c)$$

As the potential approaches the standard potential $E^{0/+}$, the oxidation current starts increasing. It reaches its maximum at the standard potential, when the surface concentration of DPA becomes zero at the Pt electrode. At higher magnitudes of the positive potential, the current progressively decreases

because of the depletion of oxidizable DPA in the layer of solution adjacent to the electrode, by diffusion. This can be understood from the definition of the faradaic diffusion controlled current, I_F .

$$\frac{I_F}{nFA} = - D \left(\frac{\partial C_{DPA}}{\partial x} \right)_{x=0} . \quad (2.1.1d)$$

Clearly, as the diffusion front extends further and further into the electrolyte, the concentration gradient at the electrode ($x = 0$) decreases, and so does the current. At the switching potential, the sweep becomes reverted, and the reduction current corresponding to the conversion of DPA^{+} to the neutral DPA, increases slowly and follows the same trend near and beyond the standard potential for reduction, $E^{+/0}$. This is because, in the initial oxidation sweep, the diffusion layer becomes depleted of DPA and populated with DPA^{+} at a concentration of C_{DPA}^* . The conditions in the diffusion zone are similar for reduction as compared to oxidation in the initial sweep.

In the considered case of a reversible reaction, the surface concentrations of oxidized and reduced species at the electrode (Pt) are defined by the Nernst equation:

$$\frac{C_{DPA^{+}}(0,t)}{C_{DPA}(0,t)} = \exp \left[\frac{nF}{RT} (E(t) - E^{0'}) \right]. \quad (2.1.1e)$$

This was used to derive the expressions for the anodic and cathodic peak currents and potentials:

$$i_p = (2.69 \times 10^5) n^{3/2} A D_{DPA^{+}}^{1/2} v^{1/2} C_{DPA^{+}}^*, \quad (2.1.1f)$$

where i_p is the current in amperes at 25 °C, A is the electrode area in cm^2 , $D_{DPA^{+}}$ is the diffusion coefficient in $cm^2 s^{-1}$, v is the scan rate in Vs^{-1} and $C_{DPA^{+}}^*$ is the concentration in $mol cm^{-3}$. For a reversible electrochemical reaction, the plot of i_p vs. $v^{1/2}$ is a straight line, from which the diffusion coefficient of the reactant can be calculated, knowing the other parameters. In addition, the ratio $i_{pa}/i_{pc} = 1$ for reversible oxidation and reduction reactions. Any deviation in this ratio reflects kinetic complications, i.e., irreversible or quasi-reversible electrochemical reactions at the electrode. The difference between E_{pa} and E_{pc} (ΔE_p) is another useful tool to test the reversibility of the electrochemical process, which is close to $2.3 RT/nF$ at 25 °C for a Nernstian reaction.

The cyclic voltammetry of a polymer-coated electrode in the electrolytic solution is similar to that of a bare electrode, except with some important differences: The first change is brought about by the thickness of the polymer. This poses limitations to the progress of the diffusion front in the polymer. If the polymer thickness is lower than the diffusion layer thickness, the diffusion becomes hindered abruptly. This results in shortening of the diffusion tail in the cyclic voltammogram, and the current peak is now depicted by

$$i_p = \frac{n^2 F^2 v V C_{O^*}}{4RT}, \quad (2.1.1g)$$

where C_{O^*} is the bulk concentration of the oxidized polymer moiety and V is the volume of the polymer. Thus, the peak current becomes proportional to v , when the thickness of the polymer is smaller than the diffusion layer thickness (l), defined by the diffusion coefficients of the reactant and the time ($l = \sqrt{2Dt}$), for a linear diffusion. Thus, the cyclic voltammogram gives clues about the kinetic and transport parameters of the concerned electrochemical reaction.

2.1.2. Potential step experiments

2.1.1.i. *Electrode reaction kinetics*

Let us consider a single potential step to understand the current characteristics, by taking the example of 1 mM DPA in 0.1 M TEAClO₄ in acetonitrile (AN).

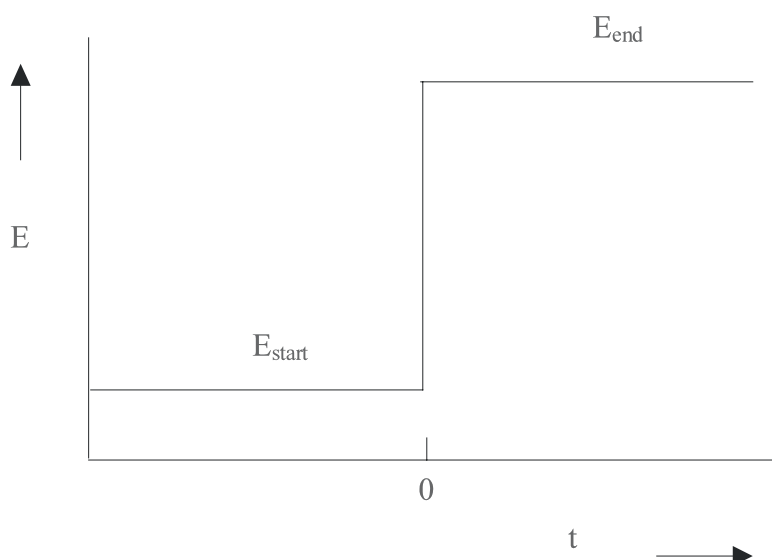


Fig. 2.1.2a: Scheme of a single positive potential step.

In these experiments the working electrode is initially kept at a potential where there will be no electrochemical reaction. And then the potential is stepped at $t = 0$, to a positive potential, which is above the standard potential $E^{0/+}$ for the oxidation of the DPA in the electrochemical cell. The reactant at the electrode surface will become converted to positive radical ion, DPA^+ . This provokes subsequent diffusion of DPA towards the electrode generating a concentration gradient within the diffusion layer. Since DPA becomes instantaneously oxidized to DPA^+ , the concentration gradient at the electrode surface defined by the diffusion, controls the current. At $t = 0$, the concentration gradient is maximum, because the concentration of DPA remains the same throughout the bulk except at the electrode surface, where it goes to 'zero'; this leads to maximum current in the chronoamperometry. Subsequently, decreasing current is recorded, since the concentration of DPA in the diffusion layer depletes with time due to the electrochemical reaction. The current is obtained by solving the concentration terms using the relationship,

$$\frac{\partial C_O(x,t)}{\partial t} = D_O \frac{\partial^2 C_O(x,t)}{\partial x^2}, \quad (2.1.2a)$$

where O stands for the oxidized species, DPA^+ . Even a sluggish electrochemical reaction can be made diffusion controlled, by increasing the applied potential, and the current is derived to be

$$i(t) = \frac{nFAD_O^{1/2} C_O^*}{\pi^{1/2} t^{1/2}}. \quad (2.1.2b)$$

This equation is known as Cottrell equation. The plot of $i(t)$ vs. $t^{-1/2}$ is linear for a diffusion controlled reaction, from which the value of the diffusion coefficient can be calculated. As with the case of cyclic voltammetry, the thin layer condition imposed by the polymer thickness can be inferred from the break in linearity of the $i(t)$ vs. $t^{-1/2}$ plot. This is because when the diffusion layer exceeds the thickness of the polymer film, there is no oxidizable species, and hence the current drops to zero all of a sudden.

2.1.1.ii. Measurement of double layer parameters

Electrode potentials, at which electrochemical charge transfer does not take place, the electrochemical systems: electrode/solution or electrode/polymer/solution behaves like an RC circuit upon application of potential to it. The double layer at the interface electrode/solution (or the electrode/polymer/solution) behaves like a capacitor. The potential drop across this capacitor supplies the potential for an electrochemical reaction. In addition, the current has to flow through the electrolytic solution (or polymer/electrolytic solution), which offers resistance to the current flow. This can be schematically shown as below:

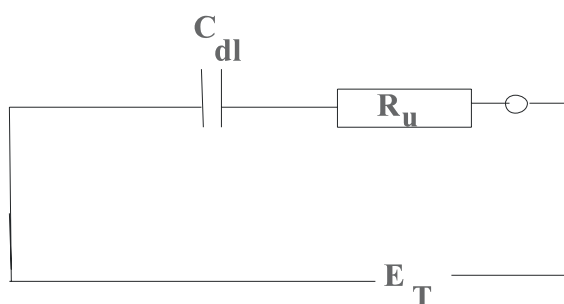


Fig. 2.1.2.b: Equivalent circuit description of an electrochemical system in the absence of electrode reaction.

E_T is the total potential applied to the electrochemical system. The values of the uncompensated resistance R_u and the double layer capacitance C_{dl} are essential for the quantitative analysis of the kinetics and transport properties. Their product, $R_u C_{dl} = \tau$ determines the time constant of electrochemical kinetics. Their measurement was achieved by stepping the potential to a value far below the standard potential for oxidation or reduction of the electrochemical system and by measuring the current. The current in potential step experiment in this potential range is due to double layer charging (i_{dl}) which is expressed as,

$$i_{dl} = \frac{E}{R_u} \exp \left(-\frac{t}{R_u C_{dl}} \right). \quad (2.1.2c)$$

When $\log i_{dl}$ is plotted against the time (t), the uncompensated resistance (R_u) can be calculated from the intercept; knowing which, the double layer capacitance C_{dl} can be estimated from the slope.

2.1.1.iii. Double layer charging and charge transfer

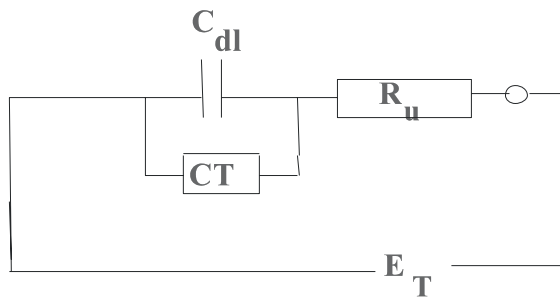


Fig. 2.1.2.c: Equivalent circuit description of an electrochemical system in the presence of an electrochemical reaction.

CT is the resistance for the charge transfer reaction. Due to the IR_u drop in the electrochemical system, the electrode potential that is effective for the interfacial charge transfer reactions E_{CT} is diminished from the applied potential E_T [52]. Considering potential steps as in Fig. 2.1.2a, and defining the start and end potentials of a step as E_{start} and E_{end} , we can write

$$E_{CT}(t) = E_{end} - I(t)R_u$$

or

(2.1.2d)

$$E_{CT}(t) = E_{start} + \int_0^t \frac{I_{dl}}{C_{dl}} dt.$$

The total current (I) at any time t is a sum of faradaic current I_F and the charging current I_{dl} :

$$I(t) = I_F(t) + I_{dl}(t).$$
(2.1.2e)

Following these equations, Eq. (2.1.2c) can be re-written as

$$I_{dl} = \frac{E_{end} - E_{start}}{R_u} \exp\left(-\frac{t}{R_u C_{dl}}\right).$$
(2.1.2f)

2.2. Experimental procedures

The polymer coating was done by dissolving the polymer in CHCl_3 to make a saturated solution. Then, the polymer solution was applied to the electrode in drops with subsequent spinning of the electrode at a rate of 3 rps to ensure uniform coating. The Pt substrate was polished with 3, 1 and 0.7 μm diamond paste and cleaned ultrasonically. The surface was checked for uniformity with a Nikon PFX 104 optical microscope before and after the deposition of the polymer. The amount of polymer was estimated separately by evaporating part of the solution on a Pt disc and weighing it in a microbalance. The approximate polymer thickness was estimated from the amount of the polymer applied to an electrode using the value of dry density of the polymer.

Electrochemical experiments were carried out in a three-electrodes configuration with the polymer coated Pt as the working electrode and Pt wires as the quasi-reference (QRE) and counter electrodes. Anhydrous CH_3CN obtained from Aldrich was used as the solvent and 0.1 M tetraethylammonium tetrafluoroborate (TEABF_4), tetraethylammonium hexafluorophosphate (TEAPF_6), tetrabutylammonium tetrafluoroborate (TBABF_4), or tetraethylammonium perchlorate (TEAClO_4) were used as the supporting electrolytes. The electrolytes were stored in desiccators over silica. Prior to the experiment they were dried in the oven for 12 hours to remove the traces of water present. Further care was taken for the removal of water, by heating the mixing cell containing the supporting electrolyte for half an hour, prior to mixing it with the solvent. The solvent acetonitrile, was stored in a closed vessel and was pressed inside the mixing cell by applying Ar pressure. Immediately after mixing the solvent and the supporting electrolyte, the solution was bubbled with argon and was also heated at intervals with proper care of the pressure development inside it, for nearly an hour [53]. The solution was then pumped to the electrochemical cell containing the working, counter and reference electrodes and was filled with Ar. Electrochemical measurements were accomplished with a homemade potentiostat. Potential pulses were applied by Agilent 33250 A function generator via the potentiostat. ECL emission intensities were measured with an RCA photomultiplier tube (type 7326), which

was polarized at -1000 V by a Keithley 246 high voltage supply. The polymer coated Pt working electrode was cycled in the respective potential range at 100 mV s⁻¹. The range of potential used in the sequential potential step experiment to generate the ECL was determined from the oxidation and reduction peaks in the cyclic voltammetry, which was recorded using Volta Lab 4.

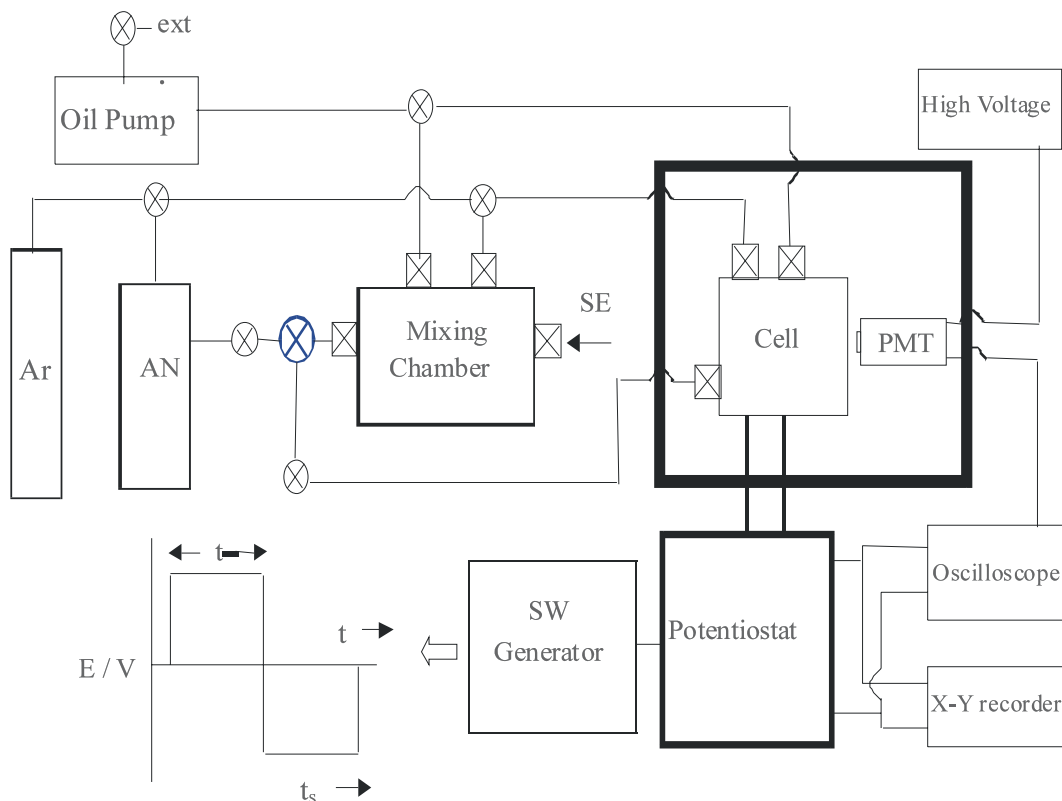


Fig. 2.2a: Scheme of the setup for the ECL experiment.

2.3. Optical methods

2.3.1. Absorbance and fluorescence spectroscopy

Every elementary system, whether nucleus, atom, or molecule has a number of discrete, quantized energy states. When an electromagnetic radiation of energy equivalent to one of the quantized energy levels of a substance is applied, there is interaction between the two, leading to absorption of the incident radiation. It can be schematically denoted for a substance X as



where X^* is the excited state of the substance. The term $h\nu$ is the energy of the incident radiation. It is related to the energy level of the substance X by the Bohr equation,

$$h\nu = E_f - E_i. \quad (2.3.1b)$$

Here h is the Planck's constant, ν is the frequency of the incident radiation, E_f and E_i are the energies of the final (excited state X^*) and initial (ground state X) states of the substance. The measurement of the intensity of the absorbed light against energy, the absorption spectrum, yields clues about the nature of the excited bond.

The average lifetime of an undisturbed excited atom or molecule X^* is estimated to be on the order of 10^{-8} s or shorter than that. The excited state therefore dissipates the excess energy in some form and returns to the ground state. If the mode of relaxation is by emission of radiation, then it is called fluorescence or phosphorescence depending on the spin of the electron in the excited state configuration of the system X .



In fluorescence, the delay between absorption and reemission is only about 10^{-4} to 10^{-8} s, while for phosphorescence it ranges from 10^{-4} to 10 s or more. Hence, fluorescence appears as instantaneous. Further, the emission occurs at longer wavelengths than the absorbed radiation. This is because part of the incident radiation is lost through other modes of deactivation, e.g., dissipation to vibrational, rotational levels leading to heating up of the substance, intersystem crossing, etc.. The plot of energy versus emission intensity yields the fluorescence spectrum, which is again a tool to investigate the nature of the excited bond.

The processes taking place in a substance upon application of an electromagnetic radiation can be understood from the following schematic picture.

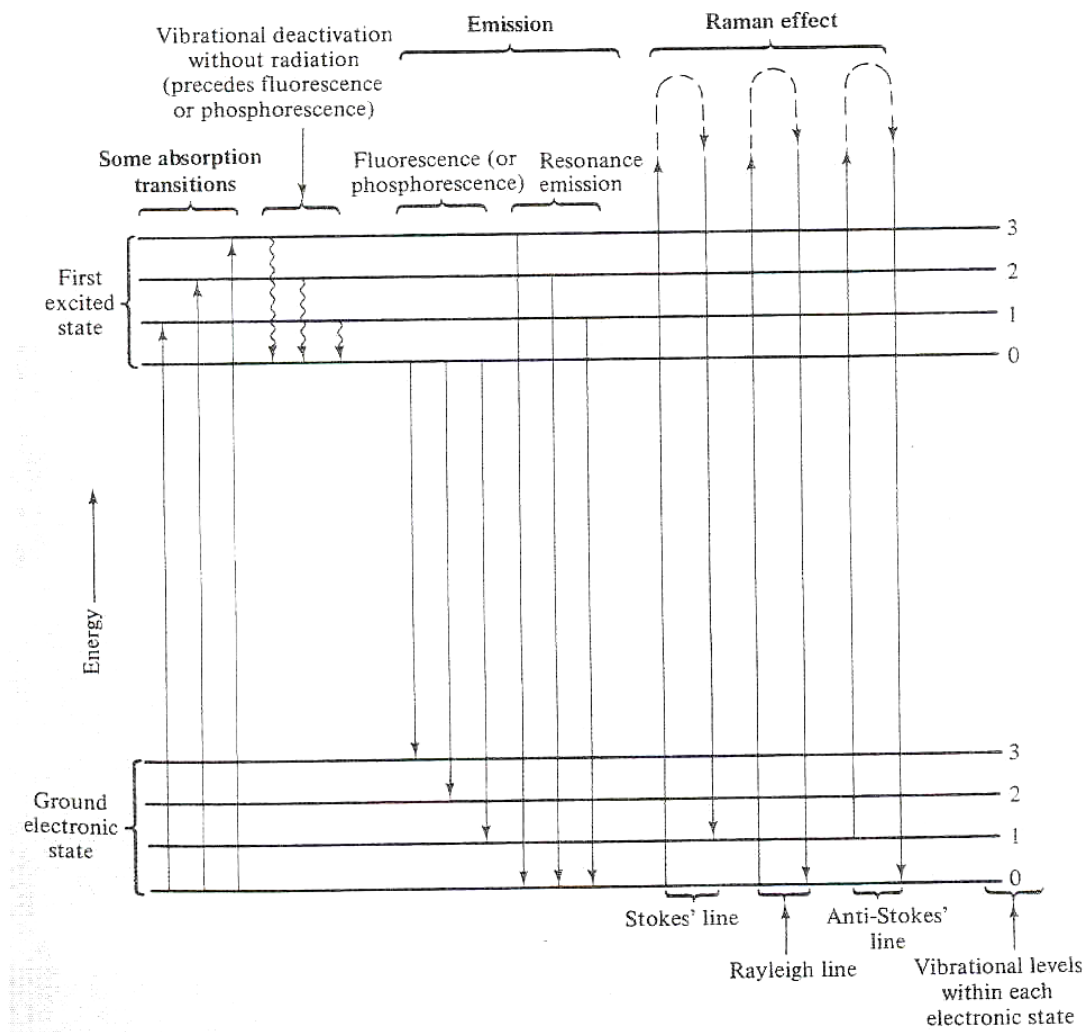


Fig. 2.3.1a: Scheme of the interaction of radiation with energy levels of a substance.

The absorbance and fluorescence measurements were made with a dilute CHCl_3 solution by using a blue laser, with the solvent CHCl_3 as the blank. The absorbance measurement was made with Unicam UV/Vis spectrometer UV4, and the fluorescence was done with Aminco. Bowman® series 2 Luminescence spectrometer.

2.3.2. Raman spectroscopy

In Raman spectroscopy, when molecules are irradiated with monochromatic light, a portion of the light is scattered; most of this scattered radiation (about 99 %) has the original frequency (Rayleigh scattering), but a small portion (<1 %) is found at other frequencies. The difference in frequency between these new frequencies (Raman lines or bands) and the original frequency is characteristic

of the molecule irradiated and numerically identical with some of the vibrational and rotational frequencies of that molecule.

The cause of this phenomenon is that, in Raman spectroscopy, the molecules are also vibrationally and rotationally excited to a higher level. The energy of the incident radiation is not just equivalent to the electronic excitation energy, as with the case of molecular emission and absorption spectroscopy. This causes polarization of the bonds of the molecule. If the polarized bond resonates with the incident light, it emits radiation of the same frequency, called Rayleigh scattering. If emission occurs at a lower frequency, it is called Stoke's line, and that occurring at higher frequency than the exciting radiation is called anti-Stokes line. Stoke's lines are generally accounted since they are more intense than the anti-Stokes lines while providing the same information about the molecule. The plot of the emission intensity versus energy in wave numbers, yields clues about the nature of excited bonds [54].

For a particular mode of vibration to appear in the Raman spectrum, i.e., to be Raman-active, the molecule's polarizability must change during the course of this vibration. The polarizability of a molecule is the ability of the molecule to be polarized under the action of an electric field such as the alternating field of a light wave, and it can be defined in terms of the dipole moment μ produced by the electric field, E:

$$\mu = \alpha E, \quad (2.3.2 \text{ a})$$

where α is the polarizability. The polarizability is thus a measure of the efficiency with which a varying electric field will induce a dipole moment in a molecule.

In measuring the Raman effect, visible light is almost always used as the incident radiation. Usually the 435.8 nm line from a mercury arc or the 632.8 nm line from a helium-neon laser is used. Ultraviolet light could be used, but it is not as widely applicable, not only because it is absorbed by many substances, but also because it may cause molecular dissociation and fluorescence.

Under the influence of visible (or ultraviolet) incident light, only electrons (not nuclei) oscillate, since nuclei cannot follow the rapid oscillations. Thus,

polarizability measures the ease of displacement of electrons by the electric field.

This spectroscopy has several advantages: Samples can be handled freely in any forms, solids, liquids or gases. Simple glass cells are sufficient for holding the sample. In addition, one instrument and a single continuous scan can be used to cover the entire range of molecular vibration frequencies.

Raman spectroscopic measurements were done with the solid polymer film on the electrode being subjected to red laser. The polymer coated electrode surface was analyzed before and after the ECL experiment ex-situ. The analyses were also made before and after cross-linking the polymer.

2.3.3. Photomultiplier Tubes

The ECL transients were recorded with the help of the photomultiplier tubes. Photomultiplier tubes are extremely sensitive, fast-responding types of vacuum phototube, designed so that an amplification of several million folds is achieved within one tube by the emission of secondary electrons. Radiation striking a photocathode causes the ejection of primary electrons, as in an ordinary vacuum phototube. In photomultiplier tube, these electrons are accelerated by a positive potential to a second sensitive surface, where each electron striking it causes the release of four to five secondary electrons. These electrons in turn are accelerated to another sensitive surface, where the number of electrons is again increased by a factor of 4 or 5. This practice can be repeated as many times as desired, though most commercial photomultipliers have about 10 target electrodes, or dynodes. The following figure schematically illustrates the cross section of the widely used circular-cage photomultiplier design.

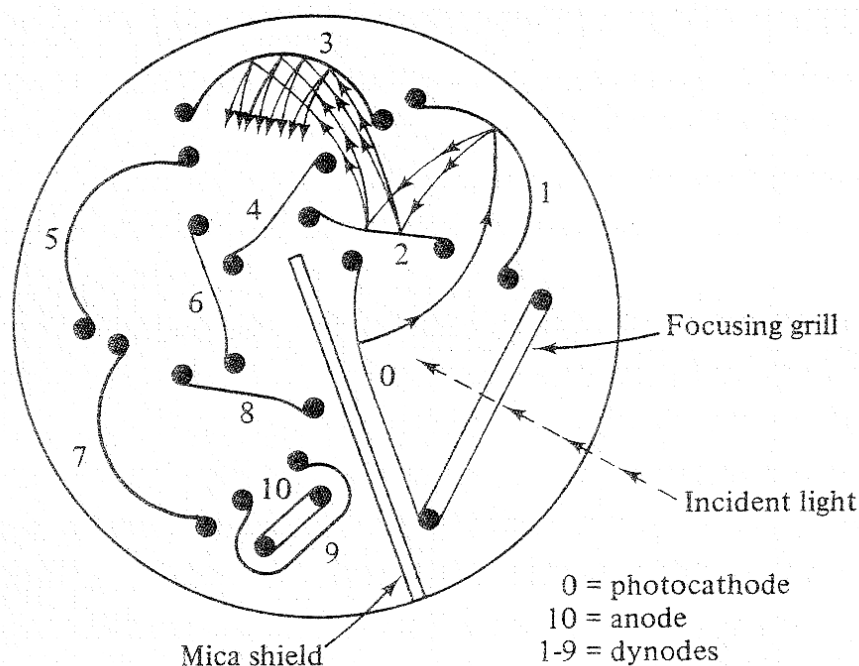


Fig. 2.3.3a: Cross section of a photomultiplier tube.

The amplification factors achieved depend critically on the voltage applied to each dynode, and a very stable high-voltage power supply is required. Typically, each dynode is made 75 to 100 V more positive than the preceding dynode, and overall amplification factors of about 10^6 are common. In addition, the output of the photomultiplier can be further amplified. The limit of detection is set by the inherent dark-current noise, which is due to thermionic emission and other random noise. The response time is extremely short, responding to light pulses as brief as 10^{-9} s. The output current is linearly dependent on illumination over a fairly wide range but becomes nonlinear at high levels of illumination.

2.4. Polymer cross-linking by synchrotron radiation

Synchrotron radiation is produced, when charged particles, such as electrons, travel close to the speed of light and are deflected by a magnet. As a result of the radial acceleration in the magnetic field (Lorentz force), the particles emit electromagnetic radiation. For a particle of mass m in circular motion with velocity $\beta = v/c$, energy E , and a radius of curvature ρ , the power (P) radiated by a single nonrelativistic accelerating particle with charge e (e.g., an electron) is given, following the Larmor formula as

$$P = 2.654 B E^3 I. \quad (2.4a)$$

The practical units are P in kW, E in GeV, ρ in meters, B in kiloGauss and I in amperes [55]. Thus, an intermediate energy storage ring with $E = 1$ GeV, $B = 10$ kG and $I = 0.5$ A would radiate 13.3 kW.

The secondary radiations are spread over a wide range of energy. By using grating or crystal monochromators, researchers can select any wavelength from the intense synchrotron radiation continuum. Thus, synchrotron radiation makes it possible for a research worker to select the wavelength most appropriate for the experiment, and also to scan the wavelength over a large range, because it provides five orders of magnitude more continuum vacuum ultraviolet (VUV) and X-ray radiations than the conventional sources such as X-ray tubes. It has several other properties that further add to its abilities as a research tool. These include an extremely broad spectral range (from infrared to X-rays), natural collimation, high polarization, pulsed time structure, high-vacuum environment, small source size, and high stability. Therefore it is preferred over many other radiation sources and has found varied application such as lithography, production of micro emulsions, chemical vapor deposition, and so on.

To stabilize a polymer in a solution and to decrease its dissolution, cross-linking of the side groups of the polymer is a known route. This cross-linking can be a chemical or radiation induced process. When a radiation of energy, higher than the energy of a particular bond, is applied to a molecule (or polymer), bond breaking results. This results in the production of a free radical at the site of a broken bond. As an example, if the polymer has a side group having C-H bond, then upon subjecting to a radiation of suitable wavelength, it breaks as



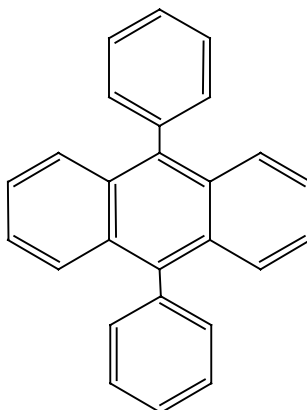
where C^{\bullet} and H^{\bullet} are the free radicals. Two C^{\bullet} radicals, of different bonds, can react with each other forming a C-C bond. Thus, the reaction between the free radicals leads to cross linking between the chains. This decreases the solubility of an otherwise slightly soluble polymer. The cross linked polymer will pose hindrance to the movement of ions, which is one adverse effect of this procedure.

The polymer-coated surface of the electrodes were mounted on a special aluminum holder and subjected to synchrotron radiation from the white beam line for lithography, of BESSY-II, Berlin, Germany. The energy range of the beam line is 1.5 - 6 keV, and the strength of the magnetic field is 0.4 T. A beryllium window (200 μm) and a graphite window (160 μm) were used. The dosage was varied from 100-500 mJ/cm^2 , corresponding to the dosage levels 19.4645 mA min/cm to 97.3225 mA min/cm.

3. The Electrochemiluminescence Experiments

3.1. Solution phase ECL: DPA

The model compound in the electrogenerated chemiluminescence experiments is 9,10-diphenylanthracene, abbreviated as DPA. Due to the consistency and the simplicity in the nature of the electrochemiluminescence process in DPA, it has been used as the compound for the standardization of the experimental conditions [56] It is chemically denoted as follows:



9,10 - diphenylanthracene (DPA).

3.1.1. Experimental details

The Pt substrate was polished with 0.7 μm diamond paste and the surface was checked for uniformity with a Nikon PFX 104 optical microscope. Electrochemical experiments were carried out in a three-electrode configuration with Pt disc as the working electrode (WE) and Pt wires as quasi-reference (QRE) and counter electrodes. Anhydrous CH_3CN (Aldrich No. 27,100-4) was used as the solvent. DPA corresponding to the concentration 1 mM, tetrabutylammonium perchlorate (TBAClO_4) or tetraethylammonium perchlorate (TEAClO_4) corresponding to 0.1 M in concentration were taken in the evacuated mixing chamber. The mixture was continuously heated while evacuating the container. (The supporting electrolyte and DPA were also dried in the oven for 12 hours to remove traces of water present in them prior to transferring them to the mixing vessel). Acetonitrile was pumped in to make the solution of the DPA and the supporting electrolyte. The solution was bubbled with argon (Ar) to chase out the traces of oxygen and was heated frequently to accelerate the

solubility of DPA in acetonitrile. It was then transferred to the electrochemical cell in-situ. Electrochemical measurements were accomplished with a homemade potentiostat. Potential pulses were applied by a Agilent 33250 A function generator via the potentiostat. ECL emission intensities were measured with an RCA photo multiplier tube (type number 7326), which was polarized at -700 V by a Keithley 246 high voltage supply. The Pt working electrode was cycled in the potential range from -2.1 V to +1.6 V vs. Pt (QRE) at a scan rate of 100 mV s^{-1} . The range of potential used in the sequential potential step experiment to generate the ECL was determined from the oxidation and reduction peaks in the cyclic voltammetry.

3.1.2. Cyclic voltammetry

The cyclic voltammogram has the same features for both TEAClO_4 and TBAClO_4 . The potentials for the oxidation and reduction of the polymer in the ECL experiment were determined from the E° value from the cyclic voltammogram.

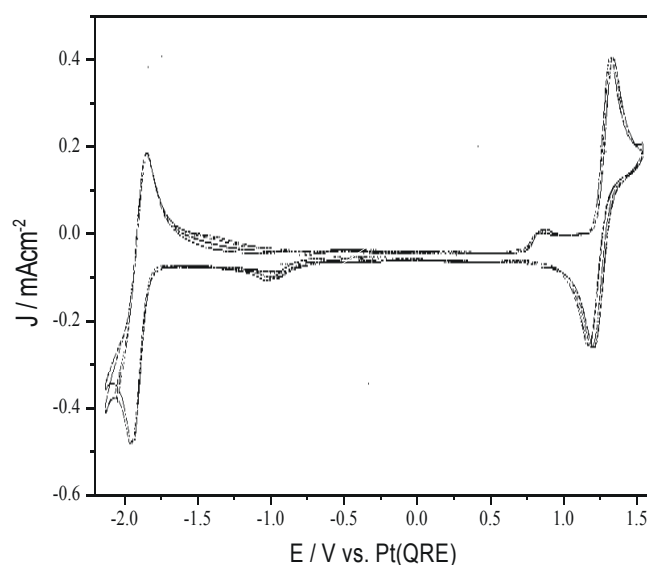


Fig. 3.1.2a: Cyclic voltammogram (CV) of Pt in 1mM DPA + 0.1M TBAClO_4 in acetonitrile at a scan rate of 100 mV/s .

3.1.3. Current transients

Current transients are obtained from the potential step experiments. Under the

conditions of potential step experiments, initially the charging of the electrode/solution interface takes place for a duration depending on the time constant τ (see section 2.1.2.ii and 2.1.2.iii) followed by the electron transfer reaction. The parameters determining the time constant, the resistance of the electrolytic solution (R_u) and the double layer capacitance C_{dl} were evaluated first by a separate experiment where the potential step was made to a lower magnitude, thereby avoiding the electron transfer reaction at the electrode. In the case of DPA, the potential steps were made from 0 V to 0.5 V or - 1 V of duration 50 ms. From the decay characteristics of the corresponding current transients, the uncompensated solution resistance R_u and the double layer capacitance were calculated. For the cathodic transient they were 71 Ω , 1.99 μF and for the anodic transient 148 Ω , 0.9 μF respectively. The values of the resistance and capacitance were averaged out to be 109.5 Ω and 1.5 μF , respectively. The area of the electrode is 0.07065 cm^2 .

Then the rate parameters of diffusion were calculated by making potential steps of higher magnitudes past the standard potentials for oxidation/reduction. These lead to the production of radical cations or radical anions depending on whether it is a negative or a positive potential step. The current flow after capacitive charging of the electrode in this case is controlled by the diffusion of the radical ions which is described by the Cottrell equation (Eq. (2.1.2b)) The diffusion coefficient was evaluated to be $5 \times 10^{-6} \text{ cm}^2 \text{ s}^{-1}$ from the slope of the diffusion current (i) vs. the inverse square root of time ($t^{-1/2}$).

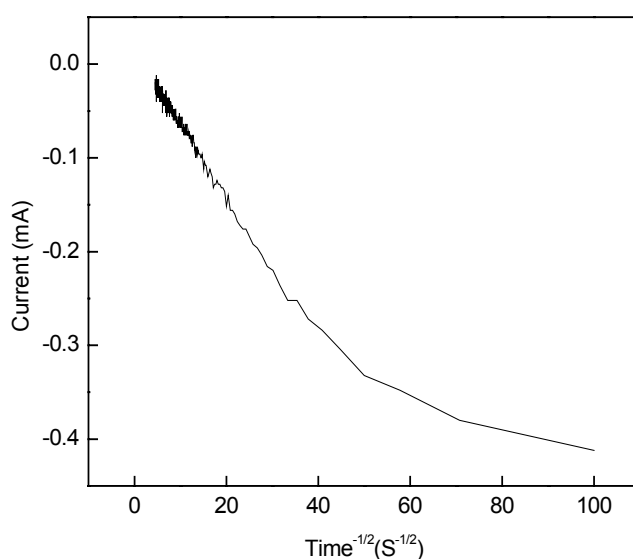


Fig. 3.1.3a: Cottrell plot for 1 mM DPA in 0.1 M TBAClO₄-AN when the potential step was made from 0 V to -1.95 V of duration 50 ms.

3.1.4. The ECL experiment

As explained in the introduction, the ECL was produced in the third step of the triple potential step experiment. The typical form of the triple potential step is shown below:

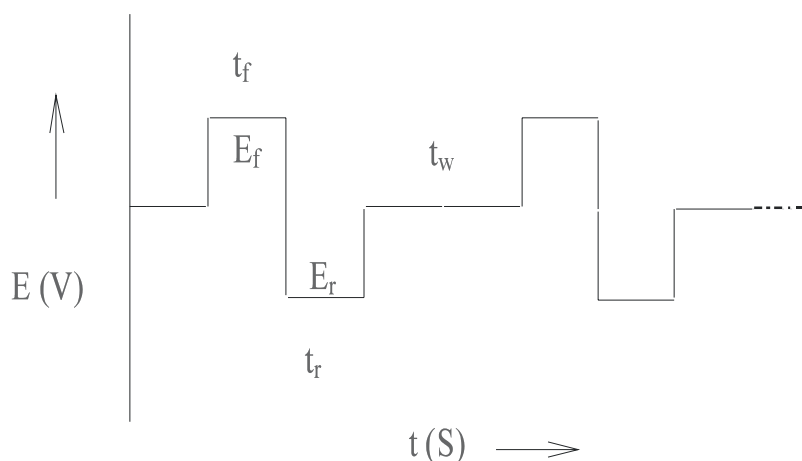


Fig. 3.1.4a: Scheme of the sequential anodic and cathodic potential steps in ECL experiments.

In this case we expect cathodic ECL. The potential step can also be reversed to produce anodic ECL. The ECL experiments were done with 1 mM DPA in 0.1 M TBAClO₄ in acetonitrile. The emission intensity increased when the magnitude of the potential step was raised due to the increased rate of formation of the reactant.

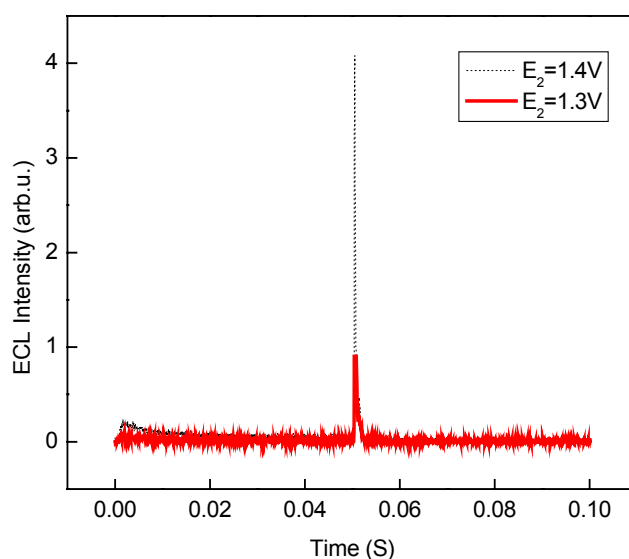


Fig. 3.1.4b: The potential step from E_f to E_r was made from -1.9 V (E_f) to a positive (E_r) value given in the inset. $t_f, t_r = 0.05$ s and $t_w = 0.2$ s.

The mechanism of ECL generation should be the same, irrespective of the potential step sequence. Contrary to the expectation, the intensity and the kinetics of the anodic and cathodic ECL are found to be different. Several researchers have tried to reason out the difference. In DPA, it has been reported in the literature that the intensity of the anodic ECL is more pronounced than the cathodic ECL. However, the occurrence of cathodic ECL is more consistent than the anodic ECL. The various reasons proposed for the occurrence of non-symmetrical ECL in DPA are as follows:

(1) The difference in the life times of the radical ions. It was analyzed with electron spin resonance (ESR) spectroscopic studies. The DPA radical cations and anions were turned out to be almost of equal stability. The half-lives of the radical cations are 0.5 min and radical anions are 1min [57].

(2) Different possibilities are there for the formation of the excited states. There are two major routes – the singlet route (S route) and the triplet route (T route).

In the singlet route the annihilation between radical cation and anion results directly in the production of the singlet-excited state, whereas in the T route first a triplet-excited state is formed. Two formed triplets undergo mutual annihilation resulting finally in the singlet-excited state. Due to the paramagnetic spin of the triplet-excited state, its resultant magnetic field can interact with an external magnetic field. Some experiments were done in this direction. Since there were no appreciable effects, it was concluded that it forms the excited state predominantly by the singlet route [58 and references therein]. Also the efficiency of the DPA ECL agrees with that expected for an energy sufficient system [51 and references therein]. The S route is reported to be predominant under the conditions of cathodic ECL than that of anodic ECL in DMF solvent [59]. The major criteria set for the S route behavior are (i) the congruence of transients generated by the two possible reactant generation sequences and (ii) an ability to linearize the transients with the inverse square root of time [60, 61]. Although discrepancies were reported [62, 63], the absence of any effect on the DPA ECL by a magnetic field suggests that DPA follows the S route for the generation of the excited state.

(3) Ionic association of the radical ions with the counter ions from the supporting electrolyte could lead to slow diffusion of one of the ions. This could also result

in the non-symmetry of the ECL process. To analyze this feature, the ECL experiments were performed with different supporting electrolytes such as TBABF₄, TBACF₃SO₃ and TBAP. It was found that the maxima of the intensity as well as the time taken for its decay to zero for anodic ECL were roughly twice than for the cathodic ECL, in the former two supporting electrolytes. In TBAP, the cathodic ECL was nearly invisible in comparison to the anodic ECL. In addition, the anodic ECL showed a delay for the onset of the luminescence and decayed fast to zero. The results with the perchlorate were interpreted by assuming the ion pair formation between the radical cations and the perchlorate, with the rate constant on the order of 0.1 ms. However, there are several unsolved questions: How would a stable ionic association exist in acetonitrile which does not promote ion pair formation. Also pre-treatment procedures of the electrode have made changes in the ECL transients, which could not be explained based on the concept of ion association. It is also peculiar that perchlorate alone shows such an ion-pairing effect [64].

(4) The other possibility could be the adsorption of some species on the electrode other than the precursor molecule DPA, changing the kinetics of the electrochemiluminescence reaction. In fact, this had already been speculated and some analyses were made in this direction. The electrode material was changed to gold and glassy carbon. However, the responses were not reliable for analyzing this phenomenon. There were some electrochemical pre-treatments followed earlier, as, e.g., by changing the direction of the potential cycling prior the ECL reaction and polarizing the electrode at 1.3 V. The former could not be taken as a favorable pre-treatment procedure as the results were complicated [64]. In the latter process the potential of the Quasi Reference Electrode shifts due to the application of such a high voltage to the working electrode [65].

In earlier experiments, either a continuous rectangular AC voltage [66] or continuous potential pulses of unequal widths, i.e., t_f is not equal to t_r , were applied. Unequal pulse widths were preferred to verify the linearity between the current transient with an inverse square root of t_r (or t_f). This would result in the unequal concentration distribution of radical cations and anions, which would complicate the comparison of the ECL intensities. Hence, in this present study, the property of non-symmetrical ECL has been analyzed by varying the potential step width, magnitude, sequence and duration between the potential

steps. The electrolyte was chosen to be TBAP–acetonitrile, since this was reported to be the controversial system in the literature. Also the durations t_r and t_f were chosen to be the same, to provide similar conditions for the generation and distribution of radical cations and anions.

Under the conditions of normal potential steps ($E_+ = E^{+/0} + 250$ mV, $E_- = E^{0/-} - 250$ mV), of duration 5–10 ms when applied continuously, only cathodic ECL of low intensity was observed (Fig. 3.1.4c). ECL could not be observed on reversing the potential step. When the waiting period (t_w) between the successive double potential steps was increased, the intensity of the cathodic ECL also increased (Fig. 3.1.4d).

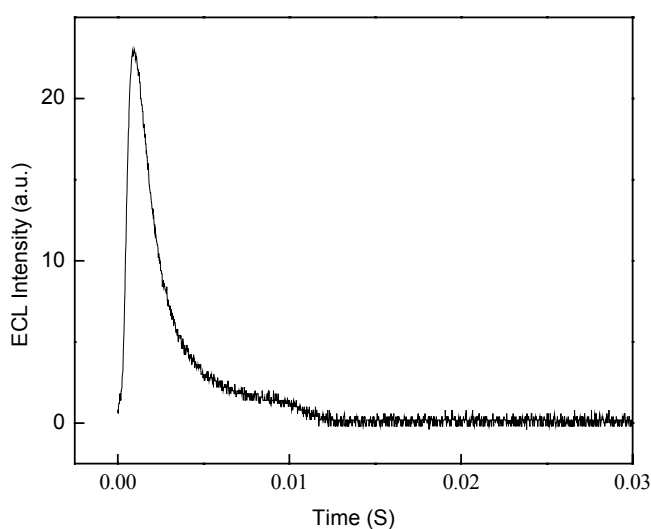


Fig. 3.1.4c: The potential step was made from 1.55 V (E_f) to - 2.05 V (E_r). t_f , t_r = 0.01 s and t_w = **0.02 s**. No ECL was observed when reversing the potential step.

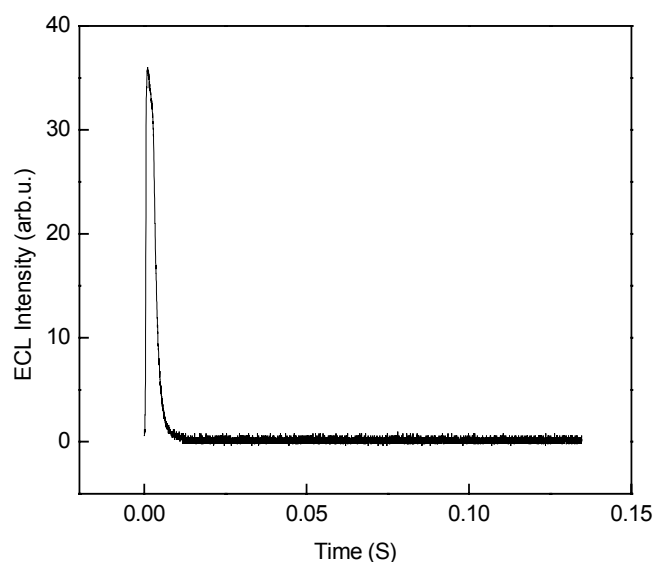


Fig. 3.1.4d: The potential step was made from 1.55 V (E_f) to -2.05 V (E_r).
 t_f , t_r = 0.01 s and t_w = **0.28 s**.

On increasing the potential step width to 50 ms (t_f and t_r), the ECL intensity increased and anodic ECL was also observed. Unlike the cathodic ECL, the anodic ECL was independent of the waiting period (t_w), which is shown in Figs. 3.1.4e and 3.1.4f.

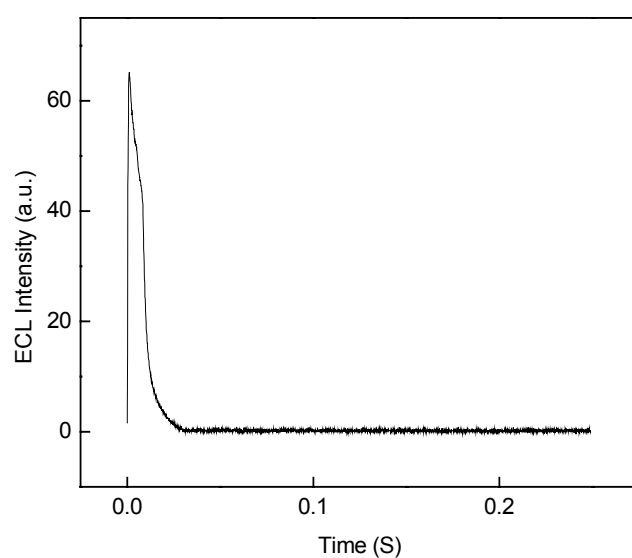


Fig. 3.1.4e: The potential step was made from - 2.1 V (E_f) to 1.6 V (E_r).
 t_f , t_r = 0.05 s and t_w = **0.20 s**.

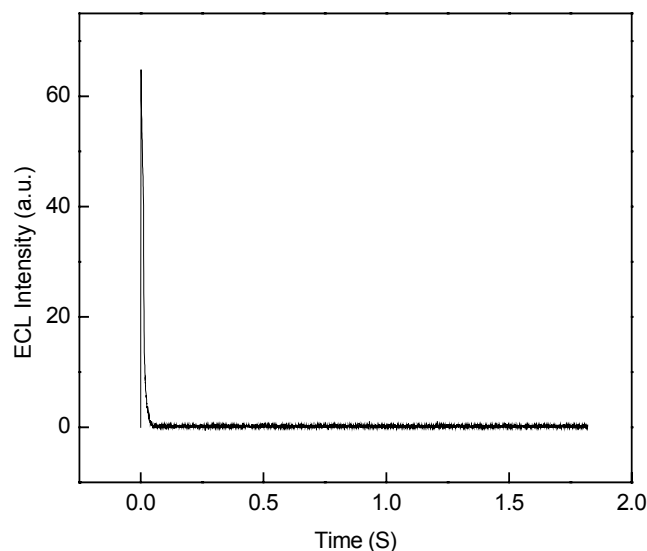


Fig. 3.1.4f: The potential step was made from - 2.1 V (E_f) to 1.6 V (E_r). t_f , t_r = 0.05 s and t_w = **1.80 s**.

Further on, at t_f and t_r = 50 ms, cathodic and anodic ECLs occurred with equal intensities under the appropriate magnitudes of the oxidation and reduction potentials. These results are contradicting the ones reported earlier which stated that no cathodic ECL was observed with TBAP. And also in the case of ECL experiments with another supporting electrolyte it was reported that the anodic ECL and cathodic ECL were of different intensities, the anodic being more intense than the cathodic.

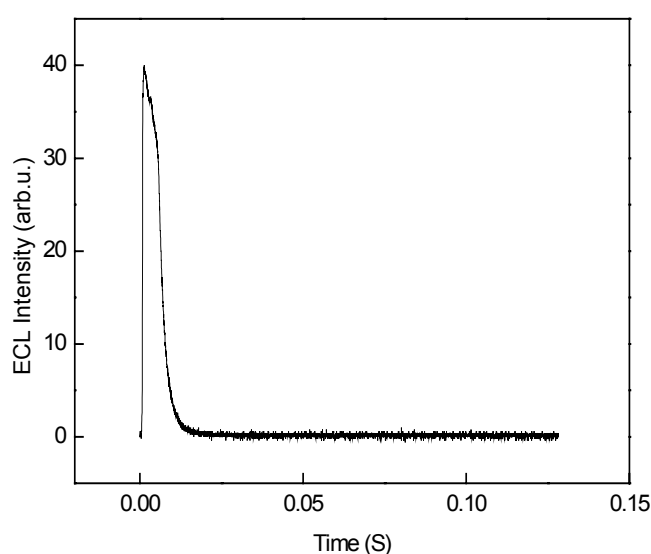


Fig. 3.1.4g: Anodic ECL when the potential step was made from - 2.05 V (E_f) to 1.6 V (E_r). t_f , t_r = 0.05 s and t_w = 0.24 s.

Thus, the observation of equal intensities of anodic and cathodic ECLs in the TBAP-acetonitrile at a specific time scale in our experiments is a new result to be considered.

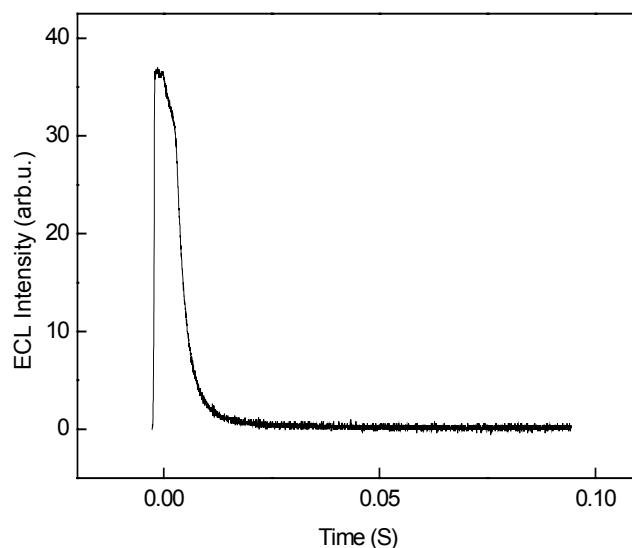


Fig. 3.1.4h: Cathodic ECL under the similar condition as in Fig. 3.1.4g; potential step was from 1.6 V (E_f) to - 2.05 V (E_r). t_f , t_r = 0.05 s and t_w = 0.24 s.

Equal intensities of anodic and cathodic ECLs could be observed under the same conditions as above with only changing the cation of the supporting electrolyte, to TEAClO_4 .

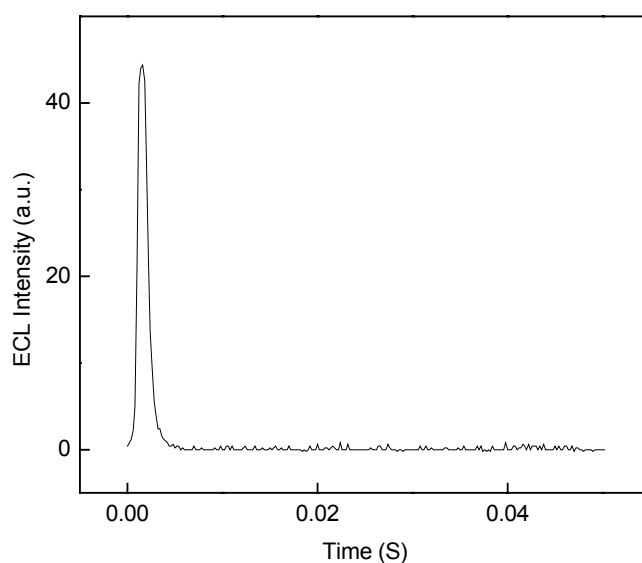


Fig. 3.1.4i: Anodic ECL for potential step from - 2.05 V (E_f) to 1.5 V (E_r).

$t_f, t_r = 0.05$ s and $t_w = 0.24$ s.

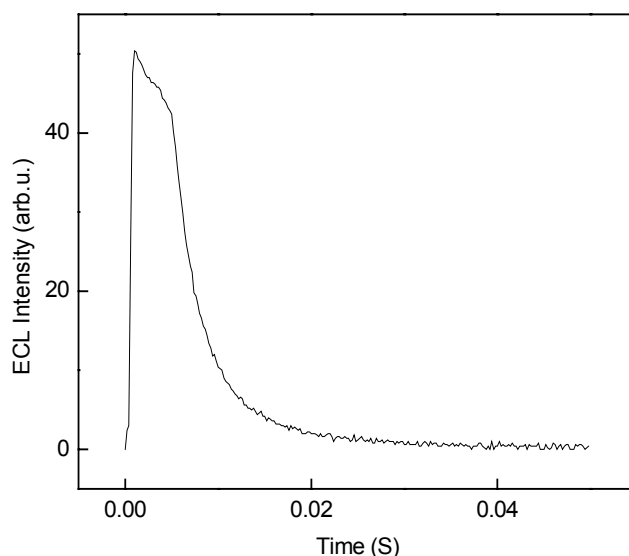


Fig. 3.1.4j: Cathodic ECL under the similar condition as in Fig. 3.1.4g; potential step was from 1.5 V (E_f) to - 2.05 V (E_r). $t_f, t_r = 0.05$ s and $t_w = 0.24$ s.

These results show that polarizing the electrode at 0 V during the period $t_w = 240$ ms causes an increase in the ECL intensity. This could be due to the stripping off some electro inactive species from the electrode surface. The adsorption of this species should have occurred during the negative potential step, since only cathodic ECL shows variation with the increase in t_w .

In an earlier publication, it was found that the addition of cyclohexanone in small concentration [0.05 M] makes the DPA anodic and cathodic ECLs to be almost similar in the cases of TBACF₃SO₃ or TBABF₄ as the supporting electrolytes [65]. The hydrogen absorbed in platinum electrodes can be reduced to hydride in non-aqueous media when a sufficiently negative potential is applied. The hydride is very reactive and reacts with solvents to produce various products near the electrode surface [67]. At low temperatures ideal electrochemical behavior was observed in non-aqueous solvents, since the diffusion of hydrogen in Pt is sharply reduced as a consequence of its relatively high activation energy [68]. Cyclohexanone can react fast with hydride to produce its alkoxide, thus scavenging the hydride away. Thus, its addition improved the intensity and the decay of the cathodic ECL, where hydride could easily react

with the DPA radical ions. This is in accordance with the present observation and thus, the effect of polarization of the Pt electrode at 0 V was interpreted as a method of removing adsorbed hydrogen and thereby its interference with ECL.

3.1.5. The ECL Emission spectrum

The ECL was caused by the annihilation reaction (4.1.1c) between the radical cations and the radical anions of DPA [69 and 70]. Further evidence for the cause of electron transfer between the radical cation and anion for the generation of the excited state was provided by the effect of ionic strengths of the solvents [71] and the temperature effect [72] on the ECL. The free energy of the pair of radical ions compared with that of the ground state DPA pair was estimated to be 3.06 eV on the basis of the cyclic voltammogram in acetonitrile. The free energy of $^1R^* + R$ was calculated from the 0-0 transition energy in the fluorescence spectrum as 3.0 eV. The solvation energy was estimated as 0.4 eV based on the values for similar compounds in acetonitrile [73]. Thus, the formation of the singlet-excited state is in the 'normal region' ($-\Delta G^\circ < \lambda$) of electron transfer reactions.

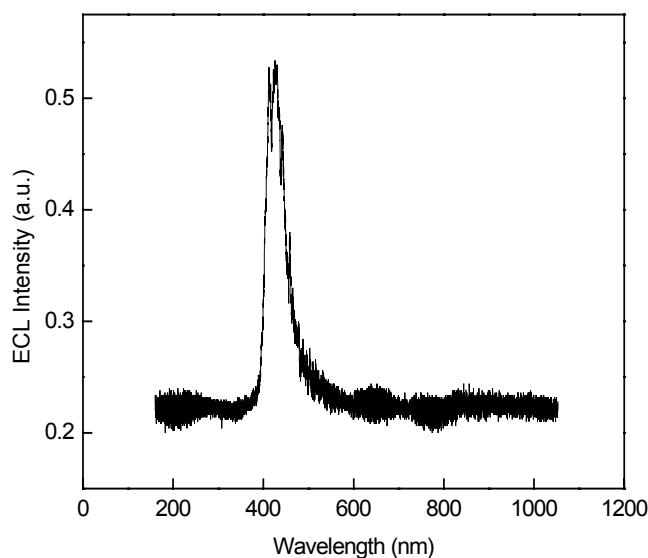


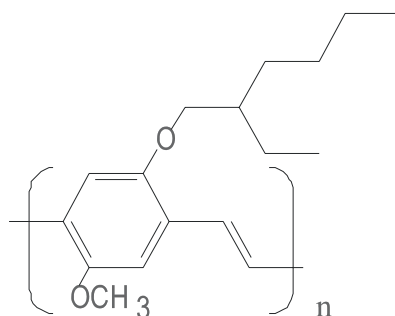
Fig. 3.1.5a: ECL emission spectrum of DPA.

The experimental verification to find out the nature of the excited state is the ECL emission spectrum. The spectra of anodic and cathodic ECLs were taken by manipulating the waiting period (t_w) to produce one kind of ECL at a time.

The conditions of the potential steps were corresponding to that for the observation of equal intensities for anodic and cathodic ECLs. The spectra of both were found to be identical with the emission maximum at 427 nm (≈ 2.91 eV) confirming that the emission was from the singlet excited state (Fig. 3.1.5a). The singlet excited state can also be generated by a triplet-triplet annihilation reaction, which can be analyzed by the effect of the magnetic field as discussed in the previous section.

3.2. Polymer phase ECL: MEH-PPV

The electrogenerated chemiluminescence (ECL) from a conducting polymer (CP) poly(2ethylhexyloxy 5 methoxy 1,4 phenylenevinylene), abbreviated MEH-PPV, was studied. The ECL experiment was carried out with the system configuration as electrode/polymer/solution. The effect of the supporting electrolyte on the ECL was examined.



poly(2-ethylhexyloxy-5-methoxy-1,4-phenylenevinylene) (MEH-PPV).

3.2.1. Experimental details

The polymer MEH-PPV was coated on the Pt electrode (with a surface area of approximately 0.09 cm^2) by evaporating a solution of the polymer in CHCl_3 in the dark. The Pt substrate was polished with $0.7 \text{ }\mu\text{m}$ diamond paste, and the surface was checked for uniformity with a Nikon PFX 104 optical microscope before and after the deposition of the polymer. Electrochemical experiments were carried out in a three-electrode configuration with the polymer coated Pt as the working electrode (WE) and Pt wires as quasi-reference (QRE) and counter electrodes. Anhydrous CH_3CN (Aldrich 27,100–4) was used as the solvent and 0.1 M tetraethylammonium hexafluorophosphate (TEAPF_6),

tetraethylammonium tetrafluoroborate (TEABF₄) or tetrabutylammonium tetrafluoroborate (TBABF₄) were used as the supporting electrolytes. The preparation of the electrolytic solution was done in dried Ar atmosphere following the procedure utilized by Orlik et al. [53], which was described in detail in section 2.2. Electrochemical measurements were accomplished with a homemade potentiostat. Potential pulses were applied by an Agilent 33250 A function generator via the potentiostat. ECL emission intensities were measured with an RCA photo multiplier tube (type number 7326), which was polarized at –1200 V by a Keithley 246 high voltage supply. The polymer coated Pt working electrode was cycled in the potential range from –1.9 V to +1.5 V vs. Pt (QRE) at 100 mV s^{–1}. The range of potential used in the sequential potential step experiment to generate the ECL was determined from the oxidation and reduction peaks in the cyclic voltammetry.

3.2.2. Cyclic voltammogram

The cyclic voltammograms were reproducible, when TEABF₄ or TEAPF₆ were used as the supporting electrolytes.

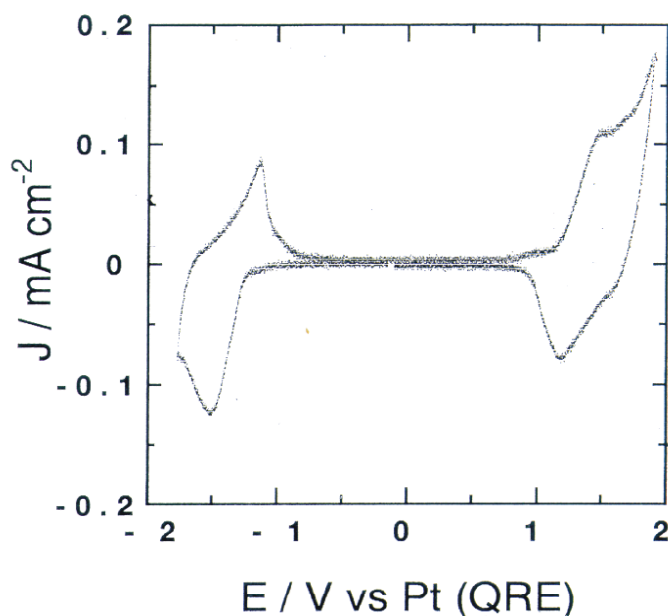


Fig. 3.2.2a: Cyclic voltammogram (CV) of Pt/MEH-PPV in 0.1M TEABF₄ in acetonitrile at a scan rate of 100 mV/s.

The ratio of the current peaks in the anodic and cathodic cycles (0.64 and 0.74,

respectively) shows that the kinetics of the oxidation and reduction of the MEH-PPV polymer is not strictly reversible but nevertheless quasi-reversible. Thus, similar to the case of the solution phase ECL process with DPA (chapter 3.1), the first requirement, the co-generation of positive and negative polarons, for the production of ECL is fulfilled with this polymer. Also the CV was devoid of any intervening peaks.

However, when the supporting electrolyte was changed from TEABF_4 to TBABF_4 , which has a comparatively bigger tetrabutylammonium cation (TBA^+), the polymer could not be reduced. The reason is the resistance offered by the polymer to the movement of bulkier ions through it. When the polymer is becoming reduced, it needs an equivalent amount of positive charged ions from the supporting electrolyte to counter balance the negative charge. If the positive ions cannot move inside the polymer, it cannot accept electrons from the electrode. This concept is discussed in detail in chapter 4. The cyclic voltammogram looks as follows:

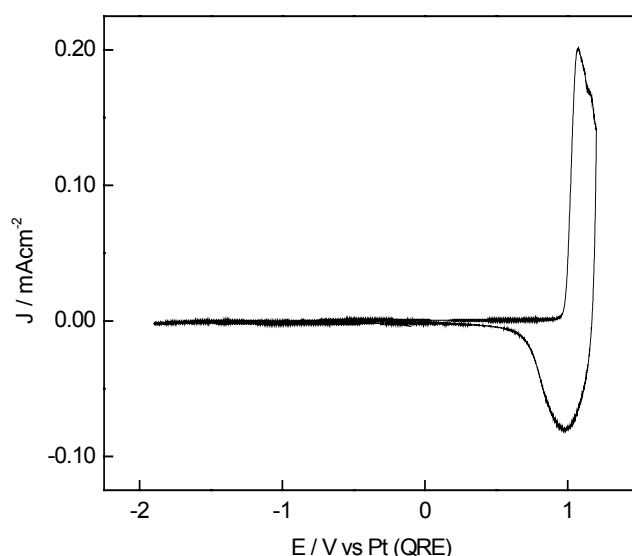


Fig. 3.2.2.b: Cyclic voltammogram (CV) of Pt/MEH-PPV in 0.1 M TBABF_4 in acetonitrile at a scan rate of 100 mV/s.

The MEH-PPV film used in Fig. 3.2.2a and Fig. 3.2.2b were of approximately the same thickness (1 μm). This shows how the size of the counterions, and hence the diffusivity of them, plays a major role in the electrochemistry of conducting polymers. Thus, the mechanism of charge transport in the polymer is different in the electrochemical environment than in the case of the solid-state electroluminescence process where such effects were not reported [74].

Some other conducting polymers were examined for ECL reaction. One is again a derivative of PPV, poly[bis(2,5-dimethyl-octylsilyl)-1,4-phenylenevinylene] (BDMOS PPV). The cyclic voltammetry showed irreversible oxidation of the polymer and no reduction at all. Thus, no ECL could be obtained from this CP, since feasible oxidation and reduction of the polymer are the foremost criteria for the generation of ECL.

Another polymer that was tried was poly(3-hexylthiophene) (PAT6). Upon oxidation the polymer was not intact on the Pt electrode. This caused instability in the cyclic voltammogram during oxidation, and no reduction could be observed. Even roughening of the electrode surface did not improve the adherence of the polymer with the electrode. These factors are the important ones in the selection of conducting polymers for ECL reaction.

3.2.3. Current transients

As with the case of DPA, the potential step was made to generate one kind of polarons. The current was linear with $t^{-1/2}$. The Cottrell equation (Eq. (2.1.2ib)) was used to evaluate the diffusion coefficient as $1 \times 10^{-13} \text{ cm}^2 \text{ s}^{-1}$ from the slope of the diffusion current (i) vs. the inverse square root of time ($t^{-1/2}$) plot.

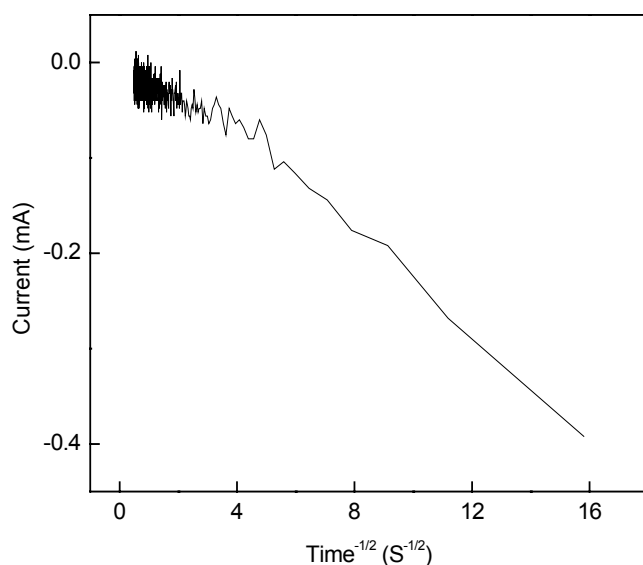


Fig. 3.2.3a: Cottrell plot for Pt/MEH-PPV in 0.1 M TEABF₄-AN, when the

potential step was made from 0 V to -1.9 V of duration 1 s.

3.2.4. The ECL experiment

As with the case of DPA, the magnitudes of positive and negative potential steps were chosen from the formal potentials calculated from the cyclic voltammogram. Using a square wave alternating between the potential for the oxidation and reduction of the polymer (or vice versa), positive and negative polarons (similar to the cationic and anionic radicals in DPA) were generated. These species combine to form the luminescent moiety. The anodic ECL was obtained, when the potential was switched from negative to positive value, which is commonly referred to as – to +; similarly, cathodic ECL is denoted as + to –. With the MEH-PPV polymer both, – to + as well as + to – were observed when TEABF₄ was used as the supporting electrolyte in the acetonitrile solvent. These are shown in the following figures:

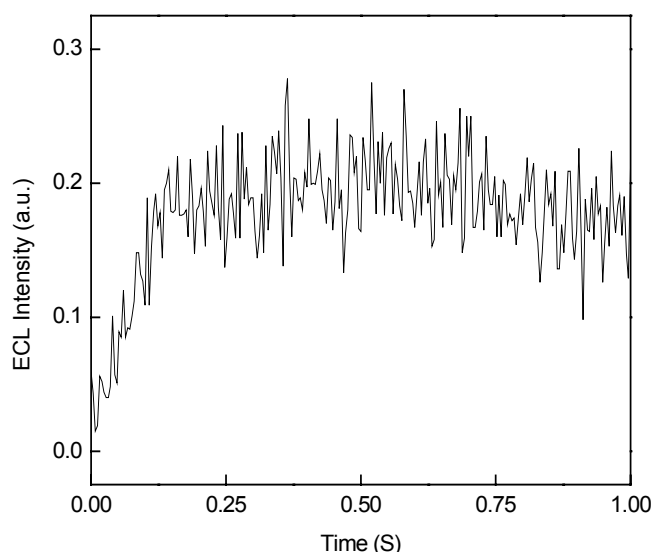


Fig. 3.2.4a: Anodic ECL when the potential was switched between –1.75 V and 1.45 V of duration 4 s each for MEH-PPV film on Pt in 0.1M TEABF₄–AN.

The ECL transient takes longer time for decaying (1 s) in the CP than the solution phase ECL with DPA (20 ms). This is due to the low transport coefficient in the conducting polymers ($\times 10^{-13} \text{ cm}^2 \text{ s}^{-1}$) compared to the diffusion

coefficient in the solution phase ($\times 10^{-6} \text{ cm}^2 \text{ s}^{-1}$). This slower kinetics is one important difference in the transport characteristics of the conducting polymers in comparison to that in the solution phase.

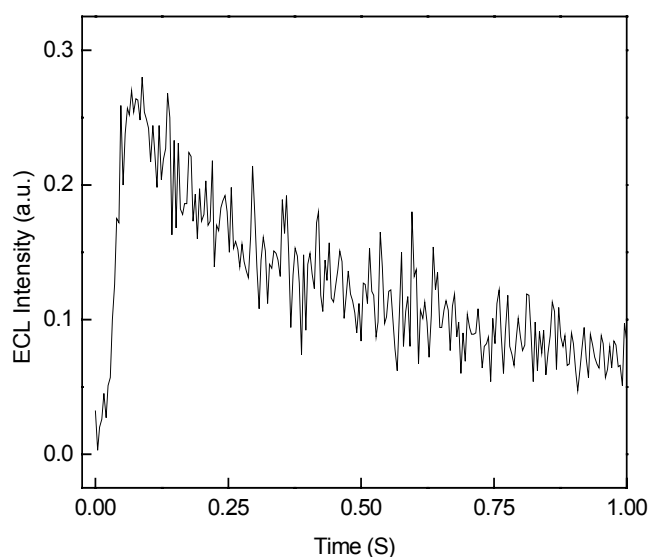


Fig. 3.2.4b: Cathodic ECL when the potential was switched between 1.45 V and -1.75 V of duration 4 s each for MEH-PPV film on Pt in 0.1 M TEABF₄-AN.

The anodic and cathodic ECLs shown in Fig. 3.2.4a and Fig. 3.2.4b have comparable intensities in the ECL experiments with MEH-PPV. The observation of ***symmetrical ECL*** is an important result of the present experiments with MEH-PPV, because in earlier experiments done with other polymers, such an observation had been difficult. This has to do with the relative stability of the positive and negative polarons [3]. In earlier studies, continuous pulsing between positive and negative potentials was done, without considering the stability aspect. As in the studies with DPA discussed in section 3.1.4, the widths of the potential steps and the waiting period were chosen to provide favorable conditions for the generation of positive and negative polarons. Also magnitudes of the potential steps were carefully chosen to prevent over oxidation/reduction of the polymer. Thus, it was possible to obtain **symmetrical ECL** in our experiments. However, the kinetics was found to be different between the anodic and cathodic ECLs as seen from differences in the onset and decay of the ECL transients. This needs to be analyzed.

The experiments were done by varying the anion; using 0.1M TEAPF₆ in acetonitrile. The ECL transients obtained are shown below:

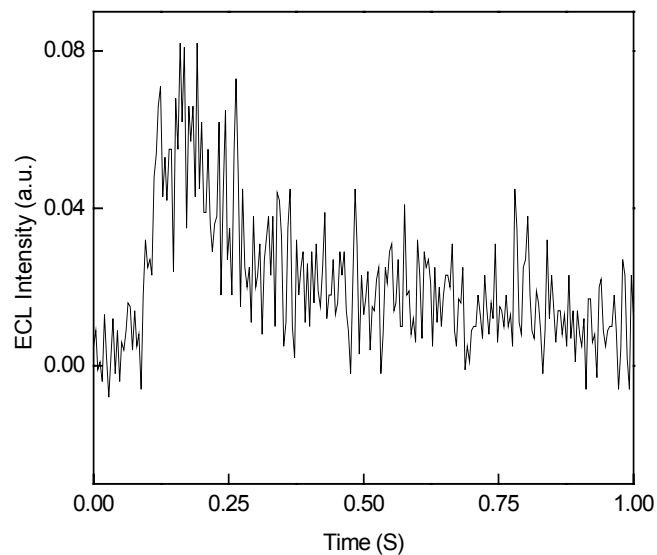


Fig. 3.2.4c: Anodic ECL, when the potential was switched between -1.85 V and 1.35 V of duration 1 s each for MEH-PPV film on Pt in 0.1 M TEAPF₆-AN.

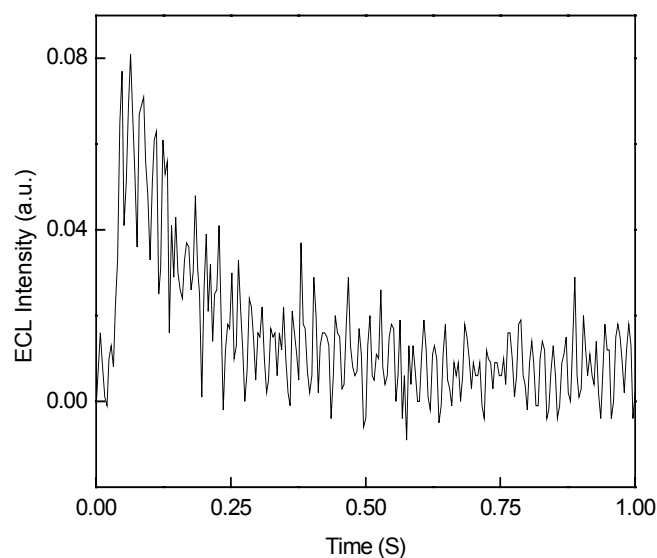


Fig 3.2.4d: Cathodic ECL, when the potential was switched between 1.35 V and -1.85 V of duration 1 s each for MEH-PPV film on Pt in 0.1 M TEAPF₆-AN.

Again the anodic (Fig. 3.2.4c) and the cathodic (Fig. 3.2.4d) ECLs are found to

have comparable intensities but differ in the kinetics. The anodic ECL has more delay (≈ 120 ms) than the cathodic ECL (≈ 50 ms) for the onset of ECL. The intensities of anodic and cathodic ECL with TEAPF_6 are lower than those obtained with TEABF_4 . This could be due to the difficulty in purifying the former. Comparing Fig. 3.2.4a and Fig. 3.2.4c, we find that the relatively larger anion PF_6^- causes more delay in the onset of ECL than the smaller one, BF_4^- . Further, one can find that even the cathodic ECL was suffering a larger delay in the presence of TEAPF_6 . This is because during the negative potential step at which cathodic ECL was observed, the charge compensation can be achieved by the movement of PF_6^- away from the polymer or the transport of the TEA^+ towards it. Thus, an increase in the size of the anion affects the cathodic ECL also, due to the coupling between the counter ion movements themselves.

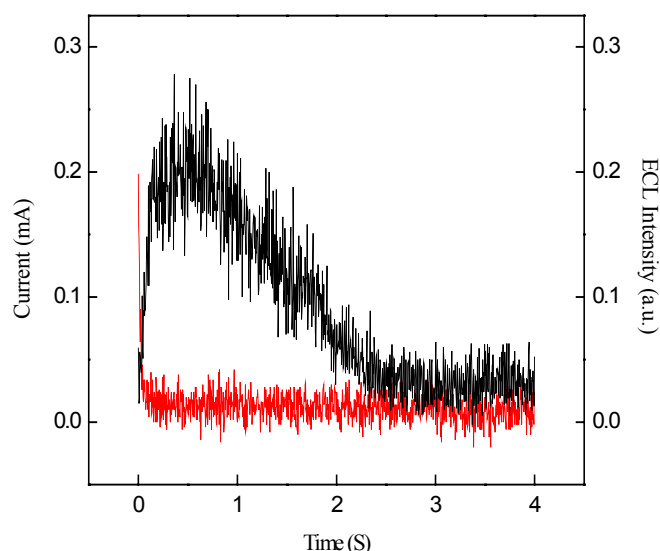


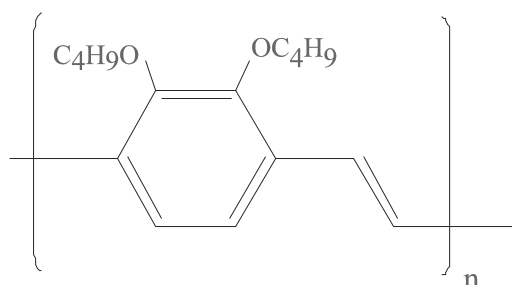
Fig. 3.2.4e: Comparison of anodic ECL and current decay for Pt/MEH-PPV in 0.1M TEABF_4 -AN.

When the anodic current and ECL transients were compared, the decay of current seems almost instantaneous compared to the decay of the ECL in the conducting polymer (MEH-PPV in the present case). This is due to the slow transport of charges in the CP and the slow reaction kinetics for the annihilation reaction between the polarons - both are the parameters describing the ECL transient. This can be compared with the decay of the current and luminescence intensity in the solid-state electroluminescence (EL) process of the CP, in which both of them almost follow the same path [50]. This is because, in the ECL process, the transport is dominated by the slower moving

counterion ($D_{ap} \leq \times 10^{-11} \text{ cm}^2 \text{ s}^{-1}$) from the supporting electrolyte in contrary to the usual electron (or hole) drift mode of charge transport in the CPs in the EL experimental conditions ($D_{ap} \leq 10^{-6} \text{ cm}^2 \text{ s}^{-1}$) Thus the ECL process in the CP differs from the solid-state EL process.

3.3. Polymer phase ECL: DB-PPV

The electrogenerated chemiluminescence (ECL) from a conducting polymer (CP) 2,3- dibutoxy-1,4-polyphenylenevinylene (DB-PPV) was studied. The ECL experiment was carried with the system configuration as electrode/polymer/solution.



poly(2,3dibutoxy 1,4-phenylenevinylene) DB-PPV.

3.3.1. Experimental details

The polymer DB-PPV was coated on the Pt electrode (with surface area of approx. 0.07 cm^2) by evaporating a solution of the polymer in CHCl_3 in the dark. The Pt substrate was polished with $0.7 \text{ }\mu\text{m}$ diamond paste, and the surface was checked for uniformity with a Nikon PFX 104 optical microscope before and after the deposition of the polymer. Electrochemical experiments were carried out in a three-electrode configuration with the polymer coated Pt as the working electrode and Pt wires as quasi-reference (QRE) and counter electrodes. Anhydrous CH_3CN (Aldrich 27,100-4) was used as the solvent and 0.1 M tetraethylammonium perchlorate (TEAClO_4), tetraethylammonium hexafluorophosphate (TEAPF_6), tetraethylammonium tetrafluoroborate (TEABF_4), or tetrabutylammonium tetrafluoroborate (TBABF_4) were used as the supporting electrolytes. ECL emission intensities were measured with an RCA photo multiplier tube (type number 7326), which was polarized at -1000 V by a Keithley 246 high voltage supply.

3.3.2. Cyclic voltammogram

The cyclic voltammograms were reproducible, when TEABF_4 or TBABF_4 were used as the supporting electrolytes. With TEAClO_4 and TEAPF_6 the oxidation and reduction were both irreversible, oxidation being the most affected reaction (Fig. 3.3.2a). The reason could be the difficulty in drying them.

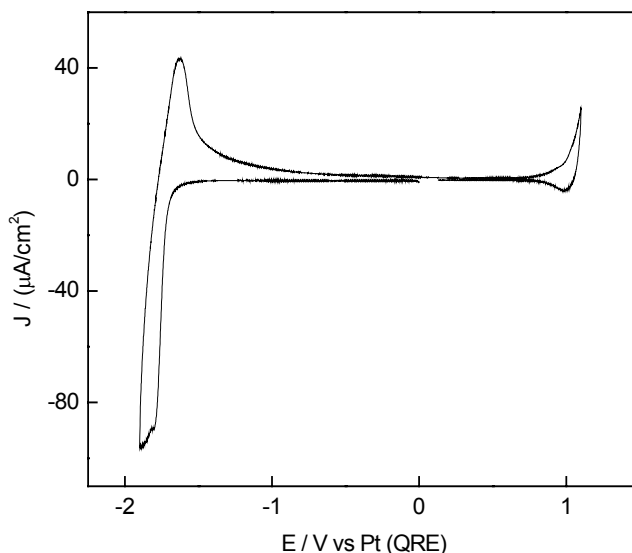


Fig. 3.3.2a: Cyclic voltammogram (CV) of Pt/DB-PPV in 0.1M TEAClO_4 in acetonitrile; scan rate: 100 mV/s.

Acetonitrile was found to be the best solvent for this purpose. The choice of the solvent was limited by the potential range and the purity of the solvent. As an example, when benzonitrile was used oxidation of the polymer could not be observed but there were multiple peaks. The presence of multiple electrochemical reactions is destructive for the production of ECL. Further, the high boiling point of benzonitrile (191 °C), as compared to acetonitrile (82 °C), caused difficulty in evacuating the vacuum lines between successive experiments.

The cyclic voltammetry did not show a marked difference between TBABF_4 and TEABF_4 , when DB-PPV films of equal thickness were used (Figs. 3.3.2b and 3.3.2c).

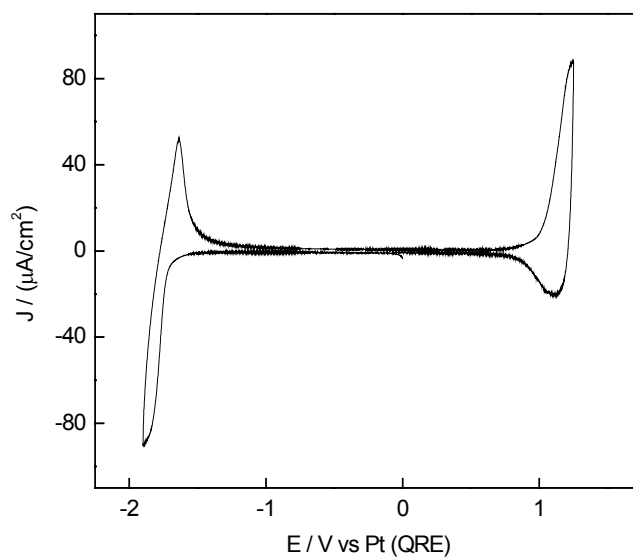


Fig. 3.3.2b: Cyclic voltammogram (CV) of Pt/DB-PPV in 0.1 M TBABF₄ in acetonitrile; scan rate = 100 mV/s.

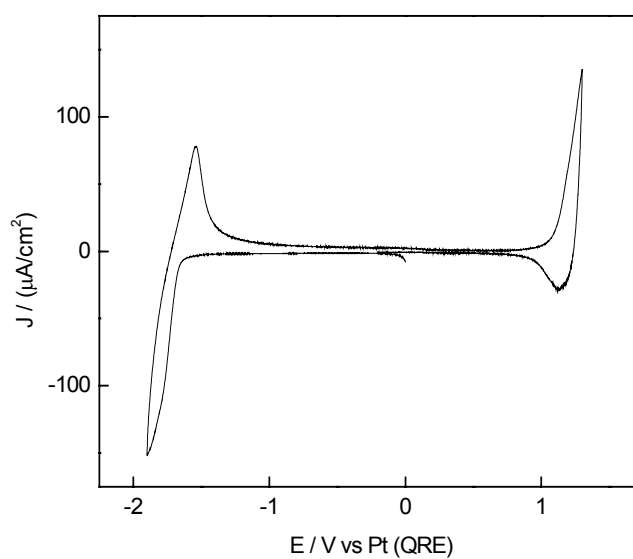


Fig. 3.3.2c.: Cyclic voltammogram (CV) of Pt/DB-PPV in 0.1 M TEABF₄ in acetonitrile; scan rate = 100 mV/s.

However, the anodic sweep was found to be less reversible than the cathodic one, which by itself, was quasi-reversible (Figs. 3.3.2d and 3.3.2e).

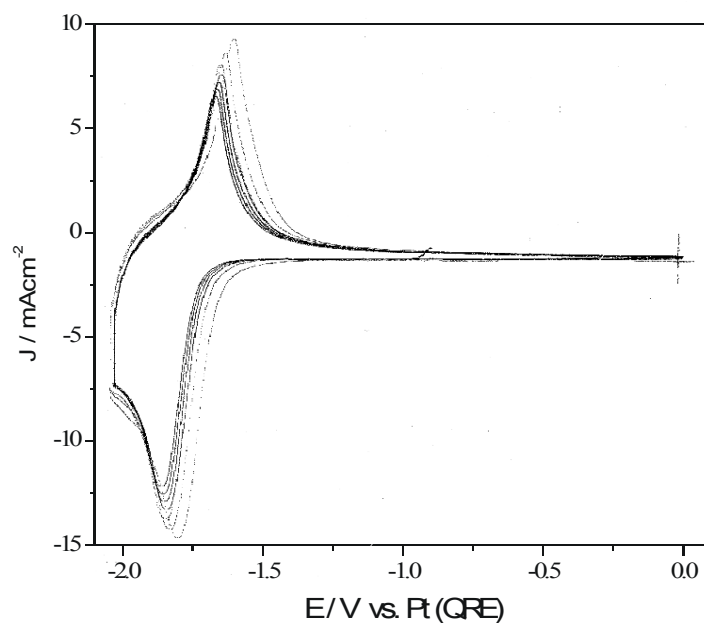


Fig. 3.3.2d: Cathodic potential sweep of Pt/DB-PPV in 0.1 M TBABF₄ in acetonitrile; scan rate = 100 mV/s.

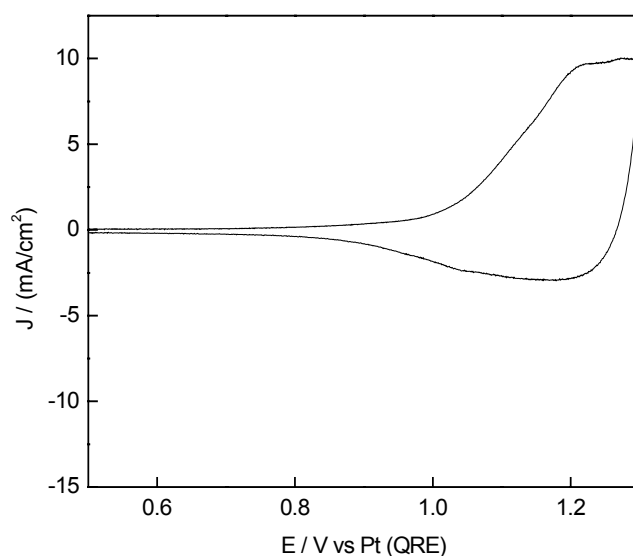


Fig. 3.3.2e: Anodic potential sweep of Pt/DB-PPV in 0.1 M TBABF₄ in acetonitrile; scan rate = 100 mV/s.

The cross-linked films did not show much difference from the uncross-linked polymer. But indeed, they show effect by the bulkier nature of the supporting electrolyte.[75]. When TBA⁺ was used instead of TEA⁺, there was no reduction. This is due to the restriction for the transport of bulkier cation (which is required for charge compensation in cathodic sweep) by the cross-linked polymer film.

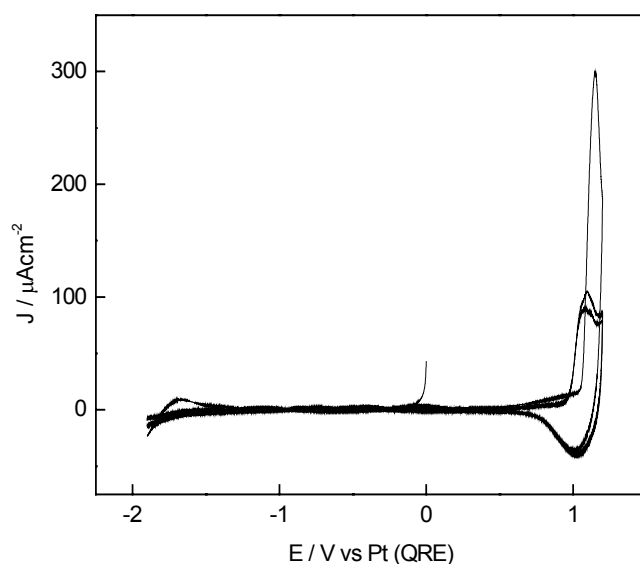


Fig. 3.3.2f: Potential sweep of Pt/DB-PPV (thickness = $1\mu\text{m}$, energy of cross-linking = 400 mJ/cm^2) in 0.1 M TBABF₄ in acetonitrile; scan rate = 100 mV/s.

3.3.3. Current transients

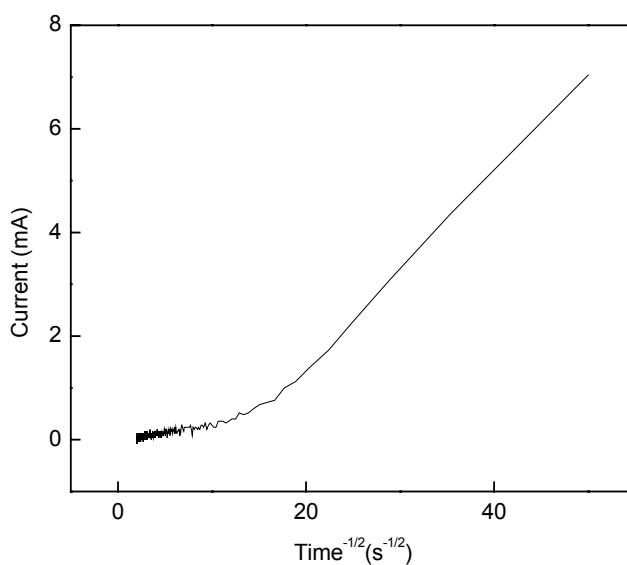


Fig. 3.3.3a: Cottrell plot for the anodic current on the positive potential step of the square wave between 0 and 1.3 V with step width of 150 ms each, for Pt/DB-PPV in 0.1 M TBABF₄ in acetonitrile.

In the ECL experiments, the radical anions and cations are formed upon application of successive negative and positive potential steps. It was therefore considered essential to analyze the anodic and cathodic current transients

following the potential steps. The linearity between current and the 1/(square root of time) (i vs. $t^{-1/2}$), is a criterion for a transport controlled electrochemical process. Such plots are referred to as Cottrell plots which are shown in Figs. 3.3.3a, 3.3.3b and 3.3.3c. Note that at the shorter times ($t^{-1/2} > 10 \text{ s}^{-1/2}$), deviations from the linear behavior were observed that result from the charging current (section 2.1.2 iii). From the slope of these plots the apparent diffusion coefficient was estimated to be $2.637 \times 10^{-11} \text{ cm}^2 \text{ s}^{-1}$ using Eq. (2.1.2b) of chapter 2. The concentration term was estimated to be $6.098 \times 10^{-4} \text{ mol cm}^{-3}$ by assuming the dry density for DB-PPV as 0.6 g/cc and 4 DB-PPV units as one electroactive site. The area of the electrode is 0.07065 cm^2 .

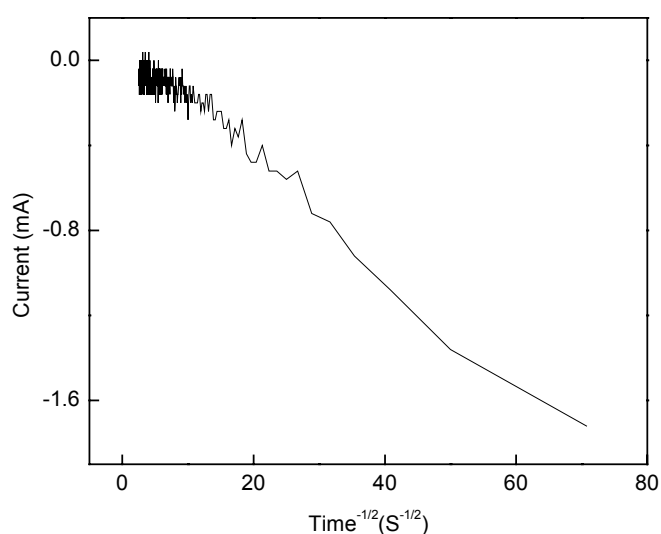


Fig. 3.3.3b: Cottrell plot for the cathodic current on the negative potential step of the square wave between 0 and -1.7 V , with step width of 150 ms each, for Pt/DB-PPV in 0.1 M TBABF₄ in acetonitrile.

The characterization of the electrode/polymer/solution also involves the evaluation of the double layer parameters: the double layer capacitance (C_{dl}) at the electrode/polymer interface and the uncompensated resistance (R_u) of the bulk consisting of the polymer and the electrolyte. Estimations of these double layer parameters were done by stepping the potential to a lower magnitude, where there will be no electrochemical reaction. The current in this region corresponds to the charging of the double layer at the electrode/DB-PPV (in the solution of the supporting electrolyte in acetonitrile). The magnitude of the current is related to the double layer capacitance and solution resistance as per

Eq. (2.1.2c) in chapter 2 from the plot of $\ln(i_{dl})$ vs. time. In a separate experiment of stepping the potential to -1V, charging current was recorded against time. The resistance of the polymer/electrolyte system was calculated from the intercept of the plot of $\ln(i_{dl})$ vs. time, as $1200\ \Omega$ and the double capacitance as $4 \times 10^{-6}\text{ F}$ from the slope. The high value of resistance compared to that in the case of solution, e.g., DPA dissolved in the electrolyte, is due to the presence of the non-conducting polymer chains under this condition.

3.3.4. The ECL experiment

ECL was generated in the triple potential step chronoamperometry experiment. The oxidized and reduced forms of the conducting polymer were generated in succession using a square wave alternating between the potential for the oxidation and reduction of the polymer (or vice versa). These species combine to form the luminescent moiety.

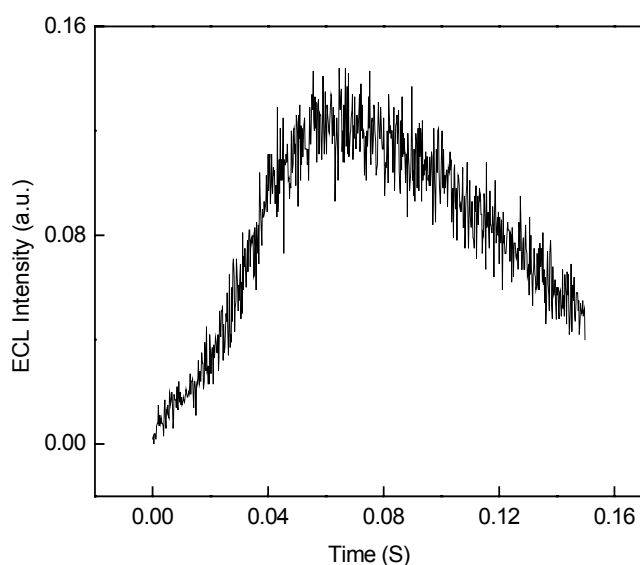


Fig. 3.3.4a: Cathodic ECL when the potential was switched between 1.3 V and -1.85 V of duration 150 ms each for DB-PPV film of thickness $\approx 0.6\ \mu\text{m}$ on Pt in 0.1 M TBABF₄ - AN.

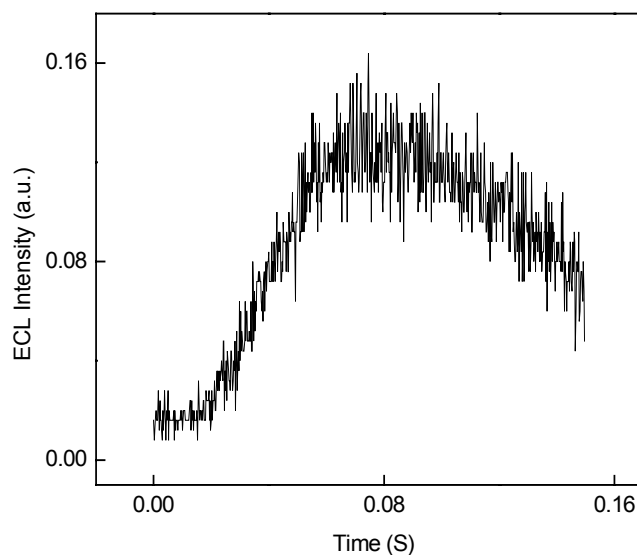


Fig 3.3.4b: Anodic ECL, when the potential was switched between -1.9 V and 1.3 V of duration 150 ms each for DB-PPV film of thickness $\approx 0.6 \mu\text{m}$ on Pt in 0.1M TBABF₄-AN.

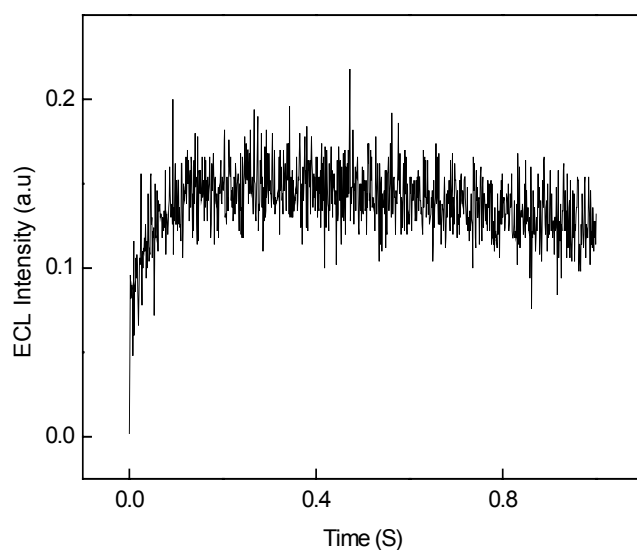


Fig. 3.3.4c: Anodic ECL when the potential was switched between - 1.9 V and 1.2V of duration 150 ms each for DB-PPV film of thickness $\approx 0.6 \mu\text{m}$ on Pt in 0.1M TEABF₄-AN.

In polymers like MDOPPV and PAT6, it has been reported that of the anodic and cathodic ECLs, one is favored over the other [3]. In MDOPPV the cathodic ECL is more predominant than the anodic ECL, which is reversed in the case of PAT6. The behavior was explained based on the results from the

chronoabsorptiometry experiments. For PAT6 the anionic form was relatively stable, subsequently when the polymer was oxidized, anodic ECL could be observed. On the other hand, in MDOPPV, the reduced form was found to be unstable, which was the cause for less occurrence of anodic ECL. They have used different pulse widths for cathodic and anodic steps.

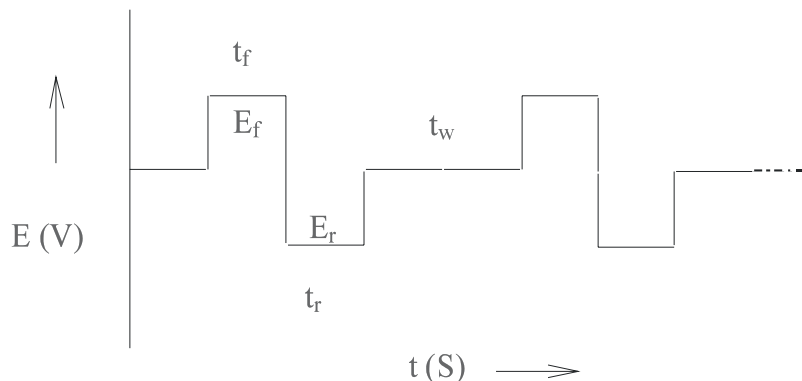


Fig. 3.3.4d: Scheme of the sequential anodic and cathodic potential steps in ECL experiments.

In the present case, equal pulse widths were used for anodic and cathodic potential steps with a waiting period t_w between adjacent potential steps at which the potential was kept at '0' V. The potential step order was also reversed in the same way. This is to ensure identical experimental conditions for the generation of positive and negative polarons. It has been found experimentally that the ECL could be found when the potential step widths starting from 150 ms to 1 s (Figs. 3.3.4a., 3.3.4b. and 3.3.4c). Reproducible results were obtained at potential widths of 100 -150 ms. No preference was observed for cathodic or anodic ECL. However, we could find anodic and cathodic ECLs of almost equal intensity (**symmetrical ECL**), when the potential step width was of duration 150 ms for each and the waiting time between successive potential steps being 200 ms, (Figs. 3.3.4a and 3.3.4b). Thus, the absence of a preference for anodic or cathodic ECL in our experiments has to do with the time allowed for the existence of the polymer in the polaronic state. At 1 s only anodic ECL could be observed (Fig. 3.3.4c). This can be explained by lesser stability of positive polaron in comparison to the negative polaron, as seen from the CV. Thus, at longer potential width, (1 s in this case) the anion produced becomes decayed, so that there is nothing left to react with the negative polaron produced in the subsequent negative potential step. Thus, cathodic ECL could not be obtained in the + to - potential step experiment at longer step widths.

The onset of ECL had a delay to the maximum of 10 ms in the case of DB-PPV. Thus, the double layer parameters of the Pt/DB-PPV in the supporting electrolyte solution were calculated. The resistance was found to be $1200\ \Omega$ for a polymer film of thickness $2\ \mu\text{m}$ and the capacitance was found to be $4\ \mu\text{F}$. The values differ from the ones we would expect from an electrode/organic solution interface (eg., Pt/DPA-SE), being larger by a factor of 10. DB-PPV was insoluble in acetonitrile in the neutral state. The higher resistance is obviously due to the presence of the polymer network on the electrode surface.

3.3.5. Studies concerning the stability of DB-PPV

Dissolution of the polymer was observed in the positive potential step. In fact, such dissolution was reported previously for other polymers [1]. This was a hindrance for the observation of ECL over a longer period. Fig. 3.3.5a shows decreasing intensity of the ECL transient with successive pulses. The dissolution has led to the change in the polymer film morphology before and after the ECL experiment.

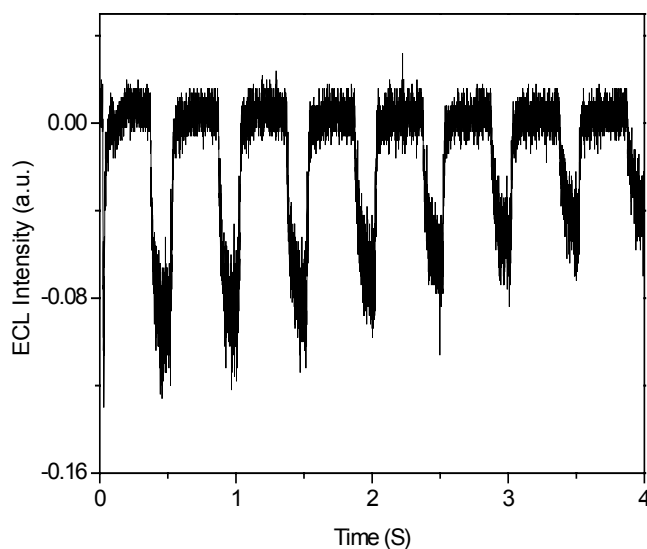


Fig. 3.3.5a: Decrease in the anodic ECL intensity with successive potential steps.

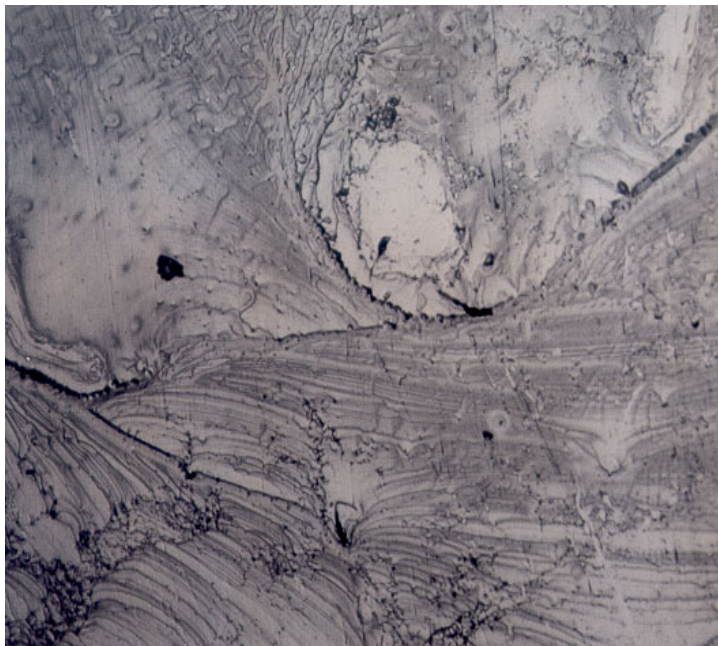


Fig. 3.3.5b: Film morphology before the ECL experiment as seen with a microscope.

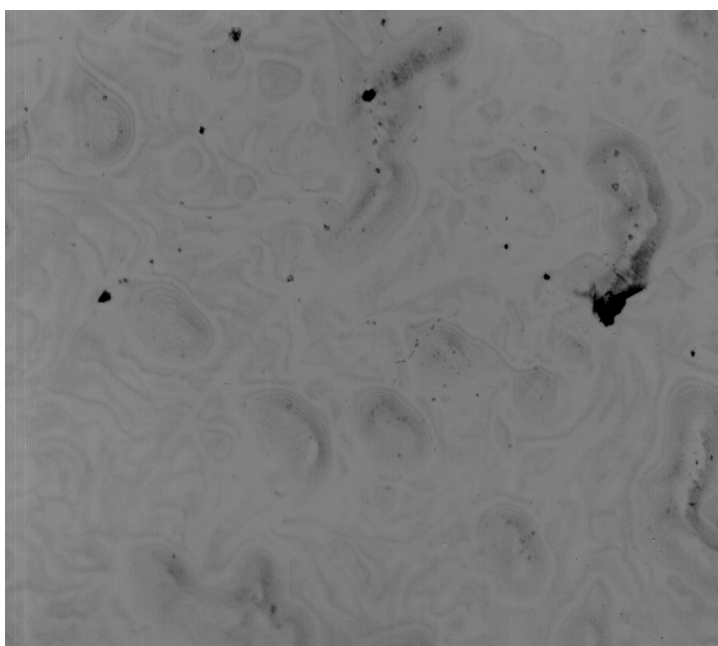


Fig. 3.3.5c: Film morphology after the ECL experiment as seen with a microscope.

To investigate whether there was complete dissolution of the polymer, which had resulted in the loss of its electroactivity, SEM (Scanning Electron Microscopy) image of the polymer coated electrode was taken after the ECL experiment.

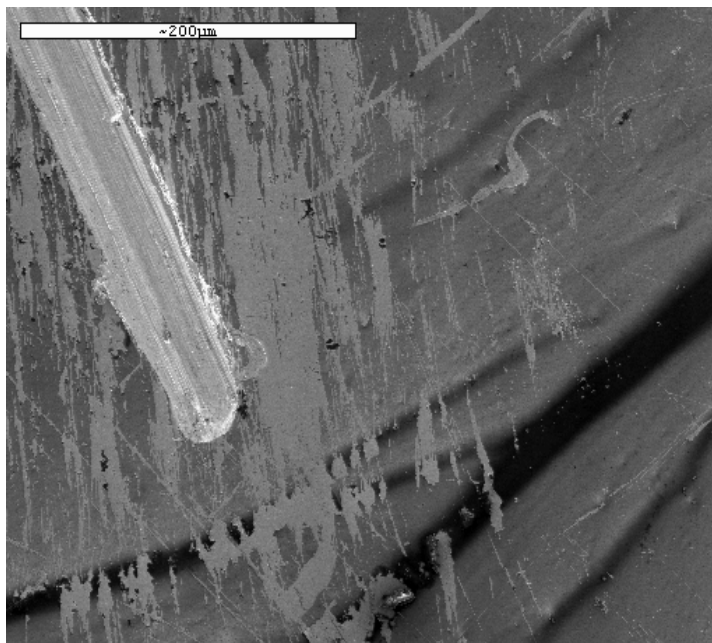


Fig. 3.3.5d: SEM image of the DB-PPV coated electrode surface.

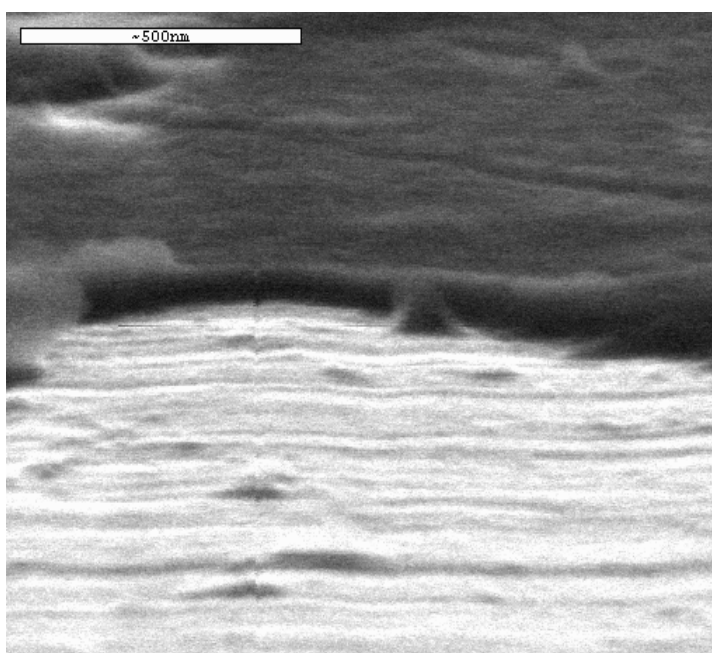


Fig. 3.3.5e: SEM image of the DB-PPV coated electrode surface at a higher magnification.

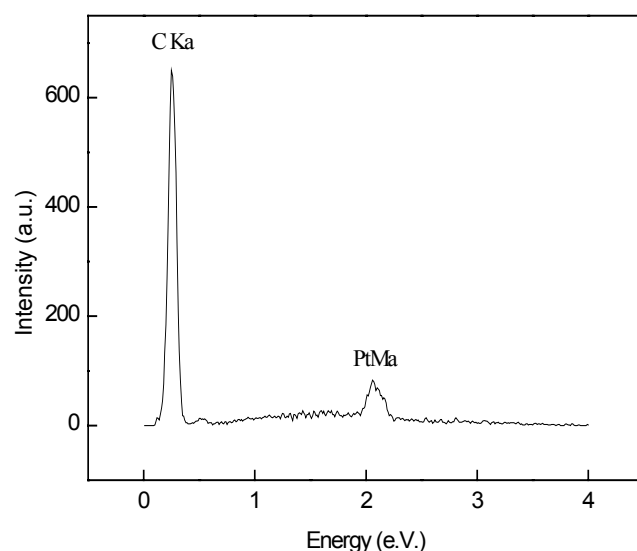


Fig. 3.3.5f: EDS analysis on the darker spots as seen in the SEM image.

The SEM pictures at two different magnifications (200 μm and 500 nm) showed the difference in the surface contour. Examination of the darker portion by EDS (Energy-dispersive X-ray Spectrometry) indicated carbonaceous material on the Pt electrode, which should be the polymer. Thus, there is polymer present on the electrode after the ECL experiment, which could not be felt by bare eyes, not even clearly under microscopic investigation. A scratch was made to analyze the interface between the polymer and the Pt electrode surface to examine the origin of dissolution, whether it is nearer to the electrode surface than the polymer bulk. But the SEM pictures did not give any insight into that aspect.

In order to prevent the dissolution, cross-linking of the polymer is one of the common procedures [76]. The DB-PPV was cross-linked using synchrotron radiation of energy in the range 100 - 500 mJ/cm^2 . The cross-linking, of course, improved the polymer stability. The degree of cross-linking was checked by coating a series of electrodes with the DB-PPV polymer of approximate thickness (0.63 μm), dipping them all into CHCl_3 for 10 min. and measuring the charging current in 0.1 M TEAP-acetonitrile solution. This is directly proportional to the resistance of the polymer film, which is the parameter that can be influenced by cross-linking. However, generating ECL in cross-linked film was found to be difficult due to the slower counterion mobility inside the cross-linked polymer during the process of electrochemical reaction in the CP.

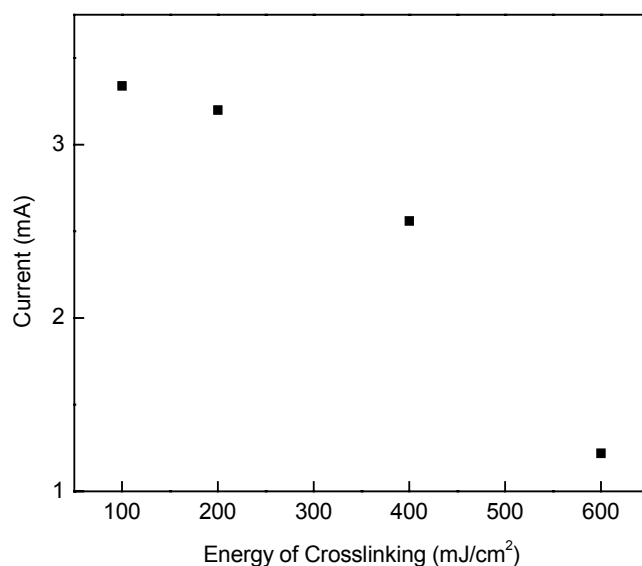


Fig. 3.3.5.g: Energy of cross-linking (mJ/cm^2) used to cross-link the DB-PPV films against the magnitude of cathodic charging current.

The experiment was also done at low temperature of $5\text{ }^{\circ}\text{C}$ with the hope that the deactivation kinetics of DB-PPV can be slowed down. Even this did not lead to observable ECL with cross-linked films. Hence, spectroscopic investigation of the polymer characteristics was undertaken. Ex-situ Raman spectroscopy data shows that the polymer was intact upon spin coating or cross-linking by synchrotron radiation of energies specified above.

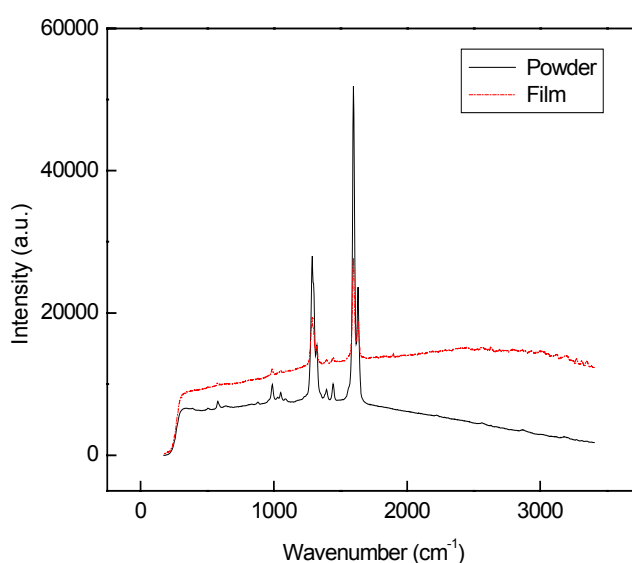


Fig. 3.3.5.h: Raman spectrum of DB-PPV when examined in the powder form and after film casting on the Pt electrode.

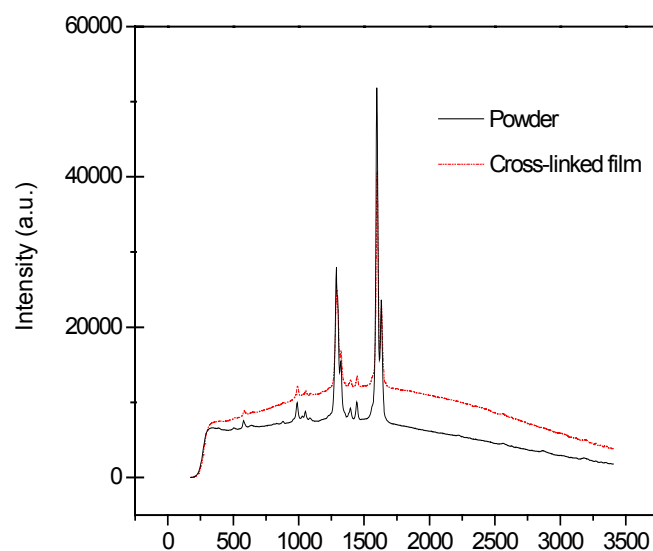


Fig.3.3.5i: Comparison of Raman spectra between the powder form and the cross-linked film of the polymer DB-PPV before the ECL experiment.

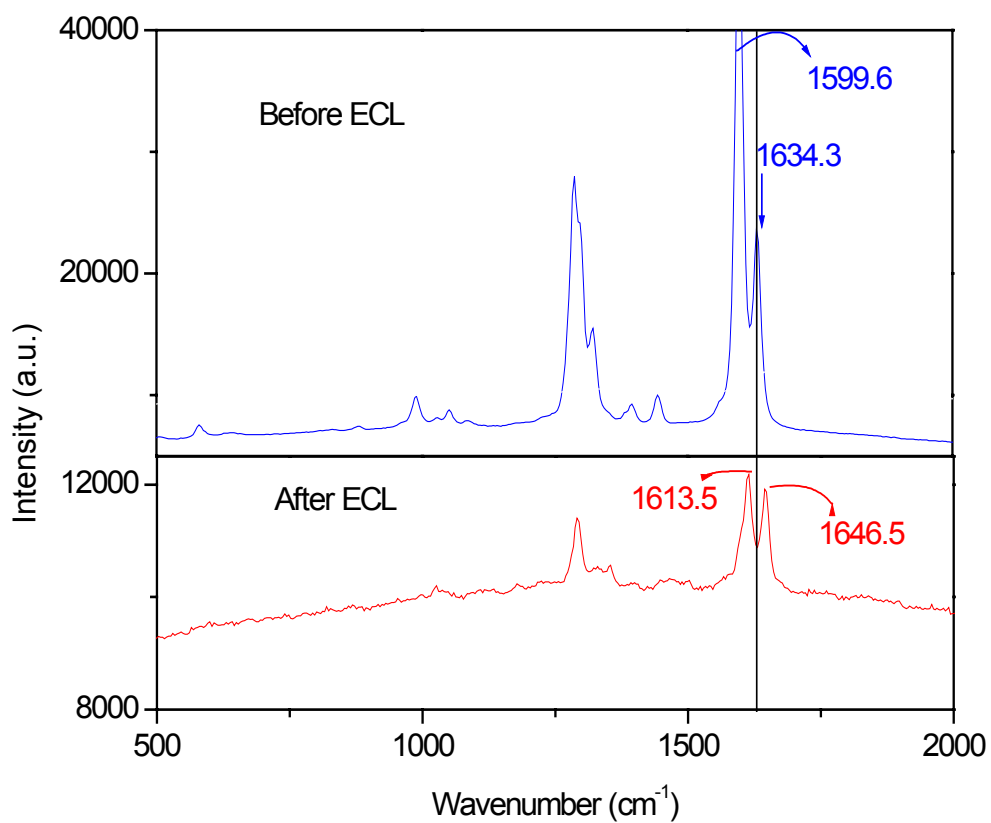


Fig. 3.3.5j: Comparison of the Raman spectra of the polymer DB-PPV before and after the ECL experiment.

But after the ECL experiment, there was a change in the spectrum when a

thinner polymer film was used. The important feature is the change in the magnitude and position of the doublets in the neutral polymer. The peak at 1599 cm^{-1} corresponds to the aromatic C–C bond, and that at 1634 cm^{-1} to the vinylic C–C bond. The intensity ratio between the two is 3:1, respectively. This shows that the aromatic system is actually a phenylic one. But after the experiment both the peaks were shifted to higher wave numbers 1613 and 1647 cm^{-1} , respectively. This shift to higher energy and the equal intensities of aromatic and vinylic C–C bonds has been attributed to quinonic structure [77]. So the polymer was disturbed during the double potential step experiment. It has been found that the positive polaronic and bi-polaronic levels co-exist in the PPV polymers [78]. The quinonic structure can be attributed to an irreversible derivative of the bi-polaronic level. The CV in the positive potential range is almost irreversible (Fig. 3.3.2e), confirming a chemical deactivation of the oxidized polymer. Further analysis suffers from the inability to characterize the product left on the electrode after the ECL experiment by spectroscopic techniques. The reason is the lesser quantity of the polymer on the electrode. Use of more polymer is limited by the slow ion transport.

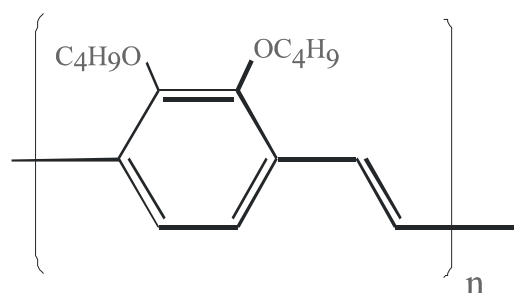


Fig. 3.3.5k: DB-PPV in phenylic form.

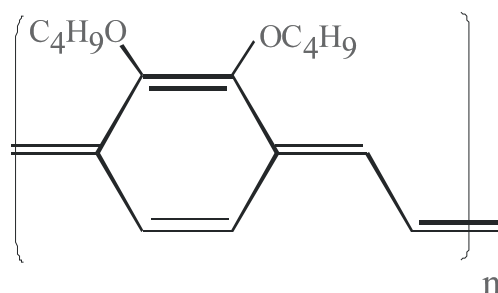


Fig. 3.3.5l: DB-PPV in quinonic form.

It has been reported that EL of DB-PPV has more PL quantum yield (40 %) than

that of MEH-PPV (15-20 %) [79]. This is also true in the case of ECL with these polymers. The ECL signals from MEH-PPV could be detected when the PMT was biased -1200V, whereas it could be observed at the PMT bias voltage of .1000V. However, as it is seen from the results, the ECL process has complications due to the stability of the polymer. Such complications were not reported in the solid-state electroluminescence (EL) or photoluminescence (PL) experiments [80]. So the electrode/polymer/solution configuration and the transport properties associated with the ECL experiments could be more sensitive to the polymer characteristics. In DB-PPV, the two butoxy substituents are in the ortho positions to each other. The presence of two ortho substituents has two effects: 1. The steric repulsion between the two butoxy groups – makes the substituents to stay away from each other, which might be the cause for the porous appearance of the film. This is because poor orientation of the substituents was found to affect the film forming property of these polymers [81]. 2. The adjacent alkoxy groups repel from each other. As a result, the phenyl rings are tilted at an angle of 30° with respect to each other, as found from theoretical quantum chemical calculations for the ortho substituted PPVs. This strain in the aromatic system can result in the less conversion of the neutral form to the polaronic form as well as to their low stability. This explains why we could not go to higher potential step widths. The longer the duration of the potential step, the lesser will be the polarons remaining intact in the polymer. Since positive polarons are found to be less stable, we could not observe cathodic ECL, when the potential step widths were of magnitude 1 s. When the potential was switched between positive to negative steps of duration 1s, the positive polarons become deactivated in the first potential step itself, thereby not yielding any ECL in the subsequent negative potential step. The lower limit of 150 ms for the potential step width is a consequence of the solid-state transport process, i.e., the slower ionic transport within the polymer.

3.3.6. Energetics of the ECL in DB-PPV

In order to understand the energy of the ECL process, the ECL emission spectra were recorded. The emission spectra from anodic and cathodic ECLs occur at the same wavelength. This shows that both anodic and cathodic ECLs are generated by the same process, the recombination of positive and negative

polarons.

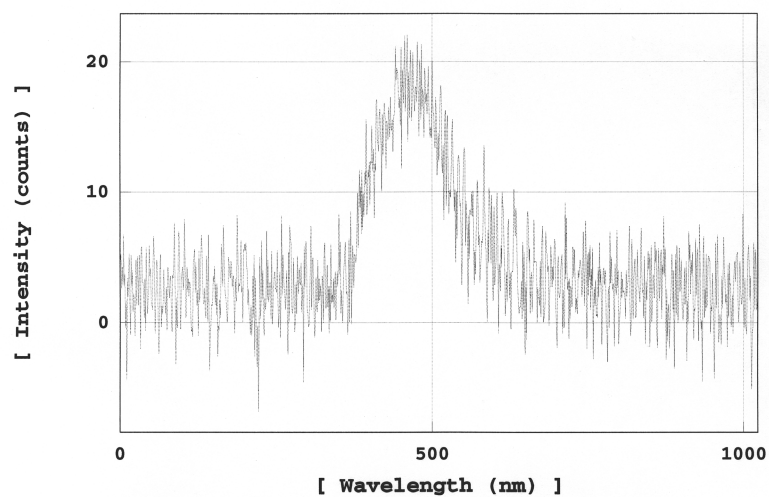


Fig. 3.3.6a: Cathodic ECL spectrum.

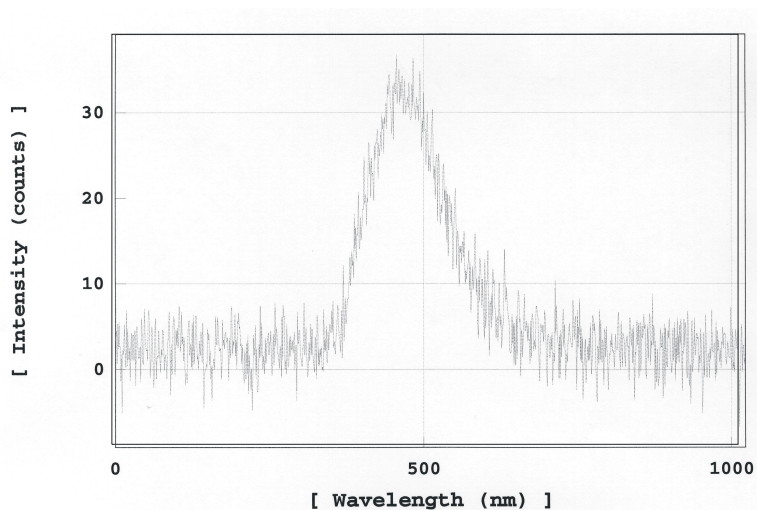


Fig. 3.3.6b: Anodic ECL spectrum.

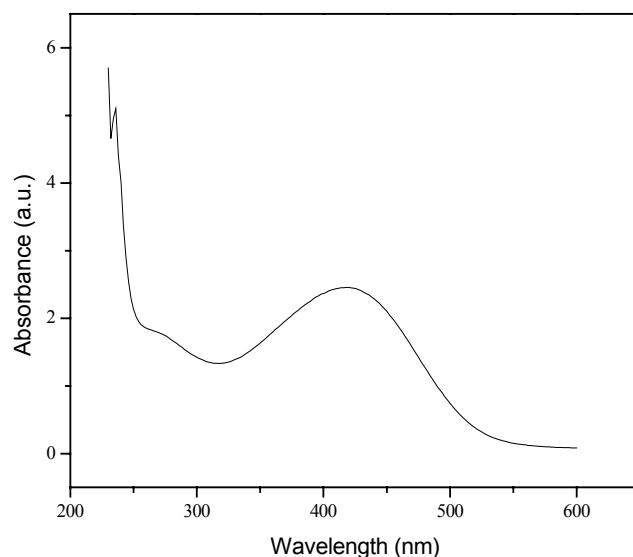


Fig. 3.3.6c: Absorption spectrum of DB-PPV in CHCl_3 .

The wavelength of ECL emission was approximately 485 nm. This energy corresponds to the energy of the singlet state. This was compared with the emission spectrum from the solid state Electroluminescence (EL) process, where there will not be any liquid phase in contact with the polymer. The value of emission maximum reported for this polymer was 519 nm [82,83]. The polymer was also dissolved in CHCl_3 and absorbance and fluorescence studies were made. The spectra are shown below:

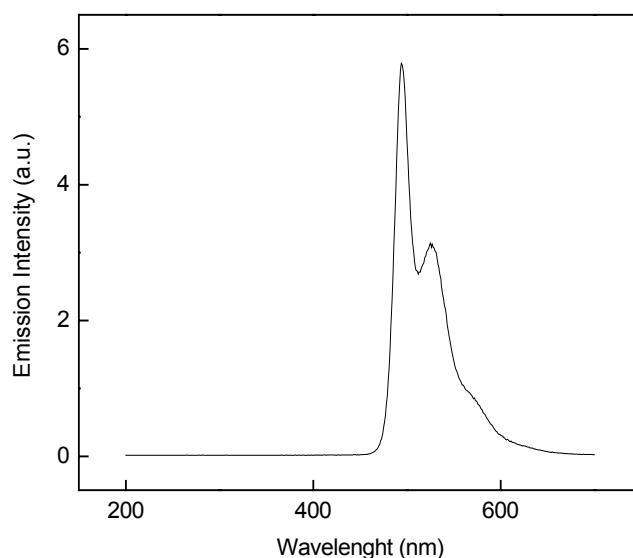


Fig. 3.3.6d: Fluorescence spectrum of DB-PPV in CHCl_3 .

The emission maximum seems to be different in the solid-state EL process, in

the ECL process where the solid polymer was kept in contact with electrolytic solution, and in the solution phase fluorescence process. The difference between the first and the others can be speculated, since solvent plays a major role in stabilizing the ground and excited states of an aromatic compound, which will in turn affect the energy of the emission. The difference between the emission maxima between ECL and fluorescence needs some consideration. The emission maximum occurs at approximately 500 nm in the solution phase. ECL occurs at a shorter wavelength in acetonitrile, 485 nm. One reason could be that in a good solvent such as CHCl_3 of low dielectric strength, the polymer can exist with extended conjugation, which shifts absorption and emission to longer wavelengths [84]. More detailed explanation can be given from the knowledge about the nature of the ground and excited states. The electronic state having lower dielectric strength will be stabilized by CHCl_3 .

4. Theoretical Analysis of the Kinetics of ECL

4.1. Solution phase ECL - 9,10 diphenylanthracene (DPA)

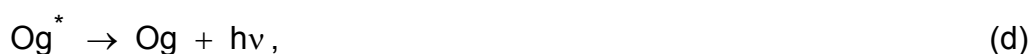
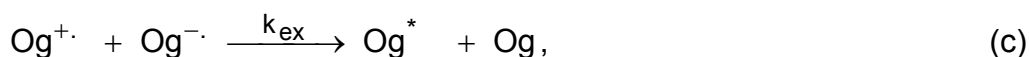
4.1.1. Kinetics of the ECL process in solution phase

As reported in chapter 3, ECL was produced by applying a series of triple potential steps to the electrode immersed in the electrochemical solution containing the organic compound (Og). The generation of luminescence in the electrochemical environment involves the following reactions:

At the positive potential step and during t_f



At the negative potential step and during t_r



where Og refers to the aromatic precursor of the luminescent moiety Og^* , $\text{Og}^{\cdot+}$ and $\text{Og}^{\cdot-}$ are the positive and negative radical ions produced by the electrochemical oxidation and reduction of Og, and k_{ex} is the rate constant for the bimolecular annihilation reaction (c). Here the luminescence is produced during the negative potential step and is referred to as cathodic ECL. (It can be the other way around where first the negative radicals are produced followed by the production of positive radicals, resulting in the generation of anodic ECL). The luminescence process, represented by equation (d), is faster in the time scale of the experiment, irrespective of the mode of production of the excited state (i.e., through direct singlet formation or by triplet-triplet annihilation reaction). Hence, the kinetics of the ECL process is defined by the annihilation reaction (c), which, in turn, depends on the transport of the radical cations and anions. Thus, the shape of the ECL transient, corresponding to the decay of the luminescence intensity with time, depends on the rate constant of the annihilation reaction (c) as well as on the rate parameters of the electrochemical reactions (a) and (b).

The simulation of the ECL transient is of interest since it serves as a tool to study the kinetics of both the ECL and electrochemical reactions [85] (see the scheme of reactions above). The following points are considered in the simulation:

1. Initially the electrochemical solution consists of a uniform concentration of the neutral organic molecule (e.g., DPA) of concentration C° (in the supporting electrolyte solution). The electrode potential was chosen for the reactant to stay in the neutral state.
2. In the first potential step of duration t_f to a positive value, the organic molecule was oxidized. Since it is a potential step experiment, the magnitude of the potential step was increased to a higher positive value ($E^{\circ'} + 250$ mV) to ensure the kinetic feasibility of the electrode reaction (a). Therefore, the current in this step is controlled by the diffusion of the Og towards the electrode and $Og^{+ \cdot}$ away from the electrode which can be described by Fick's second law:

$$\left(\frac{\partial C_{Og}}{\partial t} \right) = D_{Og} \left(\frac{\partial^2 C_{Og}}{\partial x^2} \right), \quad (4.1.1a)$$

and

$$\left(\frac{\partial C_{Og^{+ \cdot}}}{\partial t} \right) = D_{Og^{+ \cdot}} \left(\frac{\partial^2 C_{Og^{+ \cdot}}}{\partial x^2} \right), \quad (4.1.1b)$$

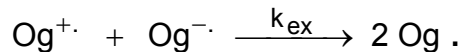
where D_{Og} and $D_{Og^{+ \cdot}}$ are the diffusion coefficients, C_{Og} and $C_{Og^{+ \cdot}}$ are the concentrations of the neutral and oxidised species, respectively and x is the distance. As the orders of the diffusion coefficients D_{Og} and $D_{Og^{+ \cdot}}$ do not differ much [86], it is a common practice to use a single diffusion coefficient D to describe the transport. Concentration profiles of, say, the neutral species can be obtained by solving the linear equation (4.1.1a).

$$C_{Og}(x,t) = C^\circ \operatorname{erf} \left[\frac{x}{2(Dt)^{1/2}} \right]. \quad (4.1.1c)$$

The concentration distribution of the radical cation can then be calculated by applying the condition $C_{Og}(x,t) + C_{Og^{+ \cdot}}(x,t) = C^\circ$.

3. When the potential was stepped to a negative value ($E^{\circ'} - 250$ mV) of duration t_r , there will be the formation of radical anion $Og^{\bar{\cdot}}$ (b). Now the

diffusion of Og and $\text{Og}^{+\cdot}$ will take place towards the electrode and $\text{Og}^{-\cdot}$ away from the electrode. When both $\text{Og}^{-\cdot}$ and $\text{Og}^{+\cdot}$ meet with each other, there will be the bimolecular annihilation reaction (c) giving rise to luminescence. The luminescence process is considered to be instantaneous in the time scale of the experiment. Eq.(c) becomes modified as



Therefore, the following equations have to be solved to describe the kinetics and concentration profiles in the second potential step (b):

$$\left(\frac{\partial C_{\text{Og}}}{\partial t} \right) = -D \left(\frac{\partial^2 C_{\text{Og}}}{\partial x^2} \right) + 2k_{\text{ex}} C_{\text{Og}^{+\cdot}} C_{\text{Og}^{-\cdot}} , \quad (4.1.1d)$$

$$\left(\frac{\partial C_{\text{Og}^{+\cdot}}}{\partial t} \right) = -D \left(\frac{\partial^2 C_{\text{Og}^{+\cdot}}}{\partial x^2} \right) - k_{\text{ex}} C_{\text{Og}^{+\cdot}} C_{\text{Og}^{-\cdot}} , \quad (4.1.1e)$$

$$\left(\frac{\partial C_{\text{Og}^{-\cdot}}}{\partial t} \right) = -D \left(\frac{\partial^2 C_{\text{Og}^{-\cdot}}}{\partial x^2} \right) - k_{\text{ex}} C_{\text{Og}^{+\cdot}} C_{\text{Og}^{-\cdot}} . \quad (4.1.1f)$$

4.1.2. Double layer charging

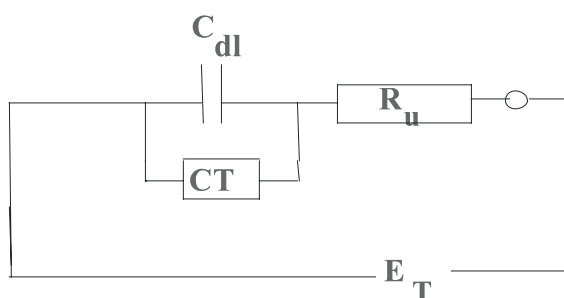


Fig. 4.1.2a: Equivalent circuit representation of the electrochemical processes.

The electrochemical system behaves as a resistance and capacitance (RC) circuit. When the electrode is subjected to a potential step, the ions from the supporting electrolyte build up near the electrode trying to counteract the charge

on the metal. Thus, the electrode/solution interface behaves as a capacitor, of capacitance C_{dl} , although the ions do not strictly confine to a single layer on the solution side. Initially the current corresponding to charging of this double layer flows through the circuit, the magnitude of which is determined by the resistance of the electrochemical solution (R_u). For a detailed discussion see sections 2.1.2ii and 2.1.2iii. The product $R_u \cdot C_{dl} = \tau$ is termed as the time constant; it determines the time for the decay of the charging current and the onset of conditions for faradaic reactions. Hence, consideration of the double layer charging process becomes important in ECL experiment, the generation of which, in turn, depends on the electrochemical production of the radical ions [57].

4.1.3. Digital simulation technique

It is difficult to solve the diffusion-reaction equation (Eqs.(4.1.1d-f)) by analytical methods. Hence, the technique of digital simulation was followed. The point model was considered. In the point model, the concentration of each species is represented as a two-dimensional array of time and distance; the array of time starts from the time of application of the potential step, and the array of distance starts from the electrode surface. The points on the time axis are uniformly separated by an interval Δt , and those on the distance axis are equally separated by the diffusional length Δx . As an example, the concentration is denoted in general terms 'C'; it can be described in the point model as follows:

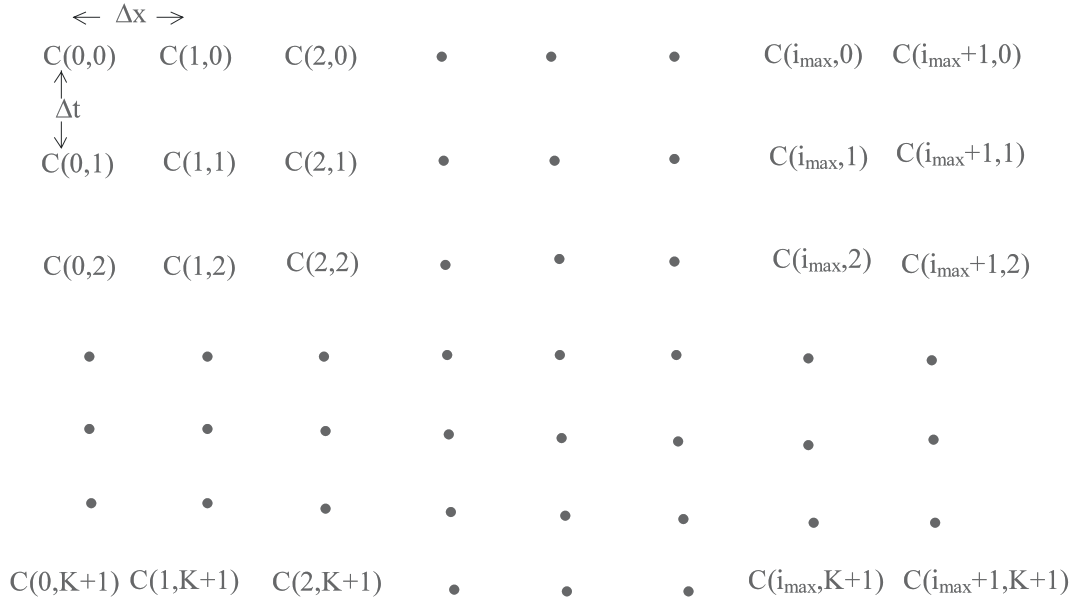


Fig. 4.1.3a Representation of concentration array in point model.

The partial differential equations (Eqs.(4.1.1d-f)) are expressed in finite difference forms by selecting very small values for Δx and Δt . The electrode potential fixes the concentration at the point zero. The concentration at each point on the distance axis, starting from the first point to the point i_{\max} corresponding to the diffusion layer thickness can be calculated from the finite difference equations:

$$\left(\frac{\partial C}{\partial t} \right) = \frac{C(t + \Delta t, i) - C(t, i)}{\Delta t} \quad (4.1.3a)$$

Therefore, $\left(\frac{\partial C}{\partial t} \right) = D \left(\frac{\partial^2 C}{\partial x^2} \right)$, i.e.,

$$\frac{\partial C}{\partial t} = \frac{D}{\Delta x^2} [C(t, i+1) - C(t, i) - C(t, i) + C(t, i-1)], \quad (4.1.3b)$$

$$C(t + \Delta t, i) = C(t, i) + \frac{D \Delta t}{\Delta x^2} [C(t, i+1) - C(t, i) - C(t, i) + C(t, i-1)]. \quad (4.1.3c)$$

Another important consideration is the *dependence of the diffusion layer thickness on the duration* of the potential step, which is crucial for experiments done under transient conditions. The diffusion layer thickness (κ) is connected

to the duration of the experiment by the equation,

$$\kappa = 2(Dt)^{1/2}. \quad (4.1.3d)$$

4.1.4. Conditions for simulation

The simulation of the concentration, current and luminescence profiles are obtained by the methodology described below:

Time is denoted by the vector 'k' ($= t/\Delta t$) and distance by 'i' ($= x/\Delta x$). The diffusion coefficient was converted to the dimensionless parameter D_M ($= D\Delta t/\Delta x^2$). The value of D_M should be ≤ 0.45 for the simulation to be consistent [86]. Initially the electrochemical solution consists of a uniform concentration of the neutral organic molecule Og. The point $k = 0$ represents the time from the point of application of the first potential step (in our case the positive potential step) until the time prior to the application of the second one. The concentrations of the species Og^{+} and Og are obtained by using the error functions (cf. Eq.(4.1.1c)). The concentration of the negative species, Og^{-} is zero during this interval. The maximum value of the 'i' vector is calculated using the expression $i_{\max} = (2 D_M k_{\max})^{1/2}$. The concentration array is constructed until $i > i_{\max}$.

The point $k = 1$ represents the time of the application of the second potential step, i.e., $k = 1$ implies $t_r > 0$ where t_r denotes the duration of the second potential step. The concentrations of the different species at the electrode surface ($i = 0$) are fixed by the Nernst equation:

$$\frac{[Ox]}{[Red]} = \exp\left(\frac{nF}{RT} (E - E^{\circ'})\right). \quad (4.1.4a)$$

The concentrations for $i > 0$ are assumed to have the same values fixed in the earlier time, i.e., the concentrations calculated using error function at $k=0$.

The diffusion-reaction process is allowed to occur from $k = 1$ to until k_{\max} , and for each value of k , the value of i_{\max} is calculated as described earlier. This simulation yields the profiles of concentration with time and distance profiles.

Since the luminescence decay is assumed to be instantaneous, the concentration-time profile of $0.5 C_{Og}$ can represent the luminescence transient. The current transient is calculated as follows:

$$j_F = F \sum z_n J_n, \quad (4.1.4b)$$

Where ' j_F ' represents the faradaic current density, F is the faraday's constant, J is the flux of the species, and z is the charge of the same; ' n ' denotes the number of electroactive species. Since the iteration is done for the second potential step, the faradaic reaction of interest, in the present case is the conversion of Og^+ to $Og^{\cdot-}$ and Og to $Og^{\cdot-}$. Hence, the current density can be represented as follows:

$$j_F = F \left\{ z_{Og^+} J_{Og^+} + z_{Og^{\cdot-}} J_{Og^{\cdot-}} \right\}. \quad (4.1.4c)$$

For the system under consideration, the flux balance equation can be written as $J_{Og} + J_{Og^+} + J_{Og^{\cdot-}} = 0$. By making use of this condition and Fick's first law, the final expression for the current density is obtained as follows:

$$\frac{j}{F} = 2D \left\{ \frac{C_{Og^+}(i=1) - C_{Og^+}(i=0)}{\Delta x} \right\} + D \left\{ \frac{C_{Og}(i=1) - C_{Og}(i=0)}{\Delta x} \right\}. \quad (4.1.4d)$$

4.1.5. Inclusion of the IR drop in the electrochemical solution and double layer charging at the electrode/solution interface

Due to the charging process of the electrochemical interface (metal/polymer) during the initial stages of the potential step (few milliseconds), the applied potential does not reach its final value at the same time as that of its application, but after a certain time lag, which can be represented as follows:

$$E_{CT}(t) = E_{Final} \left\{ 1 - \exp \left(- \frac{t}{R_u C_{dl}} \right) \right\}. \quad (4.1.5a)$$

The effective electrode potential at a time $t + \Delta t$ can be calculated from its value at the previous time t by the empirical relationship,

$$E_{CT}(t + \Delta t) = E_{CT}(t) + \Delta E_{CT}. \quad (4.1.5b)$$

The double layer charging current can be calculated by the following relationship,

$$i_C(t) = [(E_{Final} - E_{CT}) / R_u - i_F]. \quad (4.1.5c)$$

Thus Eq. (4.1.5b) can be rewritten as follows:

$$E_{CT}(t + \Delta t) = E_{CT}(t) + \left\{ \frac{E_{Final} - E_{CT}(t)}{R_u} - j_F A \right\} \frac{\Delta t}{C_{dl}}. \quad (4.1.6d)$$

4.1.6. Simulation of the experimental ECL transient for DPA

The simulation was done by following the procedures discussed in the earlier sections. The parameter diffusion coefficient D , uncompensated solution resistance R_u and double layer capacitance C_{dl} were evaluated as discussed in section 3.1.3. The value of D_M was fixed as 0.4; knowing the value of D for DPA from the Cottrell plot, Δx was calculated from the relationship $D_M = D\Delta t / \Delta x^2$. The simulation was repeated until the calculated current agreed with the experimental current in magnitude and experimental and simulated ECL transients were of the same shape. The value of k_{ex} , corresponding to the coincidence of experimental and simulated transients, is taken as the one for the annihilation reaction (d). Following are the results of simulation of the cathodic and anodic ECL transients of DPA in 0.1 M TBAClO₄.

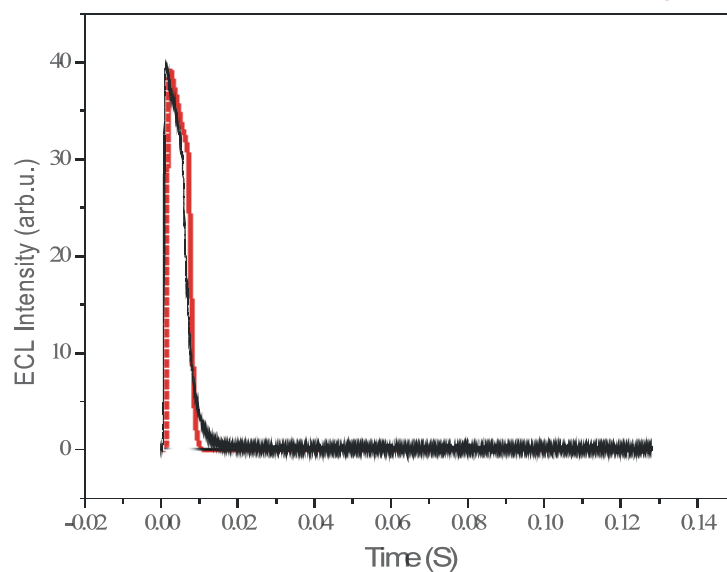


Fig. 4.1.6 a. Simulation of the anodic transient (potential step between - 2.05 V and 1.6V, duration 50ms each) with $C^{\circ} = 1 \times 10^{-6} \text{ mol cm}^{-3}$ $k_{\text{ex}} = 3 \times 10^{10} \text{ l mol}^{-1} \text{ s}^{-1}$, $D = 5 \times 10^{-6} \text{ cm}^2 \text{ s}^{-1}$, $R_u = 109 \Omega$ and $C_{\text{dl}} = 1.5 \mu \text{ F}$.

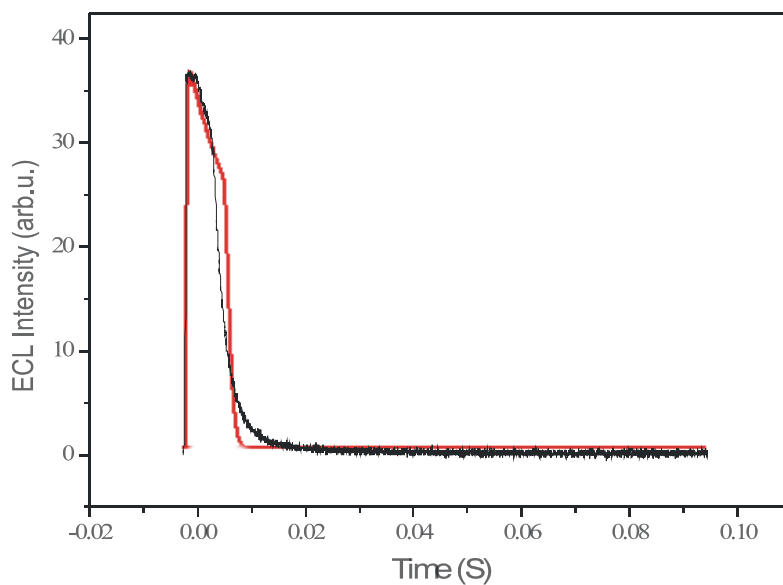


Fig. 4.1.6 b. Simulation of the cathodic transient (potential step between 1.6 V and -2.05V, duration 50ms each) with $C^{\circ} = 1 \times 10^{-6} \text{ mol cm}^{-3}$ $k_{\text{ex}} = 1 \times 10^{10} \text{ l mol}^{-1} \text{ s}^{-1}$, $D = 5 \times 10^{-6} \text{ cm}^2 \text{ s}^{-1}$, $R_u = 109 \Omega$ and $C_{\text{dl}} = 1.5 \mu \text{ F}$.

The anodic and cathodic ECL transients were found to be having almost equal values of the rate constants $3 \times 10^{10} \text{ l mol}^{-1} \text{ s}^{-1}$ and $1 \times 10^{10} \text{ l mol}^{-1} \text{ s}^{-1}$, respectively. The order of the rate constant agrees with the ones reported in the literature

[57, 66]. This shows the validity of the present theoretical simulation procedure. The effect of double layer charging on the effective potential felt by the electrochemical reaction, is shown in the following figures during anodic and cathodic ECL experimental conditions. The potential takes time approximately of 0.5 ms to reach its final value.

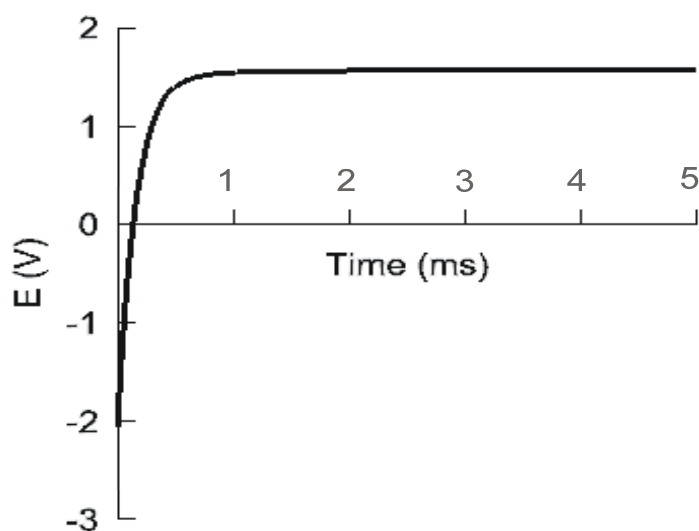


Fig. 4.1.6c: Effect of double layer charging on the potential step from -2.05 V to 1.6 V.

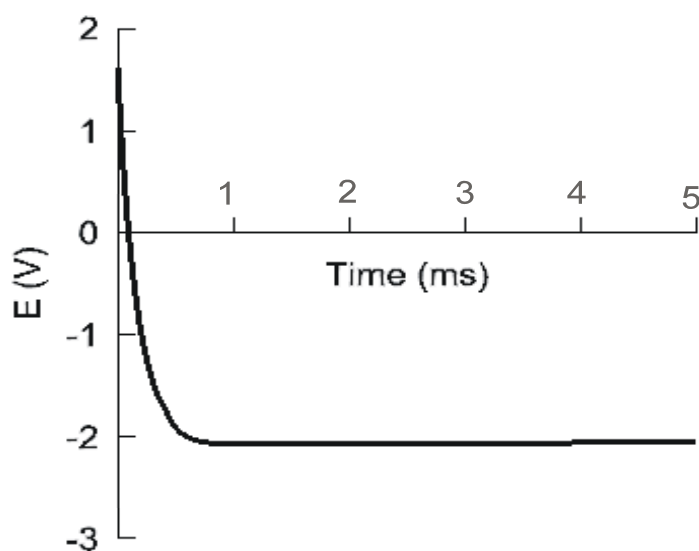


Fig. 4.1.6 d: Effect of double layer charging on the potential step from 1.6 V to -2.05 V.

It has been reported that the ECL intensity and kinetics are different for different sequences of potential steps for their generation. This concept was discussed in detail in section 3.1.4. Since the speculation and earlier analyses on this effect point to the adsorption of some species other than the electroactive species on the electrode, this concept is beyond the scope of the present theoretical analysis.

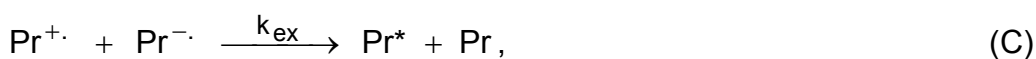
4.2. Polymer Phase ECL (MEH-PPV)

4.2.1. Kinetics of the ECL process in the polymer phase

Unlike the solution phase ECL, the ECL producing species, the conducting polymer (CP) was coated on the electrode and then dipped in the solution of the electrolyte with the solvent. As explained in the experimental section, care was taken for the CP to remain chemically and physically intact on the electrode by the appropriate choice of the solvent. ECL was produced by applying a series of triple potential steps to the CP coated electrode kept in the electrolytic solution. The kinetics can be explained on similar grounds as that of solution phase ECL: At the positive potential step and during t_f



At the negative potential step and during t_r



where Pr refers to the oxidizable/reducible unit of the neutral polymer, Pr^* is the excited polaron, $\text{Pr}^{\cdot+}$ and $\text{Pr}^{\cdot-}$ are the positive and negative polarons produced by the electrochemical oxidation and reduction of Pr, respectively, and k_{ex} is the rate constant for the bimolecular annihilation reaction (C). The cathodic ECL is considered. As with the case of solution ECL, the kinetics of the ECL process is defined by the annihilation reaction (C), since the luminescence process

represented by equation (D) is faster in the time scale of the experiment.

The annihilation reaction and the rate of formation of the positive (A) and negative polarons (B) defers from the corresponding processes in the solution phase due to the unique mode of charge transport in polymers in electrochemical environment. In the solution phase the neutral species (Og) and the positive and negative radical ions ($Og^{+\cdot}$ and $Og^{-\cdot}$) move freely to take part in the electron transfer reaction with the electrode or among them. But in the case of polymers this is not possible, since the oxidizable/reducible units (Pr) and the corresponding charged species ($Pr^{+}/Pr^{-\cdot}$) are indeed a part of the big conducting polymer network. They cannot break away from the polymer backbone for the electron transfer reactions. Instead, the electrons (or holes) themselves move towards or away from these units (Pr , $Pr^{+\cdot}$ and $Pr^{-\cdot}$) along the conjugated bonds during electron transfer reactions. On the other hand, the electrochemical environment needs to be electrically neutral. Hence, the ions of the supporting electrolyte move in and out of the polymer, depending on the charge requirement during the electron transfer reactions. This counterionic movement controls the local electroneutrality within the conducting polymer [87]. This concept is represented in the following figures:

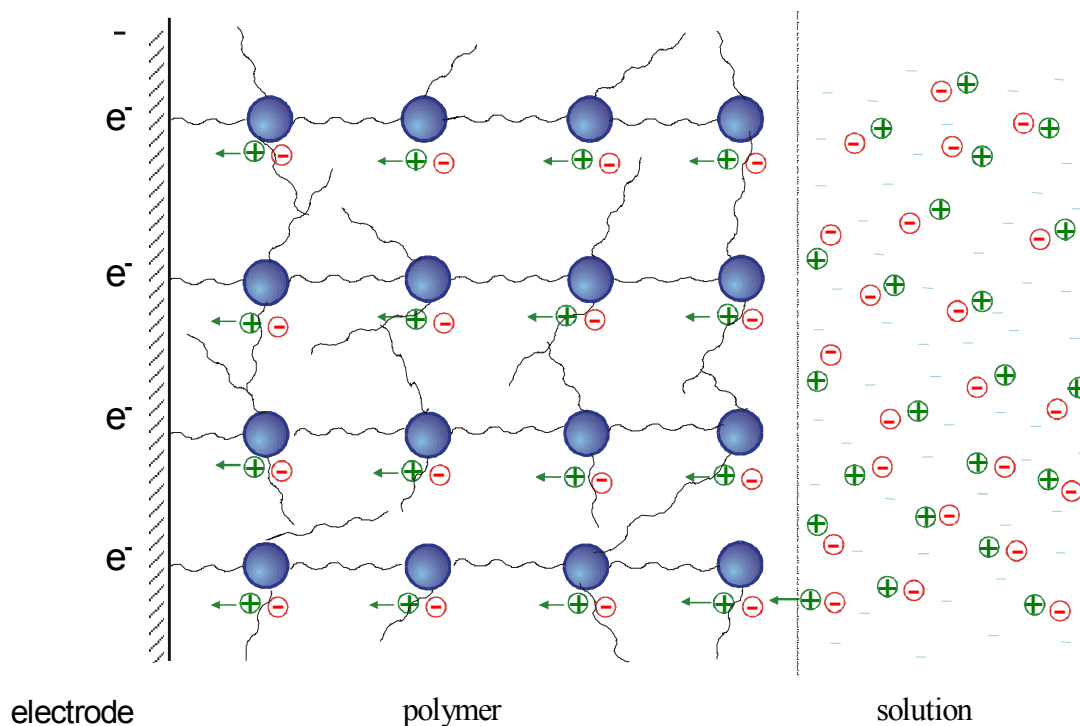


Fig. 4.2.1a. Representation of double layer charging in the

electrode/polymer/solution system: situation prior to charge transfer.

e^- — electrons,

● — active site of the neutral polymer (Pr),

— solvated negative counterion of the supporting electrolyte,

+ — solvated positive counterion of the supporting electrolyte.

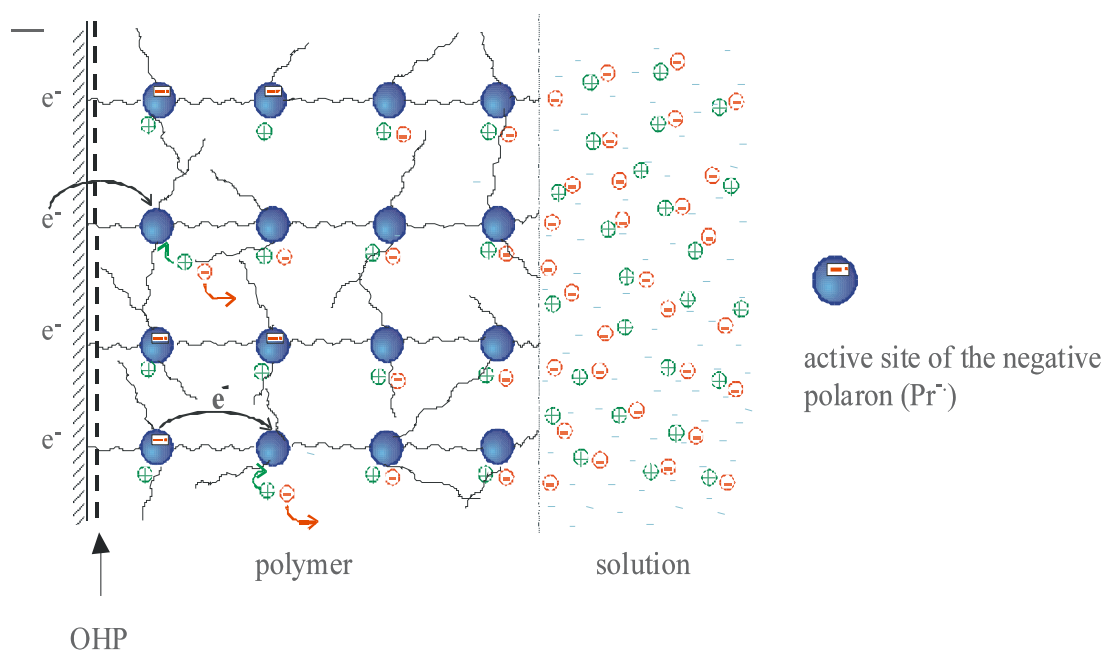


Fig. 4.2.1b. State of the polymer during charge transfer and transport maintaining bulk electroneutrality.

Since the transport of charges in the conducting polymer is different from that in the solution phase, the flux equations are also different, with the added term, due to the electric field $\partial\phi/\partial x$ [88]. Thus, the ECL reaction in the polymer phase will have the following set of equations with the flux term modified to account for the migration of the charged species under the influence of the electric field in the polymer:

$$J_{Pr^{-}} = -D \left(\frac{\partial C_{Pr^{-}}}{\partial x} \right) + \frac{F D C_{Pr^{-}}}{R T} \left(\frac{\partial \phi}{\partial x} \right) - k_{ex} C_{Pr^{+}} C_{Pr^{-}}, (4.2.1a)$$

$$J_{Pr^{+}} = -D \left(\frac{\partial C_{Pr^{+}}}{\partial x} \right) - \frac{F D C_{Pr^{+}}}{R T} \left(\frac{\partial \phi}{\partial x} \right) - k_{ex} C_{Pr^{+}} C_{Pr^{-}}, (4.2.1b)$$

$$J_{Pr} = -D \left(\frac{\partial C_{Pr}}{\partial x} \right) + 2 k_{ex} C_{Pr^{+}} C_{Pr^{-}}, (4.2.1c)$$

$$J_{+} = -D \left(\frac{\partial C_{+}}{\partial x} \right) - \frac{z_{+} F D C_{+}}{R T} \left(\frac{\partial \phi}{\partial x} \right), (4.2.1d)$$

$$J_{-} = -D \left(\frac{\partial C_{-}}{\partial x} \right) - \frac{z_{-} F D C_{-}}{R T} \left(\frac{\partial \phi}{\partial x} \right). (4.2.1e)$$

J are the fluxes, z are the charges, C are the concentrations, D are the diffusion coefficients, x is the distance, $\partial\phi/\partial x$ is the potential gradient, + and - stand for positive and negative counter-ions respectively; other terms have the conventional meanings. Note that the flux of the neutral polymer site, Pr, does not have the electric field term, as its movement is not influenced by the field.

Thus, we have three Eqs.(4.2.1a-c) to describe the transport of electrons (or holes) in the polymer, and the Eqs.(4.2.1d-e) for the counterionic transport. Besides these five equations, an equation for the potential gradient has also to be solved by iteration considering the unknown parameters: the local concentrations of the five transporting species, the diffusion coefficients of the individual species, the rate constant of the annihilation reaction and current.

The complexity of the system would render an exact solution of this diffusion-migration-reaction problem difficult. Starting from 1965, a few efforts were made to account for this migration of charges in polymers. The first one, in 1965, being that by Cohen and Cooley, who considered the migration of 'non-interacting' cations and anions in a non-conductive polymer phase under the conditions of a current step [89]. The other notable work in 1983 is by Yap et al., who did the simulations for potential step experiments [90]. Later T.R. Brumleve and R.P. Buck improved the model by considering the electroneutrality conditions in defining the concentration of different species in the polymer and

expressing the potential gradient inside the polymer film by Poisson's equation [91]. All these works were done by an implicit iterative procedure. Explicit definition of the potential drop inside the film is not possible as it depends on the concentration distribution of all the charged species inside the polymer, which makes this problem quite complicated. Hence, solving for the current, which in turn depends on the electric field in the polymer, cannot be accomplished reliably in the explicit method.

However, in 1988, the simulation of the experimental result, considering the concept of diffusion-migration was done by R. Lange and K. Doblhofer, by an iterative procedure [92,93]. The iterative procedure was used to analyze a system in which only two charged species were mobile, i.e., the reduction of Fe(CN)_6^{3-} redox ions in a polymer containing fixed positive charges to Fe(CN)_6^{4-} was considered. The local electroneutrality was maintained by these two negative ions and the immobile positive fixed charge of the polyvinylpyridinium polymer, as long as the concentration of the supporting electrolyte in the solution did not exceed 0.1 M. Thus, the complications due to counterion transport from the supporting electrolyte were avoided. Thus, the system is simpler than the one we have. In Fig. 4.2.1c [has been reproduced from 92] the current vs time^{-1/2} plot was simulated for two cases, (1) by considering diffusion-migration transport of these two ions in the polymer, (2) by considering just pure diffusion of these ions (Cottrell plot). It was found that the current holds the same dependence on $t^{-1/2}$, irrespective of the mode of transport process.

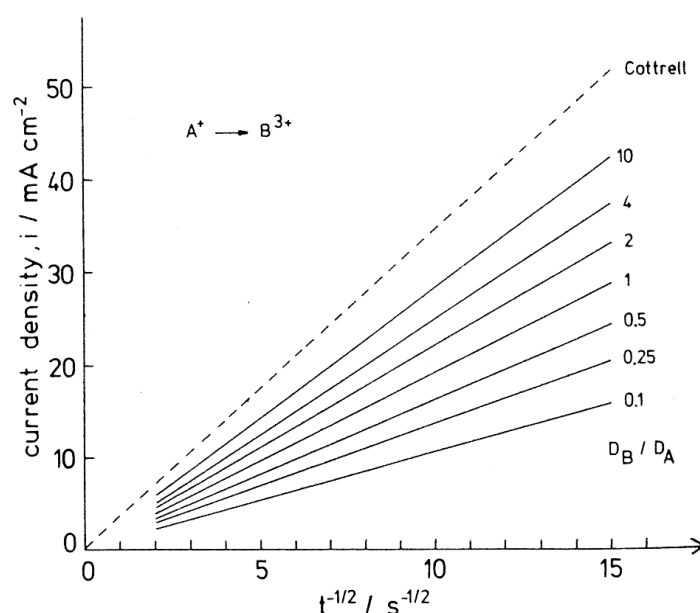


Fig. 4.2.1c: Plot of current density against $t^{-1/2}$ under diffusion-migration

conditions for the electrode reaction $A^+ \rightarrow B^{3+}$. The pure diffusion case (Cottrell) was included for comparison.

However, despite the fact that the value of the diffusion coefficient remains the same, the slopes of these plots differ from each other. Thus, charge transport inside the polymer can be approximately described by the diffusion process, but one must keep in mind that the diffusion coefficient derived from the simulations will also be approximate values.

In fact, in 1988, C.P. Andrieux and J.M. Savéant derived equations for the diffusion-migration in conducting polymers considering an electron-hopping mode of charge transport and reported that the Cottrell condition obeyed even in this case. They related the observed diffusion coefficient D_{ap} to the electron hopping diffusion coefficient D_E by the following equation:

$$D_{ap} = (\pi \Psi^2) D_E, \quad (4.2.1f)$$

where Ψ is a function which depends on the charge transfer parameters, diffusion coefficient of the mobile counterion, its charge and the number of electrons participating per electron hopping [94].

While the bulk electric field in the polymer phase is disregarded, the electric field created by the ions accelerates the slower moving charge and decelerates the faster one. Eventually both of them move at the same speed and the situation becomes the diffusion of a neutral entity. This kind of transport is termed as ambipolar diffusion in the literature [95]. For the movement of a negative polaron along the polymer coupled with that of the positive counterion from the supporting electrolyte, the observed diffusion coefficient is expressed as

$$D_{ap} = \frac{2D_{Pr^-} D_+}{D_{Pr^-} + D_+}. \quad (4.2.1g)$$

When the diffusivities of these two species differ considerably, the observed diffusion coefficient becomes that of the slowest moving species, in general that of the counterions. Thus, the simulation of the polymer system was conducted essentially in a way similar to the ECL in the solution phase system:

With these concepts in mind, it was considered that a procedure for analyzing the ECL potential step experiments should basically rely on a $t^{1/2}$ behavior. The underlying assumption is that the polarons are coupled to counterions by the condition of electroneutrality, i.e., they are moving as neutral ion pairs and follow as such the diffusion laws.

1. Initially the conducting polymer is in the neutral state with concentration of the active sites (Pr) as C° .
2. In the first potential step of duration t_f to a positive value, oxidation of Pr to $\text{Pr}^{+\cdot}$ takes place. Since it is a potential step experiment, the magnitude of the potential step was increased to a higher positive value ($E^{\circ'} + 250 \text{ mV}$) to ensure the kinetic feasibility of the electrode reaction (A). Therefore, the current in this step is controlled by the transport of the Pr towards the electrode and $\text{Pr}^{+\cdot}$ away from the electrode which can be described by Fick's second law.

$$\left(\frac{\partial C_{\text{Pr}}}{\partial t} \right) = D_{\text{ap}} \left(\frac{\partial^2 C_{\text{Pr}}}{\partial x^2} \right) \quad (4.2.1h)$$

and

$$\left(\frac{\partial C_{\text{Pr}^{+\cdot}}}{\partial t} \right) = D_{\text{ap}} \left(\frac{\partial^2 C_{\text{Pr}^{+\cdot}}}{\partial x^2} \right), \quad (4.2.1i)$$

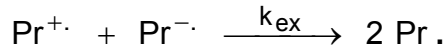
where D are the diffusion coefficients, C_{Pr} and $C_{\text{Pr}^{+\cdot}}$ are the concentrations of the neutral and oxidized species, respectively, and x is the distance. Concentration profiles of, e.g., the neutral species can be obtained by solving the linear Eq. (4.2.1h).

$$C_{\text{Pr}}(x,t) = C^\circ \operatorname{erf} \left[\frac{x}{2(D_{\text{ap}} t)^{1/2}} \right]. \quad (4.2.1j)$$

The concentration distribution of the positive polaron can then be calculated by applying the condition $C_{\text{Pr}}(x,t) + C_{\text{Pr}^{+\cdot}}(x,t) = C^\circ$.

3. When the potential was stepped to a negative value ($E^{\circ'} - 250 \text{ mV}$) of duration t_r , there will be the formation of the negative polaron $\text{Pr}^{-\cdot}$. (b). Now Pr and $\text{Pr}^{+\cdot}$ will be transported towards the electrode and $\text{Pr}^{-\cdot}$ away from the electrode.

When both $\text{Pr}^{\cdot-}$ and $\text{Pr}^{\cdot+}$ meet with each other, there will be the bimolecular annihilation reaction (C) giving rise to luminescence. since the luminescence process is considered to be instantaneous in the time scale of the experiment, i.e., Eq.(C) will be modified as



Therefore, the following equations have to be solved to describe the kinetics and concentration profiles in the second potential step (B).

$$\left(\frac{\partial C_{\text{Pr}}}{\partial t} \right) = - D_{\text{ap}} \left(\frac{\partial^2 C_{\text{Pr}}}{\partial x^2} \right) + 2 k_{\text{ex}} C_{\text{Pr}^{\cdot+}} C_{\text{Pr}^{\cdot-}}, \quad (4.2.1k)$$

$$\left(\frac{\partial C_{\text{Pr}^{\cdot+}}}{\partial t} \right) = - D_{\text{ap}} \left(\frac{\partial^2 C_{\text{Pr}^{\cdot+}}}{\partial x^2} \right) - k_{\text{ex}} C_{\text{Pr}^{\cdot+}} C_{\text{Pr}^{\cdot-}}, \quad (4.2.1l)$$

$$\left(\frac{\partial C_{\text{Pr}^{\cdot-}}}{\partial t} \right) = - D_{\text{ap}} \left(\frac{\partial^2 C_{\text{Pr}^{\cdot-}}}{\partial x^2} \right) - k_{\text{ex}} C_{\text{Pr}^{\cdot+}} C_{\text{Pr}^{\cdot-}}. \quad (4.2.1m)$$

4.2.2. Double layer charging

The double layer charging phenomena in the electrode/polymer/solution system is considered on the same grounds as in the case of solution ECL. The difference lies in the larger value for the time constant $R_u \cdot C_{\text{dl}} = \tau$, since the polymer network generally offers a larger resistance for the transport of ions through it, which are necessary for charging the double layer at the electrode/polymer interface.

4.2.3. Digital simulation technique

The point model was considered for the simulation of the ECL transient, which was discussed in detail in section 4.1.3 while dealing with the solution ECL. The partial differential Eqs.(4.2.1k-m) are expressed in the finite difference forms as discussed there.

4.2.4. Conditions for simulation

Time is denoted by the vector 'k' (= $t/\Delta t$) and distance by 'i' (= $x/\Delta x$). Initially the conducting polymer consists of the active sites Pr in the neutral state. The point k = 0 represents the time from the point of application of the first potential step (in our case the positive potential step) until the time prior to the application of the second one. The concentrations of the species $\text{Pr}^{\cdot+}$ and Pr are obtained by using the error functions (see Eq.(4.2.1j)). The concentration of the negative species, $\text{Pr}^{\cdot-}$ is zero during this interval. The maximum value of the 'i' vector is calculated using the expression $i_{\max} = (2 D_M k_{\max})^{1/2}$. The concentration array is constructed until $i > i_{\max}$.

The point k =1 represents the time of the application of the second potential step, i.e., k =1 implies $t_r > 0$ where t_r denotes the duration of the second potential step. The concentrations of the different species at the electrode surface ($i = 0$) are fixed by the Nernst equation.

$$\frac{[\text{Ox}]}{[\text{Red}]} = \exp\left(\frac{nF}{RT} (E - E^{\circ'})\right). \quad (4.2.4a)$$

The concentrations for $i > 0$ are assumed to have the same values fixed in the earlier time, i.e., the concentrations calculated using the error function at k = 0. The transport-reaction process is allowed to occur from k =1 to k_{\max} , and for each value of k, the value of i_{\max} is calculated as described earlier. This simulation yields the profiles of concentration-time and concentration-distance.

Since the luminescence decay is assumed to be instantaneous, the concentration-time profile of $0.5 C_{\text{Pr}}$ can represent the luminescence transient. The current transient is calculated as follows:

$$j_F = F \sum z_n J_n, \quad (4.2.4b)$$

where ' j_F ' represents the faradaic current density, F is the Faraday's constant, J is the flux of the species, z is the charge of the same, 'n' denotes the number of electroactive species. Since the simulation is done for the second potential step, the faradaic reaction of interest, in the present case, is the conversion of

Pr^+ to Pr^- and Pr to Pr^- . Hence, the current density can be represented as follows:

$$j = F \{ z_{\text{Pr}^+} J_{\text{Pr}^+} + z_{\text{Pr}^-} J_{\text{Pr}^-} \}. \quad (4.2.4c)$$

For the system under consideration, the flux balance equation can be written as $J_{\text{Pr}} + J_{\text{Pr}^+} + J_{\text{Pr}^-} = 0$. By making use of this condition and Fick's first law, the final expression for the current density is obtained as follows:

$$\frac{j}{F} = 2 D_{\text{ap}} \left\{ \frac{C_{\text{Pr}^+}(i=1) - C_{\text{Pr}^+}(i=0)}{\Delta x} \right\} + D_{\text{ap}} \left\{ \frac{C_{\text{Pr}}(i=1) - C_{\text{Pr}}(i=0)}{\Delta x} \right\} \quad (4.2.4d)$$

4.2.5. Inclusion of the IR drop in the conducting polymer and double layer charging at the electrode/polymer interface

Due to the charging process of the electrochemical interface (metal/polymer) during the initial stages of the potential step (few milliseconds), the applied potential does not reach its final value at the same time as that of its application, but after a certain time lag, which can be represented as follows:

$$E_{\text{CT}}(t) = E_{\text{Final}} \left\{ 1 - \exp \left(- \frac{t}{R_u C_{\text{dl}}} \right) \right\} \quad (4.2.5a)$$

The effective electrode potential at a time $t + \Delta t$ can be calculated from its value at the previous time t by the empirical relationship,

$$E_{\text{CT}}(t + \Delta t) = E_{\text{CT}}(t) + \Delta E_{\text{CT}}. \quad (4.2.5b)$$

The double layer charging current can be calculated by the following relationship,

$$i_{\text{C}}(t) = [(E_{\text{Final}} - E_{\text{CT}})/R_u - i_{\text{F}}]. \quad (4.2.5c)$$

Thus, Eq.(4.2.5b) can be rewritten as follows:

$$E_{\text{CT}}(t + \Delta t) = E_{\text{CT}}(t) + \left\{ \frac{E_{\text{Final}} - E_{\text{CT}}(t)}{R_u} - j_{\text{F}} A \right\} \frac{\Delta t}{C_{\text{dl}}}. \quad (4.2.6d)$$

4.2.6 Simulation of the experimental transients of MEH-PPV

The parameters apparent diffusion coefficient D_{ap} , uncompensated solution resistance R_u and double layer capacitance C_{dl} were evaluated as discussed in chapter 3.2. The concentration C° was calculated from the molecular weight and dry thickness of the polymer. The value of Δx was calculated after fixing D_M as 0.45 and by using the relationship $D_M = D_{ap}\Delta t / \Delta x^2$. The simulation was repeated until the calculated current agreed with the experimental current in magnitude, and experimental and simulated ECL transients were of the same shape. The value of k_{ex} corresponding to the coincidence of experimental and simulated transients was taken as the one for the annihilation reaction (D) between the positive and negative polarons. Following are the results of simulation of the cathodic and anodic ECL transients of MEH-PPV in 0.1 M TEAClO₄ and 0.1 M TEAPF₆.

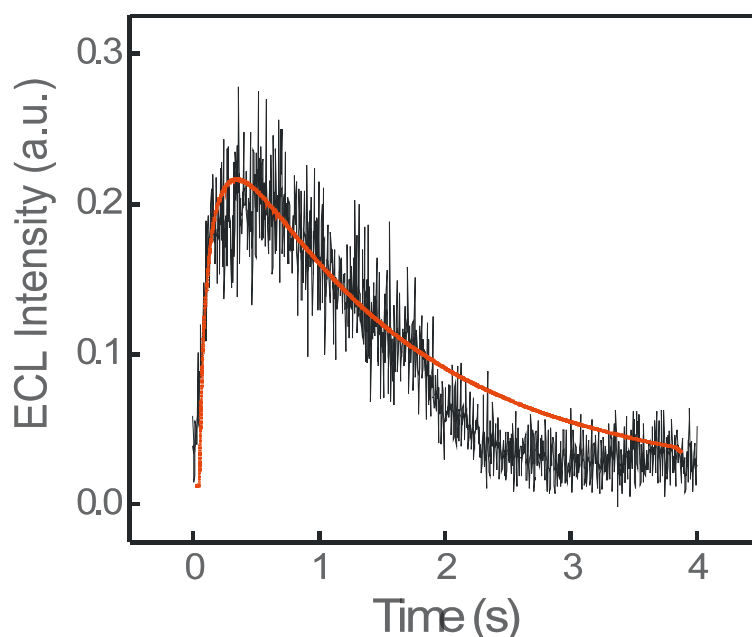


Fig 4.2.6a. Simulation of the anodic transient (for a potential step between -1.75 V and 1.45 V, SE - 0.1M TEABF₄) with $C^\circ = 5.8 \times 10^{-4} \text{ mol cm}^{-3}$, $k_{ex} = 1 \times 10^3 \text{ l mol}^{-1} \text{ s}^{-1}$, $D_{ap} = 3.2 \times 10^{-12} \text{ cm}^2 \text{ s}^{-1}$, $R_u = 1 \times 10^4 \text{ } \Omega$ and $C_{dl} = 1 \text{ } \mu\text{F}$.

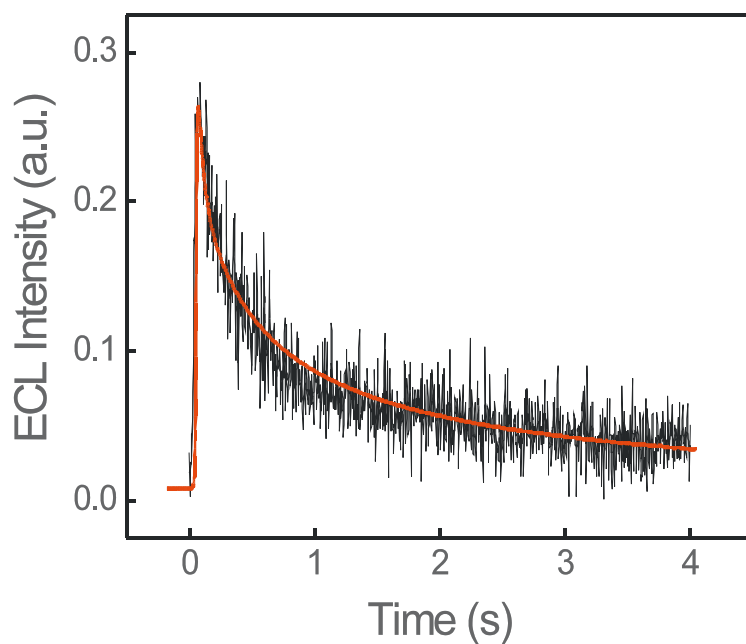


Fig 4.2.6b. Simulation of the cathodic transient (for a potential step between 1.45 V and -1.75 V, SE - 0.1M TEABF₄) with $C^\circ = 5.8 \times 10^{-4} \text{ mol cm}^{-3}$, $k_{\text{ex}} = 3 \times 10^3 \text{ l mol}^{-1} \text{ s}^{-1}$, $D_{\text{ap}} = 8 \times 10^{-13} \text{ cm}^2 \text{ s}^{-1}$, $R_u = 1 \times 10^4 \Omega$ and $C_{\text{dl}} = 2 \mu\text{F}$.

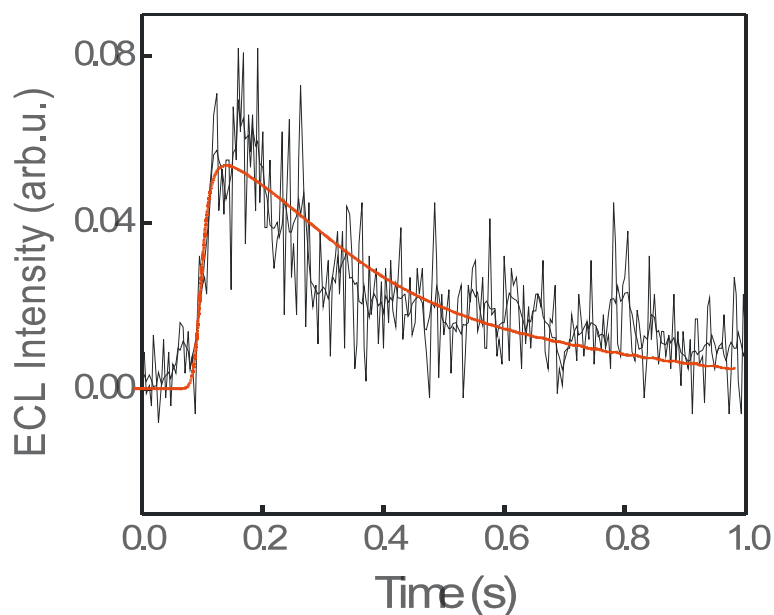


Fig. 4.2.6c. Simulation of the anodic transient (for a potential step between -1.85 V and 1.35 V, SE - 0.1M TEAPF₆) with $C^\circ = 5.8 \times 10^{-4} \text{ mol cm}^{-3}$, $k_{\text{ex}} = 6 \times 10^3 \text{ l mol}^{-1} \text{ s}^{-1}$, $D_{\text{ap}} = 0.5 \times 10^{-12} \text{ cm}^2 \text{ s}^{-1}$, $R_u = 1 \times 10^4 \Omega$ and $C_{\text{dl}} = 5 \mu\text{F}$.

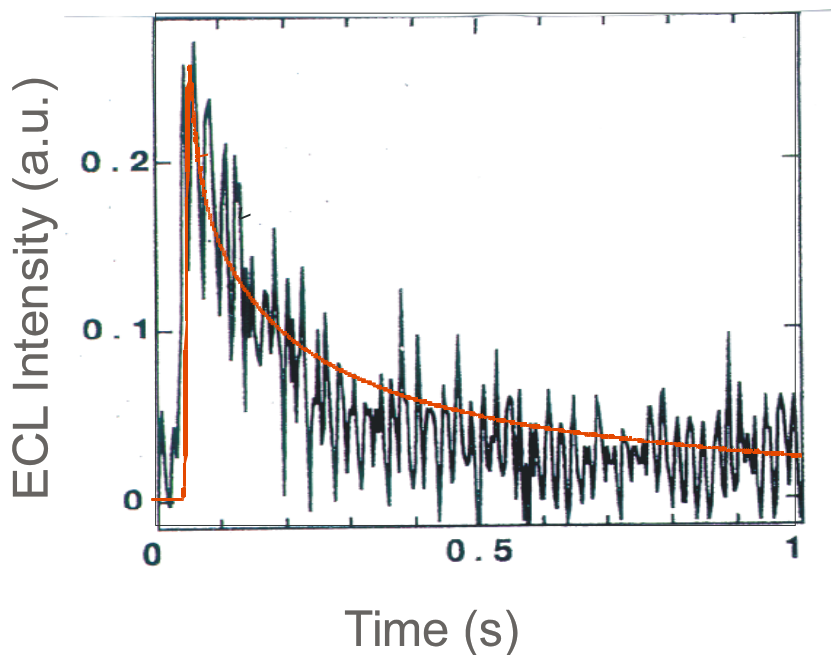


Fig 4.2.6d. Simulation of the cathodic transient (for a potential step between 1.35 V and -1.85 V, SE - 0.1M TEAPF₆) with $C^\circ = 5.8 \times 10^{-4} \text{ mol cm}^{-3}$, $k_{\text{ex}} = 5 \times 10^3 \text{ l mol}^{-1} \text{ s}^{-1}$, $D_{\text{ap}} = 1.5 \times 10^{-13} \text{ cm}^2 \text{ s}^{-1}$, $R_u = 1 \times 10^4 \Omega$ and $C_{\text{dl}} = 6 \mu\text{F}$.

When the values of the diffusion coefficients are compared between the ECL transients with 0.1 M TEABF₄ and 0.1 M TEAPF₆, they are slightly lower with the latter. This could be due to the larger size of the PF₆⁻ than that of the BF₄⁻. Though the difference is not very appreciable, the difference could be attributed to the difficulty for transportation of the PF₆⁻ ion inside the polymer. This is based on the experimental result (CV) that MEH-PPV cannot be reduced in 0.1 M TBABF₄ due to the larger size of the TBA⁺ ions that are required for the reduction reaction (section 3.2.2). The value of rate constant k_{ex} is of the order of $10^4 \text{ l mol}^{-1} \text{ s}^{-1}$ in all the cases except with the anodic ECL in 0.1 M TEABF₄ that is $10^1 \text{ l mol}^{-1} \text{ s}^{-1}$, the reason of which is hard to speculate. Nevertheless, the magnitudes are lower than that in the solution phase, cf. DPA, which is on the order of $10^{10} \text{ l mol}^{-1} \text{ s}^{-1}$. This could be due to the larger internuclear separation between the electron transfer sites in the polymer, which can be inferred from the following equation proposed by Marcus for electron transfer reaction kinetics [96]:

$$k_{\text{ex}} = A \exp \left[- \left(\frac{Ne^2}{16\pi\epsilon_0} \right) \left(\frac{1}{a} - \frac{1}{R_h} \right) \left(\frac{1}{\epsilon_{\text{op}}} - \frac{1}{\epsilon_s} \right) / kT \right] \quad (4.2.5a)$$

Where k_{ex} stands for the electron transfer rate constant, A is the pre exponential factor, ϵ_0 is the permittivity of the free space, a is the distance between the edges of the reactant species, R_h is the inter nuclear separation, ϵ_{op} and ϵ_s are the optical and static dielectric constants of the solvent, and other terms have their conventional meanings. The larger the sizes of the reactant species, a will be smaller and R_h will be larger, which will lead to a lower magnitude of k_{ex} . Thus, the lower magnitude of the rate constant for the annihilation reaction in the polymers can be understood.

4.3. Simulation of the experimental transients of DB-PPV

The discussion for the theoretical analysis of the electrogenerated chemiluminescence for DB-PPV is the same as that of MEH-PPV. The results are presented below.

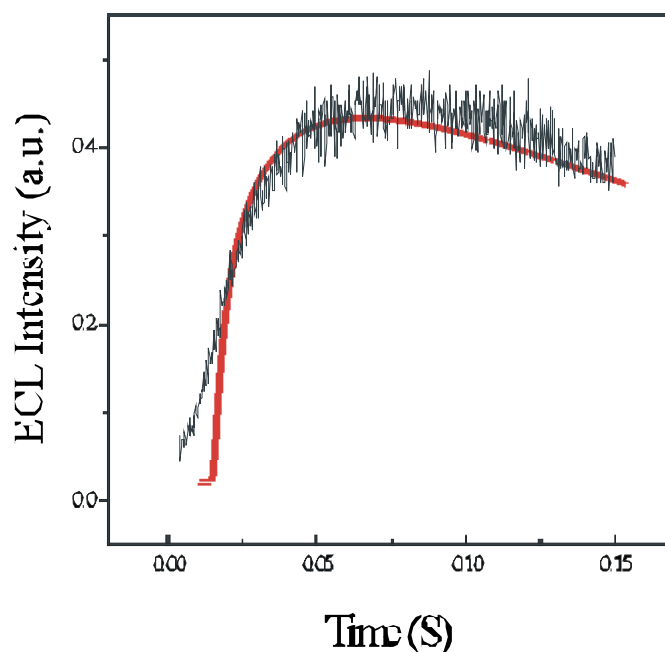


Fig. 4.3a. Simulation of the anodic ECL transient (for a potential step between -1.9 V and 1.3 V, SE - 0.1M TBABF₄) with $C^0 = 6.1 \times 10^{-4} \text{ mol cm}^{-3}$, $k_{\text{ex}} = 3 \times 10^4 \text{ l mol}^{-1} \text{ s}^{-1}$, $D_{\text{ap}} = 6 \times 10^{-11} \text{ cm}^2 \text{ s}^{-1}$, $R_u = 1200 \Omega$ and $C_{\text{dl}} = 1 \mu\text{F}$.

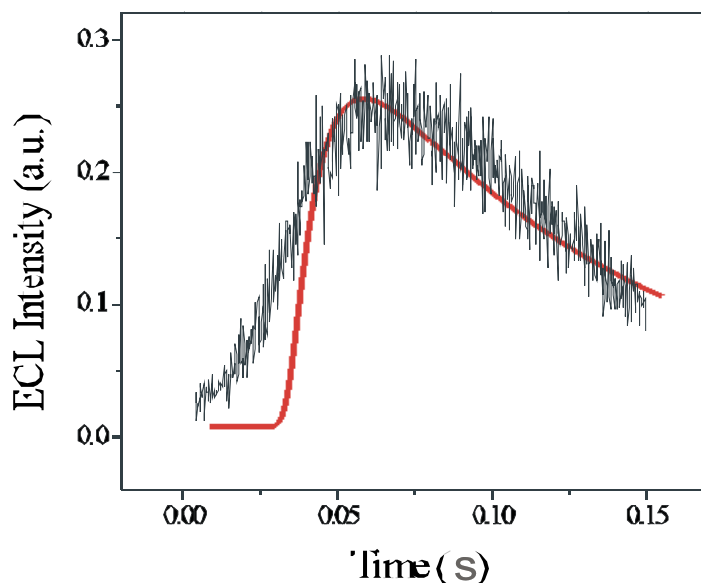


Fig. 4.3b. Simulation of the cathodic ECL transient (for a potential step between 1.3 V and -1.8 V, SE - 0.1M TBABF₄) with $C^\circ = 6.1 \times 10^{-4} \text{ mol cm}^{-3}$, $k_{\text{ex}} = 1 \times 10^4 \text{ l mol}^{-1} \text{ s}^{-1}$, $D_{\text{ap}} = 1 \times 10^{-11} \text{ cm}^2 \text{ s}^{-1}$, $R_u = 1200 \, \Omega$ and $C_{\text{dl}} = 3 \, \mu \text{ F}$.

The slow rise in the transients could not be explained by the concept of double layer charging alone. However, the progressive dissolution of polymer DB-PPV was not considered in the present simulation, as its exact mode is unknown. This could cause variation in the shape of the ECL transients due to the unequal and variable concentrations of the polarons. Also the kinetics of the transport and the annihilation reaction can change due to the disorders introduced by the dissolution. However, the values of the rate constants were calculated to be on the order $10^4 \text{ l mol}^{-1} \text{ s}^{-1}$. This is again lower than the annihilation rate constant in the solution phase. This is in accordance with the expectation for a disordered system such as a polymer phase in which the polarons are separated farther apart. (cf. discussion based on Marcus theory for electron transfer, section 4.2.5). The low magnitudes of the apparent diffusion coefficients ($10^{-11} \text{ cm}^2 \text{ s}^{-1}$) suggests that the transport is dominated by the counterion movement, as with the case of MEH-PPV. Thus the present theoretical simulation can explain the kinetics of ECL satisfactorily.

5. Summary, conclusions and outlook

ECL was generated both in the solution phase with DPA (9,10-diphenylanthracence) and in the polymer phase with PPV-derivative polymers. There are five major results from the present work. They are listed as follows.

5.1. Symmetrical ECL

In the literature on solution ECL, it has been widely reported that the emission intensity observed in the positive potential step, anodic ECL differs from that in the negative potential step, cathodic ECL (section 3.1.4). In our experiments we could observe equal intensities of anodic and cathodic ECLs by appropriately choosing the waiting period ' t_w '.

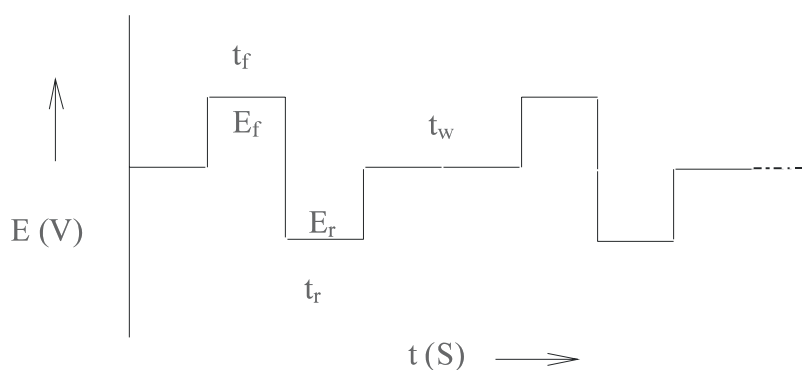


Fig. 5.1a. Typical shape of the triple potential steps including the waiting period t_w in the ECL experiments.

The longer the t_w , the better is the similarity. The potential of the pulse during t_w was kept at 0 V or -100 mV. The reasons for the improved performance can be attributed to the elimination of an adsorbed species on the electrode during the negative potential step. The adsorbate was speculated to be adsorbed hydrogen [65].

In the case of ECL with polymer-coated electrodes, symmetrical ECL has never been reported before. We did observe equal intensities from the conducting polymers MEH-PPV and DB-PPV with the proper choice of the potential step magnitude, the width and the waiting period. The absolute values of the potential steps were chosen to be larger than the absolute values of the

standard potentials for the reduction and oxidation of the polymer to ease the electrode reaction. But care was taken to avoid over oxidation or reduction leading to the formation of the bipolarons, which reduce the ECL intensity. Similarly in setting the width of the potential step, the time constant of the system ($R_u \times C_{dl} = \tau$) must be considered. Since R_u is larger in the polymers, it needs a longer time (≈ 100 ms) for charging the electrode/polymer interface compared to the case of DPA. On the other hand the thickness of the polaron diffusion layer in the polymer needs to be considered in choosing the potential step. A longer potential step width may lead to the thin layer effect in which the diffusion layer exceeds the polymer thickness (section 2.1.2i). It was found that the following values of t_w , t_f and t_r gave the most reproducible and symmetrical ECL transients. For DPA, $t_f = t_r = 50$ ms and $t_w = 200$ ms at 0 V. For DB-PPV, $t_f = t_r = 150$ ms and $t_w = 300$ ms at 0 V. The results were also obtained over a range of a waiting period, t_w ranging between 0.2 s and 1 s.

5.2. Stability of the polymers

The ECLs obtained from the conducting polymers, MEH-PPV (section 3.2) and DB-PPV (section 3.3) were less stable than that from the solution phase ECL of DPA. That is, when with DPA the triple potential steps were repeated, the intensity of the ECL remained the same for a number of cycles. Whereas in the case of conducting polymers the intensities were lower than that of the DPA ECL and also decreased by approximately 50 % within 10 cycles. Dissolution of the polymer was observed from the microscopic images of the polymer coated electrode surfaces before and after the ECL experiment. Dissolution has also been reported in the literature [1]. To avoid that, as a first approach, cross linking of the polymer DB-PPV was done by subjecting the polymer to synchrotron radiation of appropriate energy (section 3.3.5). The microscopic investigation revealed that the cross-linked polymer was quite stable under electrochemical conditions. But the observation of ECL has become more difficult than that for the un-cross linked DB-PPV. The cyclic voltammograms showed that the counterionic transport in the cross-linked film has become difficult, both for its oxidation and reduction. Thus, ECL could not be observed with heavily cross-linked film, which in our case was 500 mJ/cm^2 . However, it could be observed, when the cross linking was done with the radiation energy

100-300 mJ/cm² in the case of TEABF₄ as the supporting electrolyte. But still, the intensity was low and decreased faster than the solution phase ECL. So the possibility of a decomposition reaction in addition to the dissolution was considered.

Spectroscopic analysis was done to understand the cause and kind of the decomposition. Ex-situ Raman spectroscopic investigation was carried out on the DB-PPV polymer first. After that the film has been casted on the electrode, then after subjecting it to a synchrotron cross-linking procedure and finally after the ECL reaction. The Raman spectra of the polymer were the same in all the cases except after the ECL reaction. This shows that the polymer retains its chemical characteristics in the film casting and the synchrotron cross-linking procedure, but it becomes affected in the experimental procedures for ECL. Further analysis was done by subjecting the polymer-coated electrode to negative potential cycling and positive cycling independently. The cyclic voltammogram (CV) showed that DB-PPV is stable in the negative potential region over a number of potential cycles. Whereas in the positive potential region, the first CV itself is less reversible than the negative potential behavior and subsequent CVs showed more irreversible behavior, and a rapid decrease in the peak maximum for oxidation (i_{pa}). Thus, the decomposition of the polymer is found to happen while subjecting the polymer to a positive potential sweep/step. These analyses concerning the stability of the polymer are the first ones in the study of ECL from the conducting polymer, and the results are going to be communicated [97].

5.3. Influence of counterions

The nature and size of the counterions affect the oxidation/reduction of the conducting polymers. It is found that TEABF₄ or TBABF₄ are better supporting electrolytes yielding more intense and reproducible ECLs than TEAClO₄ or TBAClO₄. This is likely to be due to the hygroscopic nature of the perchlorates, introducing traces of water into the electrolyte.

In addition, the size of the counterions also play a major role on the electrochemistry of CPs. These counterions are needed for maintaining charge

neutrality in the CPs during electrochemical oxidation and reduction processes. Thus, the larger the counterion, the more difficult becomes its movement inside the CP and, hence, the electrode reaction. In the experiment with a MEH-PPV film coated electrode, the polymer could be oxidized and reduced with TEABF₄, but could not be reduced at all with TBABF₄ due to the larger size of the TBA⁺ cation compared to the TEA⁺ cation, which is needed for charge compensation during reduction of the polymer (section 3.2.2).

However, the TBABF₄ gave better results for the DB-PPV polymer. This is due to the difference in the molecular structure between MEH-PPV and DB-PPV. DB-PPV has two butoxy groups in the adjacent position, which produces more strain in the polymer due to steric hindrance. Thus, the DB-PPV film is less uniform than the MEH-PPV film having the two alkoxy substituents at the sterically favored opposite ends (section 3.3.5).

Even in the case of the DB-PPV films the counterionic mobility depends strongly on the degree of cross-linking. The film cross-linked with 500 mJ/cm² energy of synchrotron radiation cannot be oxidized or reduced appreciably. Whereas the less cross-linked films (when the synchrotron energy is between 100-300 mJ/cm²), can become oxidized or reduced effectively (section 3.3.2).

5.4. Kinetics of the ECL process

Since the ECL process in the conducting polymers yields more difficulty than that in the solution phase, a quantitative study has never been carried out in the literature. This task has been undertaken for the first time in the present work. The diffusion-migration mode of charge transport in the CPs is approximated by a diffusion model, which implicitly takes into account the migration process by considering the electrode/polymer interface charging process (sections 4.2.1 - 4.2.4). Digital simulation technique has been used to solve the kinetic equations and to estimate the rate parameters.

Initial evaluations of the parameters for the simulation like, concentration of the active polymer sites, uncompensated resistance of the electrochemical system, double layer capacitance, and apparent diffusion coefficients are estimated from

different appropriate experiments. First the simulation has been carried out for DPA ECL, and the rate constant was found out to be on the order of $10^{10} \text{ l mol}^{-1} \text{ s}^{-1}$, which is consistent with earlier theoretical studies of the solution phase ECL. Then the simulation was performed for the MEH-PPV polymer, yielding a value of $10^3 \text{ l mol}^{-1} \text{ s}^{-1}$ for the rate constant. In the case of DB-PPV polymer it is $10^4 \text{ l mol}^{-1} \text{ s}^{-1}$. The low value of the ECL reaction rate constant in the conducting polymers compared to the solution phase has been analyzed based on the Marcus theory (section 4.2.5). It was concluded that the small rate constants are caused by the relatively larger internuclear distance between the positive and negative polarons in the activated complex.

Though the intensity maxima of the anodic and cathodic ECLs are similar in MEH-PPV and DB-PPV, the decay kinetics are strikingly different. This feature has been found to be associated with the nature of the charge compensating counterion in the anodic and cathodic ECLs. The apparent diffusion coefficients have been found to be on the orders of $10^{-13} \text{ cm}^2 \text{ s}^{-1}$ for MEH-PPV and $10^{-11} \text{ cm}^2 \text{ s}^{-1}$ for DB-PPV. Such a low value cannot be attributed to the electron drift mode of the charge transport. Thus, the electron transport in these two polymers under ECL experimental condition must be coupled to the movement of the counterions. This is another important conclusion from the present theoretical studies. Parts of the results have been published in the Synthetic Metals [98] and in the ACS Proceedings [99].

5.5. Mechanism of ECL in PPV type polymers

The intensity of the ECL from DB-PPV is found to be 100 times higher than that from MEH-PPV. In the earlier solid-state electroluminescence (EL) studies, this has been attributed to the stabilization of the excited state in DB-PPV by the strain introduced into the polymer chain by the ortho substitution (section 3.3.5). This strain yields the loss of co planarity between the polymer backbone and the side groups. Thus, excited state deactivation by the oxygen lone pair of butoxy groups on the PPV moiety was avoided.

Hence, ECL from DB-PPV has been chosen for analysis of the ECL emission spectra. Anodic and cathodic ECLs were recorded and were found to occur at

the same wavelength (485 nm), i.e., the two modes of ECL generation yield the same excited state. This again becomes a proof that this annihilation reaction between positive and negative polarons is the only cause for the observation of ECL in DB-PPV. The ECL spectrum is identical with the solution phase luminescence spectrum in CHCl_3 . Further comparison with solid-state photoluminescence (PL) and electroluminescence (EL) showed an insignificant shift of 25 nm. In fact, the π - π^* emission band in the case of a conjugated network as the present polymer is known to show a weak environmental effect [84].

5.6. Outlook

Further analysis can be carried out in the direction of studying the orientation effect of the conjugated bonds of the conducting polymers by choosing different deposition methods like electrodeposition, Langmuir-Blodgett (LB) coating, vapor deposition and spin casting. The conjugated bonds can be oriented either parallel or perpendicular to electrode surfaces [100], which can affect the extension of the polarons and excitons in the CP. In situ FTIR studies can be done to study the exact mechanism of chemical deactivation of the conducting polymer during ECL reaction. From the theoretical point of view, migration of charges and counterions can be involved explicitly, and its effect can be analyzed on the ECL transient.

6. Literature

1. M.M. Richter, F.R.F. Fan, F. Klavetter, A.J. Heeger, A.J. Bard: Chem. Phys. Lett. 226, 1994, S. 115,
2. IUPAC Compendium of Chemical Technology. ECL stands for electrogenerated chemiluminescence or electrochemiluminescence; Band 68. 2 1996 S. 2238,
3. H. Nambu, M. Hamaguchi, K. Yoshino: J. Appl. Phys. 82, 1997, S. 1847.,
4. M. Hamaguchi, H. Nambu, K. Yoshino: Jpn. J. Appl. Phys., 36, 1997, S. L124.,
5. D. Dini, R.E. Martin and A.B. Holmes: Adv. Funct. Mater. 12, 2002, S. 299,
6. I. Prieto, J. Teetsov, M.A. Fox, D.A.V. Bout and A.J. Bard: J. Phys. Chem.A., 105, 2001, S. 520.,
7. N.R. Armstrong, R.M. Wightman and E.M. Gross: Annu. Rev. Phys. Chem., 52, 2001, S. 391.,
8. U. Mitschke and P. Bäuerle: J. Mater. Chem., 10, 2000, S. 1471.,
9. D. M. Hercules: Science., 145, 1964, S. 808.,
10. E.A. Chandross, J.W. Longworth and R.E. Visco: J. Am. Chem. Soc., 87, 1965, S. 3259.,
11. A. Zweig, D.L. Maricle, J.S. Brinen and A.H. Maurer: J. Am. Chem. Soc., 89, 1967, S. 473.,
12. A. Zweig, A.K. Hoffmann, K.L. Marice and A. Maurer: Chem. Comm. (London), 1967, S.106.,
13. R.A. Marcus: J. Chem. Phys., 43, 1965, S. 2654.,
14. G.J. Hoijtink: Ind. Chim. Belge, 12, 1963, S. 1871.,
15. W.A. Gibbons, G. Porter and M. Savadatti: Nature Lond., 206, 1965, S. 1355.,
16. M.E. Peover In: Electroanalytical Chemistry, A.J. Bard, Ed., Vol 2, Chap1, M. Dekker, New York, 1967.
17. C.A. Parker: Proc. R. Soc., A276, 1963, S. 125.,
18. S.W. Feldberg: J. Am. Chem. Soc., 88, 1966, S. 390.,
19. S.W. Feldberg: J. Phys. Chem., 70, 1966, S. 3928.,
20. R.C. Johnson, R.E. Merrifield, P. Avakian and R.B. Flippen: Phys. Rev. Lett., 19, 1967, S. 285.,
21. P. Avakian and R.E. Merrifield: Mol. Cryst., 5, 1968, S. 37.,

22. L.R. Faulkner and A.J. Bard: J. Am. Chem. Soc., *91*, 1969, S. 209.,
23. J.T. Maloy and A.J. Bard: J. Am. Chem. Soc., *93*, 1971, S. 5968.,
24. R.E. Merrifield: J. Chem Phys., *48*, 1968, S. 4318.,
25. D.J. Freed and L.R. Faulkner: J. Am. Chem. Soc., *93*, 1971, S. 2097.,
26. D.J. Freed and L.R. Faulkner: J. Am. Chem. Soc., *93*, 1971, S. 3565.,
27. A. Suna: Phys. Rev. B, *1*, 1970, S. 1716.,
28. D.L. Maricle and A. Maurer: J. Am. Chem. Soc., *89*, 1967, S. 188.,
29. E.A. Mayeda and A.J. Bard: J. Am. Chem. Soc., *95*, 1973, S. 6223.,
30. A.J. Bard: Pure Appl. Chem., *25*, 1971, S. 379.,
31. C.K. Mann In:: Electroanalytical Chemistry. *Vol. 2, Chap. 2*, 1969, M. Dekker. New York, M. Dekker, 1969.
32. H.O. House, E. Feng and N.P. Peet: J. Org. Chem., *36*, 1971, S. 2371.,
33. K. Gurunathan, A.V. Murugan, and R. Marimuthu, U.P. Mulik and D.P. Amalnerkar: Mater. Chem. Phys., *61*, 1999, S. 173.,
34. J.F. Robinson: ACS Sym. Ser., *832*, 2003, S. 2.,
35. E.W.H. Jager, E. Smela, O. Inganas: Science, *290*, 2000, S. 1540.,
36. H. Kuzmany, M. Mehring and S. Roth, Eds.: Basic Models and Applications, Band Vol. 3, *Springer*, 1989, Berlin., Springer, Berlin. 1989.
37. J.G. Kiess, Ed., In:: Conjugated Conducting Polymers, *Springer*, 1992, Berlin., Springer, Berlin. 1992.
38. W. -P. Su, J.R. Schrieffer and A.J. Heeger: Phys. Rev. Lett., *42*, 1979, S. 1698.,
39. S. Brazovskii and N. Kirova: JEPT Lett., *33*, 1981, S. 4.,
40. K. Feeser, A.R. Bishop, and D.K. Campbell: Phys. Rev. B., *27*, 1983, S. 4804.,
41. R.H. Friend, D.D.C. Bradley and P.D. Townsend: J. Phys. D: Appl. Phys., *20*, 1987, S. 1367.,
42. J.L. Bredas, R.R. Chance and R. Silbey: Phys. Rev. B., *26*, 1982, S. 5843.,
43. J. -L. Bredas, B. Themans, J.G. Fripiat, J.M. Andre and R.R. Chance: Phys. Rev. B., *29*, 1984, S. 6761.,
44. Z.G. Soos, D.S. Galvao and S. Etemad: Adv. Mater., *6*, 1994, S. 280.,
45. D. Emin: Phys. Rev., *33*, 1986, S. 3973.,
46. Z. Shuai, J.-L. Bredas and W.P. Su: Chem. Phys. Lett., *228*, 1994, S. 301.,

47. M. Zheng, A.M. Sarker, E.E. Gürel, P.M. Lahti and F.E. Karasz: *Macromolecules*, **33**, 2000, S. 7426.,
48. J.H. Burroughes, D.D.C. Bradley, A.R. Brown, R.N. Marks, K. Mackay, R.H. Friend, P.L. Burn and A.B. Holmes: *Nature*, **347**, 1990, S. 539.,
49. N.C. Greenham, R.H. Friend and D.D.C. Bradley: *Adv. Mater.*, **6**, 1994, S. 491.,
50. D. Braun and A.J. Heeger: *Appl. Phys. Lett.*, **58**, 1991, S. 1982.,
51. A.J. Bard and L.R. Faulkner In:: *Electrochemical Methods Fundamentals and Applications*, . 136., 1980, John Wiley & Sons, Chap. 5, 1980, S. 136.,
52. W. Richtering and K. Doblhofer: *Electrochim. Acta*, **34**, 1989, S. 1685.,
53. M. Orlick, J. Rosenmund, K. Doblhofer, G. Ertl: *J. Phys. Chem. B.*, **102**, 1998, S. 1397.,
54. E.D. Olsen In:: *Modern Optical Methods of Analysis*. **315**, 1975, Chap. 6.
55. H. Winick In:: *Synchrotron Radiation Research*, **12**, 1980, Plenum Press, Chap. 2, 1980, S. 12.,
56. R. Bezman and L.R. Faulkner: *J. Am. Chem. Soc.*, **95**, 1973, S. 3083.,
57. J. Rosenmund and K. Doblhofer: *J. Electroanal. Chem.*, **396**, 1995, S. 77.,
58. L.R. Faulkner, H. Tachikawa and A.J. Bard: *J. Am. Chem. Soc.*, **94**, 1972, S. 691.,
59. R. Bezman and L.R. Faulkner: *J. Am. Chem. Soc.*, 1972, **94**, S. 6317.,
60. J. D. Luttmmer and A.J. Bard: *J. Phys. Chem.*, 1981, **85**, S. 1155.,
61. R.S. Glass and L.R. Faulkner: *J. Phys. Chem.*, 1981, **85**, S. 1160.,
62. J.T. Maloy and A.J. Bard: *J. Am. Chem. Soc.*, 1971, **93**, S. 5968.,
63. L.R. Faulkner, : *J. Electrochem. Soc.*, 1977, **124**, S. 1724.,
64. J. Kim and L.R. Faulkner: *J. Electroanal. Chem.*, 1988, **242**, S. 107.,
65. J. Kim and L.R. Faulkner: *J. Electroanal. Chem.*, 1988, **242**, S. 123.,
66. M.M. Collinson and R.M: Wightman: *J. Phys. Chem.*, 1994, **98**, S. 11942.,
67. S. Pons and S.B. Khoo: *J. Am. Chem. Soc.*, 1982, **104**, S. 3845.,
67. S. Pons and S.B. Khoo: *J. Am. Chem. Soc.*, 1982, **104**, S. 3845.,
68. J. Kim and L.R. Faulkner: *Anal. Chem.*, 1984, **56**, S. 874.,
69. A. Zweig In:: *Advances in Photochemistry*, Band 6. 1968, 1968. S. 425.,
70. R.E. Visco and E.A. Chandross: *Electrochim. acta*, 1968, **13**, S. 1187.,

71. K.M. Maness, J.E. Bartelt and R.M. Wightman: J. Phys. Chem., 1994, 98, S. 3993.,
72. K. Itoh, K. Honda and M. Sukigara: Electrochim. acta, 1979, 24, S. 1195.,
73. R. P. Van Duyne and S.F. Fischer: Chem. Phys., 1974, 5, S. 183.,
74. D.D.C. Bradley, R.H. Friend: J. Phys.: Condensed Matter, 1989, 1, S. 3671.,
74. D.D.C. Bradley, R.H. Friend: J. Phys.: Condensed Matter, 1989, 1, S. 3671.,
75. F. Mohammad: Synth. Met., 1999, 99, S. 149.,
76. H. Braun, F. Decker, K. Doblhofer and H. Sotobayashi: Ber. Bunsenges. Phys. Chem., 1984, 88, S. 345.,
77. M. Baitoul, J. Wery, J.-P. Buisson, G. Arbuckle, H. Shah, S. Lefrant, M. Hamdome: Polymer, 2000, 41, S. 6955.,
78. M. Baitoul, J.P. Buisson, S. Lefrant, B. Dulieu, J. Wery and M. Lapkowski, : Synthetic Met., 1997, 84, S. 623.,
79. F. Cacialli, B.S. Chuah, J.S. Kim, D.A. dos Santos, R.H. Friend, S.C. Moratti, A.B. Holmes, J. Bredas: Synthetic Met., 1999, 102, S. 924.,
80. D. Neher, J. Grüner, V. Cimrova, W. Schmidt, R. Rulkens and U. Lauter: Polym. Adv. Technol., 1998, 9, S. 461.,
81. F. Cacialli, B.S. Chuah, R.H. Friend, S.C. Moratti, A.B. Holmes: Synthetic Met., 2000, 111-112, S. 155.,
82. B.S. Chuah, F. Cacialli, J.E. Davies, N. Feeder, R.H. Friend, A.B. Holmes, E.A. Marseglia, S.C. Moratti, J.-L. Bredas, D.A. dos Santos, : Mat. Res. Soc. Symp. Proc., 1998, 488, S. 87.,
83. B.S. Chuah, F. Cacialli, D.A. dos Santos, N. Feeder, J.E. Davies, S.C. Moratti, A.B. Holmes, R.H. Friend, J.-L. Bredas: Synthetic Met., 1999, 102, S. 935.,
84. R.M. Silverstein and G.C. Bassler In:: Spectrometric Identification of Organic Compounds, II John Wiley & Sons, 1963. S. Chapter 5, 152.,
85. S.W. Feldberg In:: Electroanalytical Chemistry, Band Vol. 3. New York, M. Dekker, 1969 S. Chap. 4.,
86. D. Britz In:: Digital Simulation in Electrochemistry. II Springer-Verlag, 1988 S. Chap. 3,
87. N.A. Surridge, C.S. Sosnoff, R. Schmehl, J.S. Facci and R.W. Murray: J. Phys. Chem., 1994, 98, S. 917.,
88. J.M. Saveant: J. Electroanal. Chem., 1986, 201, S. 211.,

89. H. Cohen and J.W. Cooley: Biophysical Journal, 1965, 5, S. 145.,
90. W.T. Yap, R.A. Durst, E.A. Blubaugh and D.D. Blubaugh: J. Electroanal. Chem., 1983, 144, S. 69.,
91. T.R. Brumleve and R.P. Buck: J. Electroanal. Chem., 1978, 90, S. 1.,
92. R. Lange and K. Doblhofer: J. Electroanal. Chem., 1987, 237, S. 13.,
93. R. Lange and K. Doblhofer: Ber. Bunsenges. Phys. Chem., 1988, 92, S. 578.,
94. C.P. Andrieux and J.M. Saveant: J. Phys. Chem., 1988, 92, S. 110.,
95. K. Doblhofer In.: The Electrochemistry of Novel Materials, VCH Publishers, 1994 S. Chap. 4, 159.,
96. R.A. Marcus: Ann. Rev. Phys. Chem., 1964, 15, S. 155.,
97. J. Umamaheswari, R.E. Martin, C. Fischmeister, A.B. Holmes, J. Piccardi and K. Doblhofer: to be communicated.
98. U. Janakiraman, D. Dini, A. Preusser, A.B. Holmes, R.E. Martin and K. Doblhofer: Synthetic Met., 2001, 121, S. 1685.,
99. Danilo Dini, Umamaheswari Janakiraman, Karl Doblhofer: Conducting Polymers and Polymer Electrolytes - From Biology to Photovoltaics. Hrsg.: J.F. Robinson and H.B. Mark: ACS Symposium Series, Band 832, 2003, S. 103.,
100. S. Hotta, Y. Ichino, Y. Yoshida and M. Yoshida: J. Phys. Chem. B., 2000, 104, S. 10316.

Table of Figures

Fig 1.2a: Scheme of potential energy surfaces for an electron transfer reaction. (5)

Fig. 1.2b: Molecular orbital representation of electron transfer reaction. (5)

Fig. 1.5a: Configuration of the exciton in PPV. (13)

Fig. 1.5b: Scheme of the valence and conduction bands of polarons and bipolarons. (14)

Fig. 1.5c: Ground and excited states of PPV polymer. (15)

Fig. 1.6a: Construction of a light emitting diode (LED). (17)

Fig. 1.6b: Absorption, photoluminescence (PL) and electroluminescence (EL) spectra of PPV. (18)

Fig. 2.1a: Scheme for controlled potential experiments. (20)

Fig. 2.1.1a. Triangular wave form of the potential in potential sweep techniques. (21)

Fig. 2.1.2a: Scheme of a single positive potential step. (23)

Fig. 2.1.2.b: Equivalent circuit description of an electrochemical system in the absence of electrode reaction. (25)

Fig.. 2.1.2.c: Equivalent circuit description of an electrochemical system in the presence of an electrochemical reaction. (26)

Fig. 2.2a: Scheme of the setup for the ECL experiment. (28)

Fig. 2.3a: Scheme of the interaction of radiation with energy levels of a substance. (30)

Fig. 2.3.3: Cross section of a photomultiplier tube. (33)

Fig. 3.1.2a: Cyclic voltammogram (CV) of Pt in 1mM DPA + 0.1M TBAClO₄ in acetonitrile at a scan rate of 100 mV/s. (37)

Fig. 3.1.3a: Cottrell plot for 1 mM DPA in 0.1 M TBAClO₄-AN when the potential step was made from 0 V to -1.95 V of duration 50 ms. (39)

Fig. 3.1.4a: Scheme of the sequential anodic and cathodic potential steps in ECL experiments. (39)

Fig. 3.1.4b: The potential step from E_f to E_r was made at time $t = 0$ from -1.9 V (E_f) to a positive (E_r) value given in the inset. $t_f, t_r = 0.05$ s and $t_w = 0.2$ s. (40)

Fig. 3.1.4c: The potential step was made from 1.55 V (E_f) to - 2.05 V (E_r). $t_f, t_r = 0.01$ s and $t_w = \mathbf{0.02}$ s. No ECL was observed when reversing the potential step. (42)

Fig. 3.1.4d: The potential step was made from 1.55 V (E_f) to -2.05 V (E_r). $t_f, t_r = 0.01$ s and $t_w = \mathbf{0.28}$ s. (43)

Fig. 3.1.4e: The potential step was made from - 2.1 V (E_f) to 1.6 V (E_r). $t_f, t_r = 0.05$ s and $t_w = \mathbf{0.20}$ s. (43)

Fig. 3.1.4f: The potential step was made from - 2.1 V (E_f) to 1.6 V (E_r). $t_f, t_r = 0.05$ s and $t_w = \mathbf{1.80}$ s. (44)

Fig. 3.1.4g: Anodic ECL when the potential step was made from - 2.05 V (E_f) to 1.6 V (E_r). $t_f, t_r = 0.05$ s and $t_w = 0.24$ s. (44)

Fig. 3.1.4h: Cathodic ECL under the similar condition as in Fig. 3.1.4g, but the potential was switched from 1.6 V (E_f) to -2.05 V (E_r). $t_f, t_r = 0.05$ s and $t_w = 0.24$ s. (45)

Fig. 3.1.4i: Anodic ECL when the potential was switched from - 2.05 V (E_f) to 1.5 V (E_r). $t_f, t_r = 0.05$ s and $t_w = 0.24$ s. (45)

Fig. 3.1.4j: Cathodic ECL under the similar condition as in Fig. 3.1.4g, but potential was switched from 1.5 V (E_f) to - 2.05 V (E_r). $t_f, t_r = 0.05$ s and $t_w = 0.24$ s. (46)

Fig. 3.1.5a: ECL emission spectrum of DPA. (47)

Fig. 3.2.2a: Cyclic voltammogram (CV) of Pt/MEH-PPV in 0.1M TEABF₄ in acetonitrile at a scan rate of 100 mV/s. (50)

Fig. 3.2.2.b: Cyclic voltammogram (CV) of Pt/MEH-PPV in 0.1 M TBABF₄ in acetonitrile at a scan rate of 100 mV/s. (51)

Fig. 3.2.3a: Cottrell plot for Pt/MEH-PPV in 0.1 M TEABF₄-AN, when the potential step was made from 0 V to -1.9 V of duration 1 s. (52)

Fig. 3.2.4a: Anodic ECL when the potential was switched between -1.75 V and 1.45 V of duration 4 s each for MEH-PPV film on Pt in 0.1M TBABF₄-AN. (53)

Fig. 3.2.4b: Cathodic ECL when the potential was switched between 1.45 V and -1.75 V of duration 4 s each for MEH-PPV film on Pt in 0.1 M TBABF₄-AN. (54)

Fig. 3.2.4c: Anodic ECL, when the potential was switched between -1.85 V and 1.35 V of duration 1 s each for MEH-PPV film on Pt in 0.1 M TEAPF₆-AN. (55)

Fig 3.2.4d: Cathodic ECL, when the potential was switched between 1.35 V and -1.85 V of duration 1 s each for MEH-PPV film on Pt in 0.1 M TEAPF₆-AN. (55)

Fig. 3.2.4e: Comparison of anodic ECL and current decay for Pt/MEH-PPV in 0.1M TEABF₄-AN. (56)

Fig. 3.3.2.a: Cyclic voltammogram (CV) of Pt/DB-PPV in 0.1M TEAClO₄ in acetonitrile; scan rate: 100 mV/s. (58)

Fig. 3.3.2.b: Cyclic voltammogram (CV) of Pt/DB-PPV in 0.1 M TBABF₄ in acetonitrile; scan rate = 100 mV/s. (59)

Fig. 3.3.2.c.: Cyclic voltammogram (CV) of Pt/DB-PPV in 0.1 M TEABF₄ in acetonitrile; scan rate = 100 mV/s. (59)

Fig. 3.3.2d: Cathodic potential sweep of Pt/DB-PPV in 0.1 M TBABF₄ in acetonitrile; scan rate = 100 mV/s. (60)

Fig. 3.3.2e: Anodic potential sweep of Pt/DB-PPV in 0.1 M TBABF₄ in acetonitrile; scan rate = 100 mV/s. (60)

Fig. 3.3.2f: Potential sweep of Pt/DB-PPV (thickness = 1 μ m, energy of cross linking = 400 mJ/cm²) in 0.1 M TBABF₄ in acetonitrile; scan rate = 100 mV/s. (61)

Fig. 3.3.3a: Cottrell plot for the anodic current on the negative potential step of the square wave between 0 and 1.3 V with step width of 150 ms each, for Pt/DB-PPV in 0.1 M TBABF₄ in acetonitrile. (62)

Fig. 3.3.3b: Cottrell plot for the cathodic current on the negative potential step of the square wave between 0 and -1.7 V, with step width of 150 ms each, for Pt/DB-PPV in 0.1 M TBABF₄ in acetonitrile. (63)

Fig. 3.3.4a: Cathodic ECL when the potential was switched between 1.3 V and -1.85 V of duration 150 ms each for DB-PPV film of thickness $\approx 0.6 \mu\text{m}$ on Pt in 0.1 M TBABF₄ - AN. (64)

Fig 3.3.4b: Anodic ECL, when the potential was switched between - 1.9 V and 1.3 V of duration 150 ms each for DB-PPV film of thickness $\approx 0.6 \mu\text{m}$ on Pt in 0.1M TBABF₄-AN. (65)

Fig. 3.3.4c: Anodic ECL when the potential was switched between -1.9 V and 1.3V of duration 150 ms each for DB-PPV film of thickness $\approx 0.6 \mu\text{m}$ on Pt in 0.1M TEABF₄-AN. (65)

Fig. 3.3.4d: Scheme of the sequential anodic and cathodic potential steps in ECL experiments. (66)

Fig. 3.3.5a: Decrease in the ECL intensity with successive potential steps. (67)

Fig. 3.3.5b: Film morphology before the ECL experiment as seen with a microscope. (68)

Fig. 3.3.5c: Film morphology after the ECL experiment as seen with a microscope. (68)

Fig. 3.3.5d: SEM image of the DB-PPV coated electrode surface. (69)

Fig. 3.3.5e: SEM image of the DB-PPV coated electrode surface at a higher magnification. (69)

Fig. 3.3.5f: EDS analysis on the darker spots as seen in the SEM image. (70)

Fig. 3.3.5.g: Energy of cross-linking (mJ/cm^2) used to cross-link the DB-PPV films against the magnitude of cathodic charging current. (71)

Fig. 3.3.5.h: Raman spectrum of DB-PPV when examined in the powder form and after film casting on the Pt electrode. (72)

Fig.3.3.5i: Comparison of Raman spectra between the powder form and the cross-linked film of the polymer DB-PPV before the ECL experiment. (72)

Fig. 3.3.5j: Comparison of the Raman spectra of the polymer DB-PPV before and after the ECL experiment. (73)

Fig. 3.3.5k: DB-PPV in phenylic form. (74)

Fig. 3.3.5l: DB-PPV in quinonic form. (74)

Fig. 3.3.6a: Cathodic ECL spectrum. (76)

Fig. 3.3.6b: Anodic ECL spectrum. (76)

Fig. 3.3.6c: Absorption spectrum of DB-PPV in CHCl_3 . (77)

Fig. 3.3.5d: Fluorescence spectrum of DB-PPV in CHCl_3 . (77)

Fig. 4.1.2a: Equivalent circuit representation of the electrochemical processes. (81)

Fig. 4.1.3a Representation of concentration array in point model. (82)

Fig. 4.1.6 a. Simulation of the anodic transient (potential step between -2.05 V and 1.6V, duration 50ms each) with $C^\circ = 1 \times 10^{-6} \text{ mol cm}^{-3}$, $k_{\text{ex}} = 3 \times 10^{10} \text{ l mol}^{-1} \text{ s}^{-1}$, $D = 5 \times 10^{-6} \text{ cm}^2 \text{ s}^{-1}$, $R_u = 109 \Omega$ and $C_{\text{dl}} = 1.5 \mu \text{ F}$. (86)

Fig. 4.1.6 b. Simulation of the cathodic transient (potential step between 1.6 V and -2.05V, duration 50ms each) with $C^\circ = 1 \times 10^{-6} \text{ mol cm}^{-3}$, $k_{\text{ex}} = 1 \times 10^{10} \text{ l mol}^{-1} \text{ s}^{-1}$, $D = 5 \times 10^{-6} \text{ cm}^2 \text{ s}^{-1}$, $R_u = 109 \Omega$ and $C_{\text{dl}} = 1.5 \mu \text{ F}$. (87)

Fig. 4.1.6 c : Effect of double layer charging on the potential step from -2.05 V to 1.6 V. (88)

Fig. 4.1.6 d : Effect of double layer charging on the potential step from 1.6 V to -2.05 V. (88)

Fig. 4.2.1a. Representation of double layer charging in the electrode/polymer/solution system: situation prior to charge transfer. (90)

Fig. 4.2.1b. State of the polymer during charge transfer and transport maintaining bulk electroneutrality. (91)

Fig. 4.2.1c: Plot of current density against $t^{1/2}$ under diffusion-migration conditions for the electrode reaction $A^+ \rightarrow B^{3+}$. The pure diffusion case (Cottrell) was included for comparison. (93)

Fig 4.2.6a. Simulation of the anodic transient (for a potential step between -1.75 V and 1.45 V, SE - 0.1M TEABF₄) with $C^\circ = 5.8 \times 10^{-4} \text{ mol cm}^{-3}$, $k_{\text{ex}} = 1 \times 10^3 \text{ l mol}^{-1} \text{ s}^{-1}$, $D_{\text{ap}} = 3.2 \times 10^{-12} \text{ cm}^2 \text{ s}^{-1}$, $R_u = 1 \times 10^4 \Omega$ and $C_{\text{dl}} = 1 \mu\text{F}$. (99)

Fig 4.2.6b. Simulation of the cathodic transient (for a potential step between 1.45 V and -1.75 V, SE - 0.1M TEABF₄) with $C^\circ = 5.8 \times 10^{-4} \text{ mol cm}^{-3}$, $k_{\text{ex}} = 3 \times 10^3 \text{ l mol}^{-1} \text{ s}^{-1}$, $D_{\text{ap}} = 8 \times 10^{-13} \text{ cm}^2 \text{ s}^{-1}$, $R_u = 1 \times 10^4 \Omega$ and $C_{\text{dl}} = 2 \mu\text{F}$. (99)

Fig. 4.2.6c. Simulation of the anodic transient (for a potential step between -1.85 V and 1.35 V, SE - 0.1M TEAPF₆) with $C^\circ = 5.8 \times 10^{-4} \text{ mol cm}^{-3}$, $k_{\text{ex}} = 6 \times 10^3 \text{ l mol}^{-1} \text{ s}^{-1}$, $D_{\text{ap}} = 0.5 \times 10^{-12} \text{ cm}^2 \text{ s}^{-1}$, $R_u = 1 \times 10^4 \Omega$ and $C_{\text{dl}} = 5 \mu\text{F}$. (101)

Fig 4.2.6d. Simulation of the cathodic transient (for a potential step between 1.35 V and -1.85 V, SE - 0.1M TEAPF₆) with $C^\circ = 5.8 \times 10^{-4} \text{ mol cm}^{-3}$, $k_{\text{ex}} = 5 \times 10^3 \text{ l mol}^{-1} \text{ s}^{-1}$, $D_{\text{ap}} = 1.5 \times 10^{-13} \text{ cm}^2 \text{ s}^{-1}$, $R_u = 1 \times 10^4 \Omega$ and $C_{\text{dl}} = 6 \mu\text{F}$. (101)

Fig. 4.3a. Simulation of the anodic ECL transient (for a potential step between -1.9 V and 1.3 V, SE - 0.1M TBABF₄) with $C^\circ = 6.1 \times 10^{-4} \text{ mol cm}^{-3}$, $k_{\text{ex}} = 3 \times 10^4 \text{ l mol}^{-1} \text{ s}^{-1}$, $D_{\text{ap}} = 6 \times 10^{-11} \text{ cm}^2 \text{ s}^{-1}$, $R_u = 1200 \Omega$ and $C_{\text{dl}} = 1 \mu\text{F}$. (102)

Fig. 4.3b. Simulation of the cathodic ECL transient (for a potential step between 1.3 V and -1.8 V, SE - 0.1M TBABF₄) with $C^{\circ} = 6.1 \times 10^{-4} \text{ mol cm}^{-3}$, $k_{\text{ex}} = 1 \times 10^4 \text{ l mol}^{-1} \text{ s}^{-1}$, $D_{\text{ap}} = 1 \times 10^{-11} \text{ cm}^2 \text{ s}^{-1}$, $R_u = 1200 \Omega$ and $C_{\text{dl}} = 3 \mu \text{ F}$. (102)

Fig. 5.1a. Typical shape of the triple potential steps including the waiting period t_w in the ECL experiments. (104)

List of Symbols

R_u	resistance of the solution phase or the polymer/solution phase in Ω
C_{dl}	double layer capacitance at the electrode/solution or electrode/polymer interface in F (farads)
k_{ex}	rate constant for the electrochemiluminescence (ECL) reaction $l\ mol^{-1}s^{-1}$
D	diffusion coefficient in cm^2s^{-1}
D_{ap}	apparent diffusion coefficient in cm^2s^{-1}
D_{ap}^f	apparent diffusion coefficient in the first potential step in cm^2s^{-1}
D_M	dimension less diffusion coefficient used in the simulation
l	diffusion layer thickness in cm
Δx	increment of distance in the simulation procedure
t	time in s (seconds)
Δt	increment of time in the simulation procedure
t_w	waiting period in s
E	potential in V (volts)
v	scan rate in Vs^{-1}
I_F	Faradaic current in A (amperes)
I_{dl}	Charging current in A (amperes).
j	current density in Acm^{-2}
C	concentration in $molcm^{-3}$
J	flux of species in $mol\ cm^{-2}\ s^{-1}$
R	gas constant $JK^{-1}mol^{-1}$
B	strength of magnetic field in kilo Gauss

Abbreviations

ECL	electrogenerated chemiluminescence / electrochemiluminescence
EL	electroluminescence in the solid-state
PL	photoluminescence
Og	organic molecule
Og ^{+·}	radical cation
Og ^{-·}	radical anion
Og*	excited state of Og
Pr	electroactive unit of the neutral polymer
Pr ^{+·}	positive polaron
Pr ^{-·}	negative polaron
Pr*	excited polaron
Ar	argon
RC	resistance-capacitance
CV	cyclicvoltammogram
SEM	scanning electron microscopy
SE	supporting electrolyte
TEAClO ₄	tetraethylammonium perchlorate
TBAClO ₄	tetrabutylammonium perchlorate
TEABF ₄	tetraethylammonium tetrafluoroborate
TBABF ₄	tetrabutylammonium tetrafluoroborate
TEAPF ₆	tetraethylammonium hexafluorophosphate
DPA	9,10-diphenylanthracene
MEH-PPV	poly(2-ethylhexyloxy-5-methoxy-1,4-phenylenevinylene)
DB-PPV	poly(2,3-dibutoxy-1,4-phenylenevinylene)
DBMOS-PPV	poly[bis(2,5-dimethyl-octylsilyl)-1,4-phenylenevinylene]
PAT6	poly(3-hexylthiophene)

List of publications

1. "Charge transport through chemically modified electrodes - a general analysis for ion exchange and covalently attached redox polymers" J. Umamaheswari and M.V. Sangaranarayanan, *J. Phys. Chem., B.* **103**, 5687 (1999).
2. "Nonequilibrium thermodynamics formalism for charge transport in redox polymer electrodes" J. Umamaheswari and M.V. Sangaranarayanan, *J. Phys. Chem., B.* **105**, 2465 (2001).
3. " Electrochemiluminescence of conjugated polymer" U. Janakiraman, D. Dini, A. Preusser, A.B. Holmes, R.E. Martin and K. Doblhofer, *Synthetic Met.*, **121**, 1685 (2001).
4. "Electrochemical Generation of Light in Conjugated Polymers" Danilo Dini, Umamaheswari Janakiraman and Karl Doblhofer in *Conducting Polymers and Polymer Electrolytes - From Biology to Photovoltaics*, Ed., J.F. Robinson and H.B. Mark, Jr, ACS Sym. Ser. **832**, 103 (2003).
5. "Comparison of ECL characteristics of PPV derivative polymers" J. Umamaheswari, R.E. Martin, C. Fischmeister, A.B. Holmes, J. Piccardi and K. Doblhofer - to be communicated.

Acknowledgements

I would like to extend my sincere gratitude to Prof. Gerhard Ertl for giving me the opportunity to do my Ph.D. in the Fritz-Haber-Institut der MPG. I am grateful to the Max-Planck-Society for the financial support. I thank Dr Karl Doblhofer for the liberty he gave me in learning this field, his valuable guidance and advices. My thanks are due to Prof. Klaus Rademann of the Humboldt Universität zu Berlin, for his suggestions and guidance on my thesis work. I am grateful to Dr M.V. Sangaranarayanan of the Indian Institute of Technology (IIT), Chennai, India, for introducing me to the field of conducting polymers.

I would like to thank my colleagues Ms Sabine Wasle for her helps to my experimental works, Dr Danilo Dini of University of Rome for his initial experimental works on the polymer MEH-PPV, Mr Gennaro Picardi of FHI, for helping me with the Raman spectroscopic measurements, Dr Albrecht Preusser of the Theory Department of FHI for his helps in introducing me to the computer simulations, Mrs Gisela Weinberg of FHI for the SEM measurements, the group of Dr Scheunemann of BESSY II for their valuable help in cross-linking of the polymer, Mr Murali Sukumaran of the Humboldt Universität zu Berlin, for helping me with the absorbance and fluorescence measurements and Dr Pranab Kumar Patra of the Freie Universität, Berlin, for his helps in the solvent purification. Above all I would like to thank, Dr Rainer Martin, Dr Cedric Fischmeister and Prof. A.B. Holmes, of the Cambridge University, UK for providing me with the PPV derivative polymers.

My deep thanks are for Ms Reinhardt of FHI for giving me the advices and the emotional support when I needed them the most. I would also like to thank, Dr. Katharina Krischer and Dr. Elena Savinova, for their kind advices. My sincere thanks are also due for Ms Todorova of FHI for being a nice friend and Dr Jae Young Lee for his inspiring words. I like to thank my land lady Ms Becker and Mrs Doblhofer for their kindness, which all made my stay in Berlin a pleasant one.

I would like to thank my Indian colleagues: Mrs Latha Ramachandran, Dr Aldrin Denny, Dr R. Saradha, Dr T. Ramnathan, Dr G. Manickam, Dr A.M.

Sembian, Dr M. Srinivasan, Dr Saroja G. and Dr K. Vijayalakshmi for their care and support and for being nice friends all along. My thanks are also for all those friends who extended their friendship, even across the distances, and filled me with joy. My special thanks is to Dr G. Natrajan of Vivekananda College, India, for his encouragements and guidance in pursuing my studies and to Dr K. Vijayamohanan of the National Chemical Laboratory, Pune, India for his encouragements.

I thank my parents, Mr R.V. Janakiraman (late) and Mrs J. Pichammal whose affection I am indebted forever. I thank my beloved sister Mrs Lalitha Rajamohan and brothers Mr R.J. Viswanathan, Mr J. Subramanian and Dr R.J. Ramamurthi for their support and care.

Lebenslauf

Name:	Umamaheswari Janakiraman
Geburtsdatum:	18. November 1974
Geburtsort:	Kumbakonam, Tamil Nadu (Indien)
1992:	Abschluss: Allgemeine Hochschulreife an der St. Antony's Girls Higher Secondary School, Chennai, Indien
Juli 1992 - Juli 1995:	Grundstudium der Chemie (B.Sc. (Chemistry)) an der University of Madras, Indien
Sep. 1995 - Juni 1997:	Hauptstudium der Physikalische Chemie (M.Sc. (Physical Chemistry)) an der University of Madras, Indien
Dec. 1996 - Juni 1997:	Senior Thesis an der University of Madras, Indien Thema: Electrochemical oxidation of catechol at glassy carbon electrode in sulphuric acid Betreuer: Dr. K. Chandrasekar Pillai
Juli 1997 - Juli 1999:	Doktorarbeit in der Indian Institute of Technology (IIT), Madras, Indien Thema: Chemically modified electrodes Betreuer: Dr. M.V. Sangaranarayanan
seit 09.09.1999:	Dissertation am Fritz-Haber-Institut der Max-Planck-Gesellschaft, Abt. Physikalische Chemie, Thema: Analysis of Electrogenenerated Chemiluminescence of PPV type Conducting Polymers Betreuer: Priv.-Doz. Dr. Karl Doblhofer

Selbständigkeitserklärung

Hiermit versichere ich, die vorliegende Arbeit selbständig und nur unter Nutzung der angegebenen Hilfsmittel angefertigt zu haben.

Berlin, den 31.03.2003

.....

(Umamaheswari Janakiraman)